POSIVA 2003-10

Glacial Rebound and Crustal Stress in Finland

Kurt Lambeck
Anthony Purcell

November 2003

POSIVA OY
FIN-27160 OLKILUOTO, FINLAND
Phone (02) 8372 31 (nat.), (+358-2-) 8372 31 (int.)
Fax (02) 8372 3709 (nat.), (+358-2-) 8372 3709 (int.)

POSIVA 2003-10

Glacial Rebound and Crustal Stress in Finland

Kurt Lambeck
Anthony Purcell
Research School of Earth Sciences
The Australian National University

November 2003

POSIVA OY
FIN-27160 OLKILUOTO, FINLAND
Phone (02) 8372 31 (nat.), (+358-2-) 8372 31 (int.)
Fax (02) 8372 3709 (nat.), (+358-2-) 8372 3709 (int.)

ISBN 951-652-124-X
ISSN 1239-3096

Posiva-raportti – Posiva Report

Posiva Oy
FIN-27160 OLKILUOTO, FINLAND
Puh. 02-8372 (31) – Int. Tel. +358 2 8372 (31)

Raportin tunnus – Report code
POSIVA 2003-10

Julkaisuaika – Date
November 2003

Tekijä(t) – Author(s)

Kurt Lambeck and Anthony Purcell
Research School of Earth Sciences,
The Australian National University

Toimeksiantaja(t) – Commissioned by

Posiva Oy

Nimeke – Title

GLACIAL REBOUND AND CRUSTAL STRESS IN FINLAND

Tiivistelmä – Abstract

The last ice age of Fennoscandinavia continues to have geological repercussions across Finland despite the last ice having retreated almost 10,000 years ago: land uplift, shoreline retreat, and the stress state of the crust continues to evolve. This report focusses on the glacial rebound signals for Finland and the Gulf of Bothnia and explores the consequences of the ongoing deformation. The rebound signals include the geological evidence as well as instrumental observations: the tide gauge and lake-level measurements of the past century, the changes in geodetic levels recorded in the repeat levelling surveys of the region and the direct measurement of crustal deformation (radial and horizontal) using high-precision space-geodesy measurements. These signals provide constraints on the Earth's rheology, its elasticity and viscosity, and the glacial history of the region. Once observationally constrained, the rebound models are used to predict both the ongoing evolution of shorelines and the changing state of stress within the crust.

This report covers:
(i) A review of glacial rebound modelling for Scandinavia (Sections 2 & 3).
(ii) Review of observational evidence relating to sea-level change and crustal rebound (Section 4).
(iii) New earth and ice-sheet model results from the inversion of the geological evidence for sea-level change, including models of shoreline evolution (Sections 5 & 6).
(iv) Earth-model results from the inversion of the geodetic evidence for sea-level change (Section 7).
(v) Development of crustal stress models for past and present stress states (Section 8).
(vi) Conclusions and recommendations (Section 9).

Specific conclusions reached pertain to:
(i) Thickness of ice cover over Scandinavia since the Last Glacial Maximum, particularly for the Lateglacial period.
(ii) Sea-level change and shoreline evolution for the Baltic area since the time the region became ice-free for the last time.
(iii) The predicted rates of present-day crustal rebound and sea-level change within the Baltic Basin.
(iv) The magnitude and orientation of the regional stress field in the crust since the time of the last glaciation, including the present-day residual stress field.

The current models have reached a state where realistic regional stress patterns can be predicted that provide the background data for developing high-resolution local numerical models. This study is confined to the regional stress field only. We use as a measure of the significance of the incremental stress the change in Fault Stability Margin (*FSM*) resulting from the changes in ice (and ocean) load with time. While ice is present, the crust is stabilized except outside the area of loading, but when the ice retreats the crust becomes less stable and faults that are close to failure may be reactivated. For much of central Finland the deviatoric *FSM* reach their maximum values at about 10 ka BP but the magnitudes relax with time and at present they represent about 20% of their original values. Thus any failure within the crust triggered by glacial loading and unloading will have occurred preferentially when the region first became ice-free and the potential for reactivating faults today by this process must be considered as negligibly

Avainsanat - Keywords
glacial rebound, stress, ice age, Scandinavia

ISBN
ISBN 951-652-124-X

ISSN
ISSN 1239-3096

Sivumäärä – Number of pages
84

Kieli – Language
English

Posiva-raportti – Posiva Report

Posiva Oy
FIN-27160 OLKILUOTO, FINLAND
Puh. 02-8372 (31) – Int. Tel. +358 2 8372 (31)

Raportin tunnus – Report code
POSIVA 2003-10
Julkaisuaika – Date
Marraskuu 2003

Tekijä(t) – Author(s)

Kurt Lambeck ja Anthony Purcell
Research School of Earth Sciences,
The Australian National University

Toimeksiantaja(t) – Commissioned by

Posiva Oy

Nimeke – Title

MAANKOHOAMINEN JA MAANKUOREN JÄNNITYS SUOMESSA

Tiivistelmä – Abstract

Viimeisen jääkauden jälkivaikutukset jatkuvat yhä Fennoskandiassa siitä huolimatta, että jäätikkö vetäytyi Suomesta lähes 10 000 vuotta sitten: maankohoamista, rannansiirtymistä ja maankuoren jännitystilan muutoksia tapahtuu edelleen. Tässä raportissa tarkastellaan maankohoamisen aikaansaamia merkkejä Suomessa ja Pohjanlahden alueella. Maankohoamisen johdosta syntyneet todisteet ovat niin geologiasia kuin mittaamalla saatujakin: meren- ja järvien pinnan korkeuden mittauksia viime vuosisatoina, toistettuja alueellisia geodeettisiä mittauksia käyttämällä tarkkoja avaruusgeodeettisiä maankuoren deformaatiomittauksia (radiaalisia ja horisontaalisia). Näistä todisteista saadaan reunaehdot Maapallon reologialle, sen elastisuudelle ja viskositeetille sekä alueen geologiselle historialle. Havaittujen reunaehtojen jälkeen maankohoamismalleja käytettään ennustamaan sekä jatkuvaa rannikkoalueiden muuttumista, että maankuoren jännitystilassa tapahtuvia muutoksia.

Tämä raportti sisältää:
(i) Katsauksen Skandinavian maankohoamisen mallintamiseen (Kappaleet 2 & 3).
(ii) Katsauksen havaittuihin todisteisiin koskien merenpinnan tason muutoksia ja maankohoamista (Kappale 4).
(iii) Uuden Maapallo- ja jäätikkömallin tulokset invertoituna havaituista merenpinnan tason muutoksista sisältäen ranta-alueiden kehitysmallit (Kappaleet 5 & 6).
(iv) Maapallomallin tulokset saatuna invertoimalla geologiset todisteet merenpinnan tason muutoksia varten (Kappale 7)
(v) Nykyisten ja aiempien maankuoren jännitystilamallien kehittyminen (Kappale 8).
(vi) Johtopäätökset ja suositukset (Kappale 9).

Johtopäätökset koskettavat erityisesti:
(i) Jään paksuutta viimeisen jääkauden maksimivaiheessa Skandinaviassa, erityisesti myöhäis-glasiaaliaikana.
(ii) Merenpinnan tason muutoksia ja rannansiirtymistä Itämeren alueella jäätikön vetäydyttyä.
(iii) Nykyisen maankohoamisen ja merenpinnan tason muutosten ennustamista Itämeren alueella.
(iv) Maankuoren alueellisen jännitystilan suuntaa ja suuruutta viimeisen jääkauden jälkeen mukaan lukien nykyinen residuaalinen jännityskenttä.

Nykyisillä malleilla on saavutettu tila, joiden avulla voidaan ennustaa realistisesti alueellista jännitystilaa ja joilla saadaan taustatiedot tarkalle paikalliselle numeeriselle mallille. Tämä tutkimus on rajattu koskemaan vain alueellista jännitystilaa. Me käytämme jännityksen merkittävän lisääntymisen mittana murtumisherkkyysmarginaalin *(FSM)* muutosta jään (ja meren) kuormittavasta vaikutuksesta johtuen. Jäätiköitymisen aikana maankuori on vakaa lukuun ottamatta jään ulkopuolisia alueita, mutta jään vetäydyttäessä kuori muuttuu epästabiiliksi ja siirrokset, jotka ovat lähellä murtumista saattavat uudelleen aktivoitua. Keski-Suomen poikkeuksellinen *FSM* saavutti maksimiarvonsa pääasiassa noin 10 ky BP, jonka jälkeen jännityksen magnitudi on alentunut ollen nykyään noin 20%:a alkuperäisestä. Siten jokainen jään kuormituksen tai kuormituksen purkautumisen aiheuttama heikkouskohta maankuoressa on ollut ensisijainen ja potentiaalinen murtumiskohta alueen ensimmäisen kerran vapauduttua jäästä, ja tämän prosessin vaikutusta tänä päivänä tulee pitää olemattoman pienenä.

Avainsanat - Keywords
maankohoaminen, jännitys, jääkausi, Skandinavia

ISBN
ISBN 951-652-124-X

ISSN
ISSN 1239-3096

Sivumäärä – Number of pages
84

Kieli – Language
Englanti

TABLE OF CONTENTS

1 SUMMARY

The last ice age of Fennoscandinavia continues to have geological repercussions across the region despite the last ice having retreated from the region almost 10,000 years ago. The most obvious consequences are the land uplift on both sides of the Gulf of Bothnia and the concomitant retreat of the sea. That this still occurs today is evidence of the Earth's viscosity, of the lagging response of the planet to past surface loads. This makes Scandinavia a natural laboratory for the study of the deformation of terrestrial materials on time scales that are beyond the reach of laboratory experiments. However it also makes Scandinavia a region of geological change on human time scales. The rebound process has not ceased, land uplift and shoreline retreat will continue into the future, and the stress state of the crust will continue to evolve.

While the glacial rebound signal is dominant in the recent geology of Scandinavia, other tectonic processes also have operated in the past and presumably operate today although at rates that are slower than the glacial processes. Erosion and sedimentation redistribute surface loads and stress the crust. Plate tectonic forces add to the regional background stress. Geological anomalies built into the crust and lithosphere during past orogenic events leave non-equilibrium stress fields that may be re-activated by the superimposed glacial stress field. Climate-change processes may cause changes in global ocean volume and in sea level in addition to the relative sea-level change resulting from the glacial rebound. Thus the glacial rebound signal has to be seen against a background of other change to the Earth's surface, change on both longer and shorter time scales than that of the characteristic glacial signal.

This report focusses on the glacial rebound signals for the Scandinavian region in general and Finland in particular and explores some of the consequences of the ongoing deformation. The rebound signals include the geological evidence for palaeo lake and sea levels that are above or below present-day positions. It also includes instrumental observations of change on recent time scales: the tide gauge and lake-level measurements of the past century, the changes in geodetic levels recorded in the repeat levelling surveys of the region and, most recently, the direct measurement of crustal deformation (radial and horizontal) using high-precision space-geodesy measurements. These recorded signals, geological and geodetic, provide constraints on two important classes of parameters: the Earth's rheology, its elasticity and viscosity, and the glacial history of the region, the thickness and retreat history of the Scandinavian ice sheet since the last maximum in glaciation ~20,000 years ago. Through a careful exploration of the combined parameter space, exploiting the spatial and temporal variability of the response signals, it becomes possible to establish constraints on both the earth response function and the glacial history and to develop physically plausible models of the phenomenon that are not just descriptive but which have a predictive capability. Such models have been derived here and used to predict both the ongoing evolution of the regions shorelines and the changing state of stress within the crust.

The rebound phenomenon of Fennoscandia does not respect political boundaries and any study must cross such boundaries: What occurs in Finland today has its origins in what occurred in the past over the Norwegian and Swedish highlands and over Arctic

Russia. Thus the development of predictive models for Finland requires that information from areas beyond Finland is also considered and a considerable part of the report is devoted to establishing regional constraints on the rebound process that are particularly pertinent to the Finland region: Thus more attention is given to the data base around the Gulf of Bothnia than for the Norwegian Coast, for example, and the predictions are largely tailored for the central region.

Specifically, the aim of this study has been to develop a predictive model for both past and future shoreline evolution and for the crustal-stress evolution caused by glacial rebound. These objectives have been addressed in several steps.

(i) A brief review of the past (circa 1998) state of glacial rebound modelling for Scandinavia (Section 2).

(ii) Review of modeling improvements since 1998 (Section 3).

(iii) Review of observational evidence relating to sea-level change and crustal rebound (Section 4).

(iv) New earth-model results and an improved rebound and ice sheet model for Scandinavia from the inversion of the geological evidence for sea-level change, including models of shoreline evolution (Sections 5 & 6).

(v) Earth-model results from the inversion of the geodetic evidence for sea-level change (Section 7).

(vi) Development of crustal stress models for past and present stress states (Section 8).

(vii) Conclusions and recommendations (Section 9).

The present work starts with the solutions for the rebound problem given by Lambeck et al. (1998 a, b) and Lambeck (1999) which present solutions based on (a) the geological evidence for the age-height relations of palaeo sea levels with respect to present sea level, (b) the Baltic Ice Lake shoreline information, and (c) the instrumental records for sea-level change and the tilting of some of the larger inland lakes of Sweden and Finland. Since 1998 improvements have been made in modelling techniques (section 3) and the decision was taken to carry out a new solution rather than base the predictions on the 1998 models. The data bases used in the current work are essentially the same as those previously used (Section 4), in part because they already were comprehensive, in part because they permit the effect of changes in modelling procedures to be separated from data constraints, and because the assessment of any new data required resources and time that go beyond the scope of the study. This has the advantage that any new data will provide good tests for the validity of the present outcomes. New data types that have been partly exploited include the GPS results for crustal displacements (Section 4) and that have not been exploited include the precise geodetic levelling data for Finland, and the highest coastline data for Finland and Sweden.

In rebound modelling both the earth rheology and the ice sheet history must be considered as at least only partially known. The margins of ice retreat have been well

mapped over land but even there uncertainties remain due to different time scales used in different regions (the radiocarbon time scale versus the varve time scales of Sweden and Finland). More important is the lack of direct observational evidence for the thickness of the ice sheet at any time during the Last Glacial Maximum and its retreat. Mostly this is based on glaciological models whose assumptions remain to be tested. During the retreat phase, the observations of shoreline elevations are quite sensitive to the geometry of the ice load and the spatial pattern of the shorelines can vary significantly from epoch to epoch. The Earth response function, filtered by the elastic lithosphere, is more sensitive to the large-scale distribution of the ice. Thus observations of sea level change after the ice has retreated tend to be more strongly dependent on rheological parameters than to the details of the ice sheet. By making use of the spatial and temporal variability of the signal it becomes possible to distinguish the parts of the signal that reflect primarily the earth response from those that reflect characteristics of the ice load. This separation of parameters is further aided by introducing global response signals, such as global sea-level signals that measure largely the total ice volumes as a function of time, or the global rotational signals that reflect primarily the rheological response of the deeper parts of the earth.

Section 5 summarizes the successive steps in the iterative solution towards new ice and rheology parameters using the age-height data base of palaeo sea levels. One feature of the inversion results is that the thickest LGM ice occurs over the northern part of the Gulf of Bothnia, ~ 2700 m, with a secondary maximum of ~2400 m over southern Sweden. There is also a suggestion of a secondary dome over northern Finland but this may be an artifact because (i) sea-level data from this region is limited, and (ii) there is inconsistency between some of the data points for this region. The evidence from northern Finland clearly needs re-examination. At the end of the Last Glacial Maximum, at ~ 19,000 years (calendar) before present (19 ka BP) a rapid reduction in ice volume appears to have occurred although the magnitude of this remains uncertain: the major reduction occurs over northern and central Finland and it is subject to the reservation that the sea-level data from this region has been correctly interpreted. This reinforces the need to revisit and expand upon the field data from northern Bothnia. The ice models for the Lateglacial period are consistent with the Gulf of Bothnia having acted as an ice stream, with ice somewhat thinner there than over Finland. The models are consistent with recent evidence that the ice thicknesses at the start of the Holocene were thin across the region north of the Younger Dryas moraines (Salpaussalkä, Central Swedish, Ra).

The Baltic Ice Lake data provides an important data set for testing the rebound model because the data is from an early period (~12 ka BP) when little information is otherwise available from the central Baltic area. The inversion of this data leads to results that are essentially consistent with that of the age-height data but some small differences occur that may be significant. First, the solution leads to a somewhat lower value for the upper mantle viscosity than does the other geological data base and this may be a consequence of the different epochs of the data sets: the BIL data corresponds to the epoch ~12 ka BP while the elevation-age data corresponds to a mean age of ~ 7.5 ka. If the earth rheology is not linear – as is assumed in the inversion – then the older

data set can lead to lower values for the viscosity (Section 6). Thus the geodetic data, because it measures very recent response, becomes particularly important. Indeed, the inversion of this data leads to higher values for upper mantle viscosity. The solutions are therefore indicative that a non-linear mantle response may not be an ideal assumption but the results are too tentative to warrant a full development of a non-linear theory at this stage. In view of these results, predictions of the stress fields have been carried separately for both the 'geological' and the 'geodetic' mantle parameters (Section 8).

In the final geological solution, the two geological data sets have been combined into a single solution for the earth rheology (eqn 10) and this, with the new ice sheet, forms the basis for mapping the shoreline progression from the time of onset of deglaciation up to the present (Figures 25, 26). They also provide the basis for forward predictions of shoreline evolution, on the basis that the residual glacial isostatic rebound is the only contribution. This result is given in Figure 28 in terms of the present day rate of change in relative sea level. Effective mapping of the future shoreline migration requires (a) a precision of the present bathymetry and topography that is not available to us, and (b) a knowledge of the change in ocean volume from either thermal expansion due to heating of the ocean column or to melting of the planet's remaining ice sheets and glaciers.

The state of stress of the planet's crust is the sum total of many processes but the one that changes on a relatively short time scale is that induced by the changes in the surface loads of ice and water. This stress field is essentially a function of higher derivatives of the displacement field of the crust. Therefore, a precise mapping of crustal displacement is required before realistic stress fields can be evaluated. We believe that we have reached a state of model development where realistic regional stress patterns can be predicted. We use as a measure of the significance of the incremental stress the change in Fault Stability Margin (*FSM*) resulting from the changes in ice (and ocean) load with time (Section 8.2). While ice is present, the crust tends to be stabilized except outside the area of loading, but when the ice retreats the crust becomes less stable and faults that are close to failure may be reactivated. For much of central Finland the deviatoric *FSM* reach their maximum values at about 10 ka BP but the magnitudes relax with time and at present they represent about 20% of their original values (Figures 34, 35). Thus any failure within the crust triggered by glacial loading and unloading will have occurred preferentially when the region first became ice free, all other factors contributing to crustal instability remaining unchanged, and the potential for reactivating faults today by this process must be considered as negligibly small (Section 8).

Despite considerable progress made when compared with the 1998 solutions, there remains scope for further improvement, both in the analyses of the field evidence and in the modelling (Section 9). The current work provides the regional setting for Finland against which local processes can be evaluated. Are there local perturbations in the crustal stress field that can be reactivated by changing rebound stresses? This can only be answered by in-situ crustal strain and stress measurements and by a very careful evaluation of the local structural geology. Are the migrating shorelines likely to have a major effect on ground water circulation over time? Again, this required greater local

knowledge than we possess. But the regional stress and displacement fields presented here provide the background data for developing high-resolution local numerical models to examine these effects.

2 REVIEW OF THE GLACIAL REBOUND MODELS FOR SCANDINAVIA

The most complete published rebound model for Scandinavia remains that of Lambeck et al. (1998a). It includes a rigorous three-dimensional and global model for the earth's response to changes in surface (ice and water) loading and high-resolution descriptions of ice sheets that are also glaciologically plausible, and is constrained by a comprehensive observational data base of sea level information (~ 1200 observations for Scandinavia, British Isles and the North Sea extending from the present to the Last Glacial Maximum.)

The model provides realistic predictions of a number of geophysical, geological and geodetic observables, demonstrating that it provides good first order predictions of the response of the earth to glacial cycles for Scandinavia. These observations include the age-height relationship of palaeo-shorelines, the history of the Baltic Sea and Baltic Lake levels since deglaciation (Lambeck, 1999), tide gauge and lake-tilting observations over the past century (Lambeck et al. 1998b), and GPS measurements of radial and horizontal crustal displacement (Milne et al., 2001). Thus the model provides a basis for predicting shoreline evolution as well as for computing the changing stress-state within the crust.

Glacial rebound is a global problem. The rebound of Scandinavia is not independent of the melting history of the other ice sheets. This complex interaction has led to the development of a process in which the rebound for different parts of the globe is evaluated iteratively. Thus the 1998-1999 solutions for the Fennoscandia ice sheet may need revision because of improvements made to the Antarctic or North American ice sheets. Also, since the earlier work several improvements have been made to the rebound theory and to its numerical implementation. It was therefore decided to defer the Finland predictions until these modifications were thoroughly tested.[1]

Milne et al. (2001) have carried out some analyses of the Scandinavian rebound. Their results compare outcomes based on different ice models and they have concluded that those of Lambeck et al. (1998b) are currently the best available. The major difference between their work and ours is that we have compiled a much more substantial data base for both sea-level and glacial history data, and that we have carried out more

---

[1] This became particularly necessary because doubt had been cast on some aspects of our solution (Peltier 2002). While we believed that this was quite unwarranted (Lambeck et al., 2002b) we did have to respond and demonstrate that our methodology was sound. The latest tests of our code were completed in June 2002. A program of numerical code comparisons with the other principal modeller in this field, Professor J. X. Mitrovica of Toronto University, has begun and so far all tested components of the respective codes agree to better than 1%. The details of this methodology have now been published (Lambeck et al., 2003), in more detail than is usually warranted. Mitrovica and Milne (2002) have examined Peltier's criticism in more detail than we were able to do because we do not have access to Peltier's numerical code. (His code is based on earlier work by Mitrovica with modifications added that are based on work by Milne.) They conclude that: '*Our* (i.e. Mitrovica and Milne's) *results for the Bonaparte Gulf data are consistent with the recent study by Yokoyama et al. (2000)*' and *'that the theories applied by Johnston (1993), Milne (1998) and Milne et al. (1999) are more accurate than the procedure advocated by Peltier (1994, 1998)*'.

comprehensive solutions for the ice sheet parameters. There is a tendency in rebound modelling to use existing ice sheet models as if they are well quantified and to invert the rebound evidence for earth-model parameters only. The result is model parameters that are only as good as the assumptions about the ice sheet. This led us to conduct much more extensive tests to separate out the ice- and earth-model parameters.

Other solutions for the Scandinavian rebound have been carried out by Fjeldskaar (1994, 1997) and follow the original formulation of Cathles (1975), in which the mantle is treated as viscous rather than visco-elastic. This means that the solutions are in principle comparable only after the bulk of the ice has melted so that the elastic components of deformation are unimportant. A more serious reservation about these results concerns the parameterisation of the mantle in which the lithospheric thickness is assumed known.

The assumed nature of the lithosphere in the analysis of rebound is a vexing matter because of the different definitions used for this layer. Seismic estimates are usually based on that part of the uppermost mantle that has high seismic shear velocities and low attenuation of seismic energy. Seismic waves are of short duration and any part of the mantle where the relaxation time is much greater than the imposed stress field will appear to be effectively elastic. Tectonic estimates are usually based on the response to loads on time scales of a million years or more (e.g. sediment or volcanic loads). Temperature increases with depth in the upper mantle and tectonically induced stresses will relax on long time scales, relaxing faster where temperatures are closer to the melting point. Thus stresses generated in the warmer part of the lithosphere migrate upwards and the load becomes increasingly supported by the cooler upper regions. Hence the effective lithospheric thickness H_l defining the response on tectonic timescales is less than the seismically defined thickness. At the time scale of glacial load cycles of $\sim 10^4$ years, the expected lithospheric thickness will lie between these limits, but exactly where remains uncertain and *a-priori* values for this parameter cannot be imposed. This becomes important because trade-offs occur between this parameter and other mantle parameters: imposing the one will influence the solution for the other (c.f. Figure 15 of Lambeck, 1993) particularly when data used to estimate the parameters is from near ice margins. Fjeldskaar's models generally impose the lithospheric thickness as being the tectonic thickness but, as shown, in Lambeck et al. (1996) this results in reduced estimates for the upper mantle viscosity. To avoid this, our strategy is not to impose *a-priori* values on any of the parameters and to search through as wide a range of earth-model parameters as is consistent with physical plausibility and computational feasibility.

A different approach developed for describing the rebound is by Påsse (2000) who uses mathematical functions to interpolate for sea levels between observed values. Such a procedure is adequate for describing observed behaviour provided that the functions chosen are sufficiently flexible. But they provide no basis for understanding the underlying physical processes or for making predictions since the functions are devoid of physical meaning and cannot be related to the physical properties of the earth and ice-sheet. Thus it is not possible to predict from the sea-level functions what the changes in gravity or stress field will be and we do not consider further this approach.

3 IMPROVEMENTS IN MODELLING METHODS AND IN EXTERNAL MODEL PARAMETERS

As noted above, the analysis of glacial rebound in Scandinavia cannot be treated in isolation of the other ice sheets in both hemispheres. Our approach has been an iterative one. In the first step we focus on one ice sheet, the Scandinavian ice sheet in this case. We make estimates of the other ice sheets (the far-field ice sheets) to predict their influences on the observations (sea level in this case) across the primary (Scandinavian) ice sheet region and invert the data within this region for ice- and earth-model parameters appropriate for the primary ice sheet. In the second step we turn to the far-field ice sheets whose influence on the primary ice sheet is important and analyse data from those regions to improve the rebound models for those regions. In the third step we iterate back to the primary ice sheet, using the improved results from the previous iteration. Thus since 1998 the emphasis of our research has been not so much on the Fennoscandian problem as on the other ice sheets and on the global ice-mass distribution (c.f. Lambeck and Chappell 2001). But we are now in a position to start the second iteration with improvements over the 1998 solution occurring in the following areas.

Time scale

All data and ice models are referred to the calibrated calendar time scale, using the Bard. (1998) polynomial for the calibration. (The age-error estimates used for all data include the uncertainties in this calibration.) A consequence of the change in scale is that the viscosities also change: the calibrated viscosities being about 10-15% greater than the radiocarbon viscosities (Lambeck 1998).

Equivalent sea-level (esl) function

The new function describing the global changes in ice volume is that of Lambeck and Chappell (2001) and Lambeck et al. (2002a) for the period before 7000 BP. In this, all melting has ceased at 7000 BP. (This is denoted here by ESL-1.) This function differs from the earlier one in that it gives a much-improved agreement with observed Last Glacial Maximum (LGM) far-field sea-level data. For the past 7000 years the far-field correction term of Lambeck (2002) is used, tapered at the older dates to avoid the introduction of a discontinuity between this function and the far-field function ESL-1 for the pre-7000 year period. This function allows for a small amount of melting of Antarctic ice during the past 7000 years, consistent with new field data (Stone et al. 2003). (This is denoted by ESL-2). The use of this function means that the far-field correction term previously introduced as an unknown (see below) is not now included in the solutions for model parameters.

The equivalent sea level functions ESL-1and ESL-2 first reach maximum ice volumes at ~30 ka BP which is earlier than previously assumed and is based on the sea-level analyses for the LGM interval at sites far from the ice margins (Yokoyama et al. 2000). This means that more time is available for the ice-earth system to approach an

equilibrium state before the onset of deglaciation. Thus, all other parameters being the same, the maximum predicted depression under the ice load is increased.

North American ice sheet model

The influence of the North American deglaciation over Scandinavia is one of long-wavelength change and errors in the North American ice model can be expected to feed back into the estimates of mantle viscosity, particularly that for the lower mantle. The previous ice sheet model, based on ICE-1, has been replaced by the model of Licciardi et al. (1998) but scaled such that the total global esl function matches the observed one.

Scandinavian ice model

The ice retreat history is the same as before. The ice thickness after 19 ka BP is that determined in 1998 but the earlier ice thickness follows the thick, quasi-parabolic profiles from the Denton and Hughes ice model. Rapid ice decrease occurs at 19 ka. This change was introduced by Lambeck et al. (2000) to increase the ice volumes for the early period so as to yield better agreement with the far-field data for the LGM and immediate post-LGM interval. Physically this means that the ice sheets were initially frozen-based and that the ice-height profiles radiating out from the central ice dome followed quasi-parabolic functions. The rapid change at ~19 ka implies a rapid reduction in ice thickness at this time and a switch from cold- to warm-based conditions at the base of the ice sheet.

Improved rebound model

Since 1997 some minor modifications to the rebound theory have been applied. The solutions are iterative, with three iterations of the sea-level equation. Ice volumes include grounded ice on shelves and any floating ice when offshore ice thickness is less than the density-scaled water column. Details of this are given in Lambeck et al. (2003).

Earth rotation

The model now includes the effects of rebound on the planet's rotation and the modification of the centrifugal force and the total gravitational potential (attraction and rotation) (Milne and Mitrovica 1998). The effect of this is to modify the long-wavelength sea-level signal and its introduction may impact on solutions for lower mantle viscosity.

4 OBSERVATIONAL DATA

4.1 Geological data

The observational data set of the height-age relations of former shorelines has remained the same for the 1998 analyses so that the effect of model improvements on the parameters can be evaluated. The data-base includes ~800 observations from Scandinavia and the North Sea and ~400 observations from the British Isles covering the time interval from the present to 21.3 ka BP (Figure 1). New information has recently been published, including data from Karelia, on both sides of the Finland-Russia border. This will be included in later comparisons of the new model results with field data.

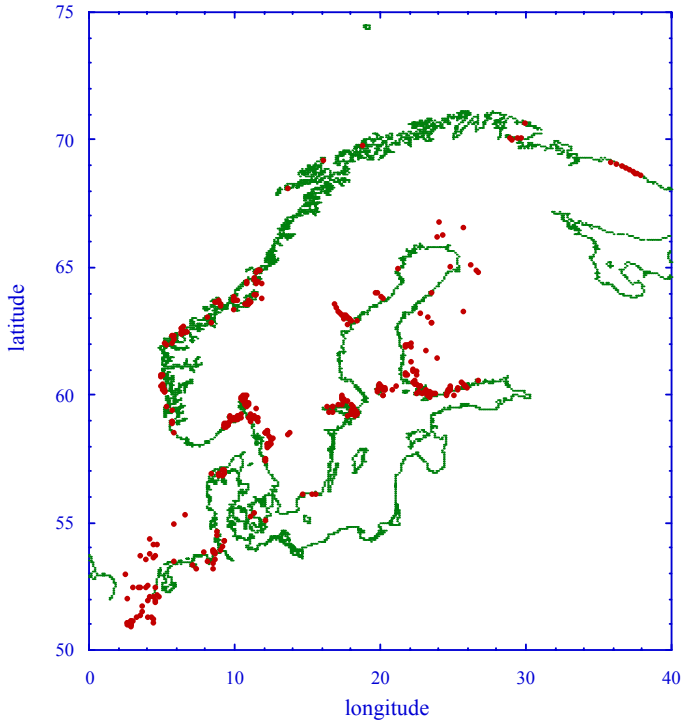

Figure 1. *Spatial distribution of geological sea-level indicators since the Last Glacial Maximum for Fenno-Scandinavia and the North Sea region. The data is based on the author's own compilation of data for the region, including the compilation of data for Finland by Eronen et al. (1995).*

Water level observations during periods when the Baltic was isolated from the sea, as during the Baltic Ice Lake or Ancylus phases, cannot be used directly as constraints in the rebound modelling because the elevation of the lake level with respect to coeval sea level will generally be unknown. But the spatial gradients of the shorelines can be used

if they formed at the same time. Of the two principal shorelines the Baltic Ice Lake that formed at ~12,000 years ago is best defined and we will use this information here. Its importance is that information is well distributed across the region, including the southern margin where there is otherwise little precise data, and because it extends the information back to the time soon after deglaciation.

4.2 Geodetic data

The geodetic observations of glacial rebound include tide gauge information on present-day relative sea-level change from the Baltic and North Sea coasts, estimates of crustal uplift and horizontal displacements measured using GPS, evidence for the tilting of lakes in Sweden and Finland, and geodetic levelling data. The most comprehensive analysis of the tide gauge data remains that of Ekman (1996) with the record extending back 100 years. When using this information to test rebound models or to estimate parameters, the challenge is to separate the rebound signal from a modern sea-level change signal caused by non-rebound processes. Earlier work (Lambeck et al., 1998b) has shown that the 1998 rebound model is consistent with this data and in the revised model a similar test will be conducted.

The GPS data for vertical crustal deformation also is consistent with the rebound model parameters of Lambeck et al. as demonstrated by Milne et al. (2001). The observational record remains short, less than 10 years for many sites, and does not yet provide strong constraints on the modelling. Recently it has become recognised that the horizontal displacements induced by the glacial rebound may be significant (James & Morgan, 1990) and this is important because of the ability to make such measurements now with, for example, GPS.

The vertical deformation of the Earth in response to surface loading has only limited resolution for the radial viscosity of the upper mantle. If there is a narrow low viscosity channel in the upper mantle, for example, then the rebound is almost insensitive to its presence. Thus three-layer mantle models, in which the upper mantle is of uniform viscosity, give essentially the same rebound results as models with a low-viscosity channel below the lithosphere and discrimination between the two models becomes possible only if there are high precision observations of sea level change of early Lateglacial age and from sites near the ice margins (Lambeck et al. 1996). But predictions for such sites are also strongly dependent on the details of the ice sheet at its margins just where the ice sheet is often least well known.

Horizontal displacements of the earth's surface due to the glacial rebound phenomenon may have a greater dependence on this upper mantle structure. Horizontal displacements do not leave a measurable geological record, with the possible exception of the displacements on faults that are believed to have been triggered by the last glacial unloading. Horizontal crustal displacements can now be measured with precisions of 1 mm/year or better and GPS results have provided a relatively dense spatial distribution of positioning results across and beyond the Fennoscandian region of former glaciation. The characteristic of these horizontal displacements is that they are small near the centre of the former load area and reach their maximum values near and beyond the former margins of the ice load (Figure 2). This is the reverse of the spatial variation of the radial displacements of the Earth's surface. Thus what the two types of measurements provide is a different dependence of the observed signals on the earth-response parameters and they may, therefore, contribute to an improved separation of model parameters in the analysis of the rebound phenomenon.

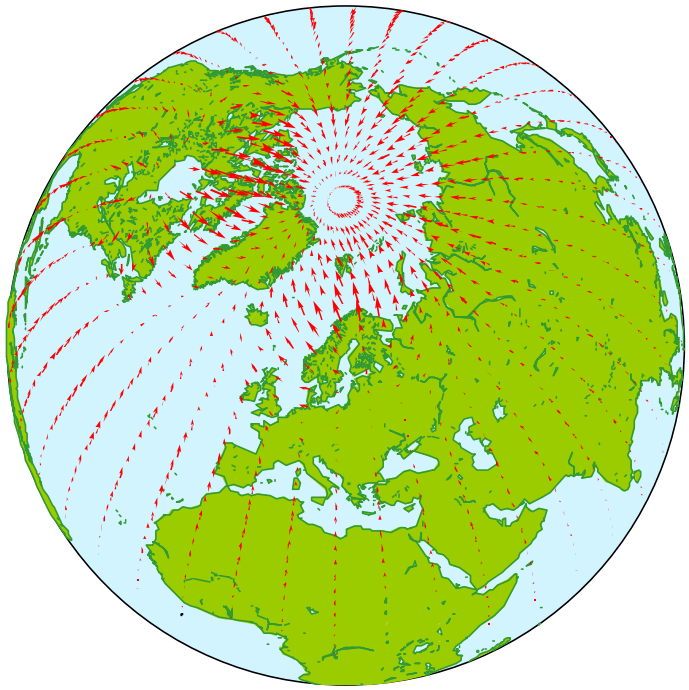

Figure 2. *Present-day directions and relative magnitudes of horizontal velocities of the crust predicted as the rebound response to the last deglaciation of the world's ice sheets, including North America and Antarctica.*

A dense network of GPS receivers has been set up around the globe in recent years and the data has been analysed for rates of displacements of the sites within a global reference frame. Such velocities are the results of (i) plate motions, (ii) the glacial rebound signal, (iii) local crustal deformation, (iv) geodetic reference frame instabilities, and (v) local GPS problems. The spatial variation of the velocities due to the Eurasian plate motion can be predicted from either geological models or from the GPS analyses themselves. GPS data from a global network of sites has been used in a preliminary

analysis. Daily solutions for the GPS orbit, site locations and ancillary parameters have been made for more than 1300 days, distributed over the 5 years, using the GAMIT/GLOBK software in a multi-step procedure (Feigl et al., 1993; Herring, 1997; King and Bock, 1999) from 32 European sites. The total number of baselines between these sites is 527. From daily solutions for site coordinates the site velocities are estimated using a Kalman filter technique, taking into consideration the red noise characteristics of GPS time series along with their full covariance matrix.

Height estimates from GPS analyses are less accurate than the horizontal positions and a number of the sites show irregular temporal variations of up to 15 mm for periods of days or longer. Some of these fluctuations may have a geophysical origin such as changes in surface loading by ground and surface water or by the atmosphere. We focus on the horizontal displacements and in the analysis we allow the daily height solutions to fluctuate with time without imposing requirements for linear or other functional motion. The rate of change of baseline length that is computed is therefore effectively the component along the great circle passing through the ends of the baseline.

Figure 3 gives the histograms for (a) the observed rates and (b) for the rates normalised by their standard deviations. For many of the baselines this latter quantity is near unity, indicating that the precisions are near the limit of being useful and that longer and more accurate time series need to be used in future analyses. Nevertheless for a substantial number of the baselines this ratio is significantly greater than unity and we have pursued the analysis as a prelude to a more extended GPS analysis in the future. (For GPS analyses at the level of precision sought one cannot accept pre-computed orbital results and it is necessary to go back to the original data and recompute the orbits and related orbital parameters. Because the definition of the geodetic reference frame is an integral part of the coordinate determinations the data set includes a global network of GPS sites. The analysis is therefore both computer intensive and time consuming.)

Figure 4 compares the predicted and observed rates of change of baseline length where the latter is based on the reference glacial rebound model (data from Spanish sites have been excluded because of problems identified with some of the data sets). Agreement between observations and predictions is broadly satisfactory. But discrepancies appear to be significant. Possibly they are indicative of a data problem, of a rebound-model problem in which the model is failing to predict properly the long wavelength features of the rebound, or local tectonic problems. We conclude that more extended analyses of the GPS data are required before this information type provides better constraints on the rebound model then do other available data types. However, we believe that the analysis conducted so far does point to the potential importance of this type of information in future analyses of glacial rebound.

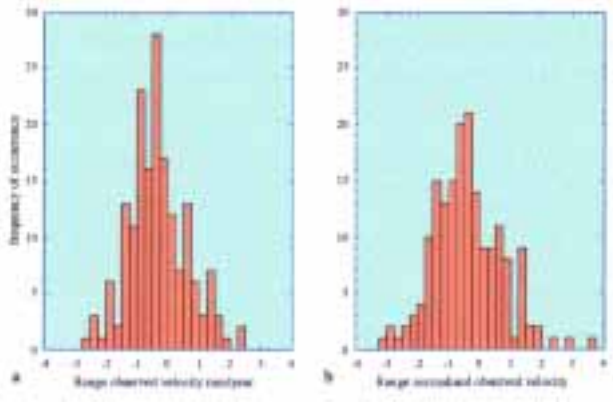

Figure 3. *Histogram of (a) the observed velocities of GPS sites in Europe with respect to a rigid-plate motion of the European Plate, and (b) the velocities normalized by the precision estimates of the rates of motion. The results are from a preliminary analysis of GPS data (by P. Tregoning at RSES-ANU) from a large number of sites in Europe both within and outside off the areas of former glaciation.*

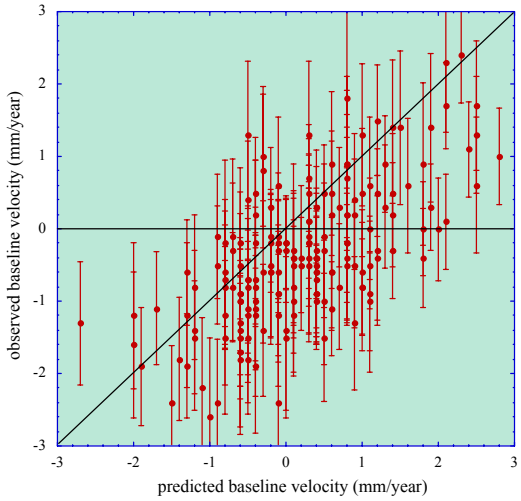

Figure 4. *The observed versus the predicted horizontal velocities at the GPS sites with the latter based on the preliminary glacial rebound model discussed in Lambeck et al. (1998a).*

The lake-tilting information from locations in Finland and Sweden has been previously analysed by M. Ekman and used in rebound modelling by Lambeck et al. (1998b). The importance of this data is that it provides information from inland sites. We do not believe that the full data set has been exploited and that a useful study would be to

examine in more detail the historic information compiled by Sirén (1951) and to complement it with post-1950 instrumental data.

The geodetic data type that has not yet been exploited is the levelling data. We have discussed this possibility with representatives of both the Finnish and Swedish geodetic surveys but cannot proceed until the most recent levelling adjustments of the two countries are completed.

5 AN IMPROVED REBOUND MODEL FOR FENNO-SCANDINAVIA

5.1 Earth rheology

Only three-layered models are considered, the limitation being imposed by computational time constraints. Three-layer mantle models have been found to be sufficient for most analyses (Lambeck et al. 1996, 1998a. More detailed resolution has been proposed by Kaufmann and Lambeck (2002) but these do not appear to offer significant improvements. The unknowns are H_l, η_{um}, η_{lm}; effective lithospheric thickness and effective average upper and lower mantle viscosity. The previous (1998) values for these parameters were:

$$H_l \sim 75 \text{ km}$$
$$\eta_{um} = (3.6 \pm 0.5)\text{x}10^{20} \text{ Pa s} \quad (1)$$
$$\eta_{lm} = 0.8\ (+0.5/-0.3)\text{x}10^{22} \text{ Pa s}$$

The boundary between the upper and lower mantle is placed at 670 km, consistent with seismological evidence for either a compositional or mineralogical boundary in the mantle.

5.2 Model-parameter estimation procedure

The observation equation for each observational data point (a sea-level age-height observation) i (i = 1...I) is (Lambeck 1993; Lambeck et al. 1998a)

$$\Delta\zeta_o(\varphi,\mathrm{t}) + \varepsilon_o(\varphi,\mathrm{t}) = \Delta\zeta^e(\mathrm{t}) + \delta\zeta^e(\mathrm{t}) + \beta^L\Delta\zeta^L + \Delta\zeta^{f-f}(\varphi,t) = \Delta\zeta_{predicted} \quad (2)$$

where:

$\Delta\zeta_o$ is the observed sea level, reduced to mean sea level at location φ and time t, with error term ε_o;

$\Delta\zeta^e$ is the nominal eustatic sea-level function for the combined ice sheets;

$\delta\zeta^e$ is the correction term to $\Delta\zeta^e$ if the ice volumes of the large and distant ice sheets are inadequately known. This is not included in these solutions because the ice volumes of these ice sheets have been scaled so that their esl function is consistent with isostatically corrected far-field sea-level data;

β^L is the scale parameter for the local ice sheet L (β^S in the study of the rebound of Scandinavia);

$\Delta\zeta^L$ is the predicted, earth-model dependent isostatic contribution to the sea-level change from the local ice sheet. It includes the glacial- and

hydro-isostatic parts and the effects of the changing gravitational field;

$\Delta\zeta^{\mathrm{f-f}}$ is the predicted isostatic crustal rebound and gravitational contribution from the ice sheets other than the local one (North America, Antarctica, British isles) and which generally lie at considerable distance from the ice sheet under investigation so as to have either negligible effect or only a spatially slowly varying effect on the local sea level.

Earth-model parameters $E(k)$ are estimated that yield the minimum variance Ψ^2_{k}

$$\Psi_k^2 = \frac{1}{M}\sum_{m=1}^{M}\left[\frac{\Delta\zeta_o^m - \Delta\zeta_{k,predicted}^m}{\sigma^m}\right]^2 \qquad (3)$$

where σ^{m} is the standard deviation of the m^{th} observation ($m = 1\ldots M$) and $\Delta\zeta^m_{k,prediced}$ is the predicted sea level for observation m and model parameters k. In practice the solution is obtained by carrying out forward modelling through the E(earth) and I(ice) model space ($k = 1....K$) and to search for parameters that minimize Ψ^2_{k}. If the model provides a comprehensive description of the sea-level change and the assessment of the σ^{m} is realistic then the expected value of Ψ^2_{k} is unity. The Earth's mantle is represented by three layers: an effective elastic lithosphere of thickness H_{l}, an upper mantle from the base of the lithosphere to the 670 km deep seismic discontinuity with an effective viscosity of η_{um} and a lower mantle from 670 km depth down to the base of the mantle with an effective viscosity of η_{lm}. The range of parameters within which the search is conducted is

$$\begin{aligned} &30 <_{\sim} H_{\mathrm{l}} <_{\sim} 150 \text{ km} \\ &5\times10^{19} <_{\sim} \eta_{\mathrm{um}} <_{\sim} 10^{21} \text{ Pa s} \\ &10^{21} <_{\sim} \eta_{\mathrm{lm}} <_{\sim} 10^{23} \text{ Pa s} \end{aligned} \qquad (4)$$

a range that is likely to encompass any plausible estimates. Within each layer the density and elastic moduli follow the depth dependence estimated from seismic data, (the Preliminary Earth Reference Model of Dziewonski and Anderson, 1981).

5.3 Results: variants of the reference model

The following results serve as tests for the various changes made in the rebound model and in the parameter estimation process.

Case 1. ESL-1 only, $\beta^S = 1$

The initial solutions were carried out with the eustatic sea level function ESL-1 defined by the ice models developed in Lambeck et al. (2000) and in which ocean volumes reached their present value at 7000 years ago and remained

constant thereafter. In these solutions the observation equations are solved for the three earth-model parameters, $E = E(H_l, \eta_{um}, \eta_{lm})$, with $\beta^S = 1$. Figure 5 illustrates a subset of the results and most of the results for the subsequent tests will be presented in this form. In this case, the minimum variance function Ψ^2_k is illustrated in two different two-dimensional sub-spaces; η_{um}-- η_{lm} for H_l=65 km and H_l -- η_{um} for $\eta_{lm} = 10^{22}$ Pa s. Within these subspaces Ψ^2_k is represented by the contours and its local minimum defines the solution within this range of parameters. The overall least variance within the three-dimensional model space (4) occurs at $H_l \sim$ 65-80 km, $\eta_{um} \sim$2-3 x10^{20} Pa s, $\eta_{lm} \sim$ 3-10x10^{21} Pa s, with $\Psi^2_k \sim$ 7.6. The solution is very comparable to that previously obtained (c.f. 1) indicating that the improvements made do not invalidate the earlier solution. However, this minimum variance is significantly greater than the expected value of unity and there is, therefore, scope for further model improvement.

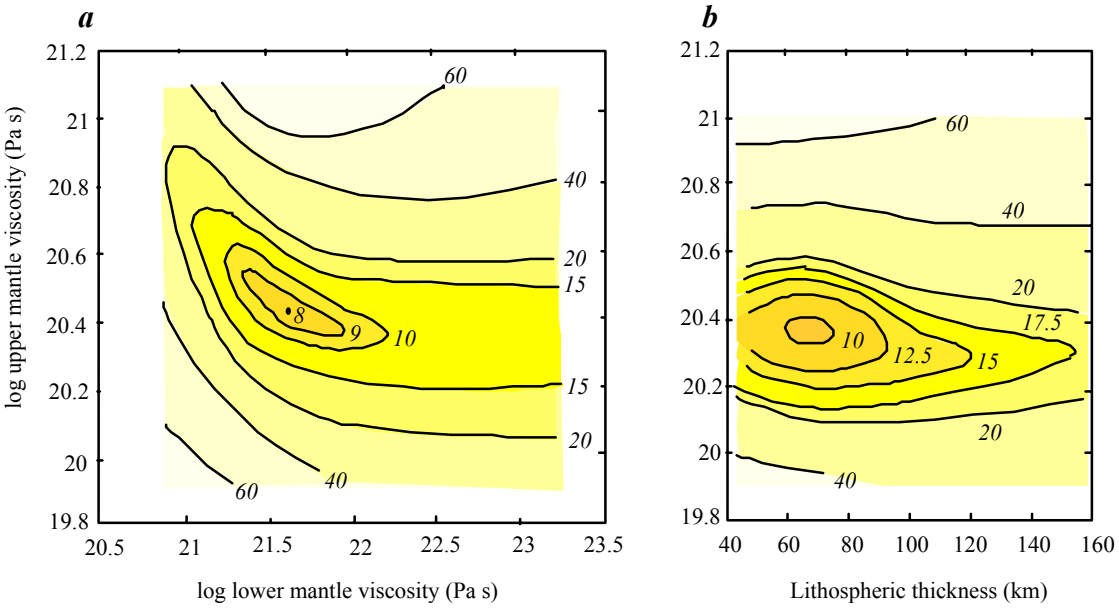

Figure 5. *Minimum variance function Ψ^2_k, defined by equation 3, in (a) the two-dimensional sub-spaces η_{um}-- η_{lm} for H_l= 65 km, and (b) for the subspace H_l -- η_{um} for $\eta_{lm} = 10^{22}$ Pa s. The model predictions are based on the Case 1 parameters. The overall least variance of Ψ^2_k=7.6 occurs at $H_l \sim$ 80 km, $\eta_{um} \sim 2.5x10^{20}$ Pa s, $\eta_{lm} \sim 5x10^{21}$ Pa s.*

Figure 6a illustrates the differences, observed - predicted sea levels, for all data points with the predicted values based on a nominal reference earth-model

$$H_{\mathrm{l}} = 80 \text{ km},$$
$$\eta_{\mathrm{um}} = 3\text{x}10^{20} \text{ Pa s}, \qquad (5)$$
$$\eta_{\mathrm{lm}} = 10^{22} \text{ Pa s}.$$

that lies close to both the solution (1) and the above-determined solution and for which $\Psi_{\mathrm{k}}^2 \sim 14.7$. Major discrepancies occur, particularly in the interval 10-13 ka, and point to either (a) an observational data problem, or (b) an ice model problem. The data for which this difference is strongly positive (the predicted values are significantly less than the observed values) correspond largely to the Oslo Graben region and this is indicative of the ice being too thin in this locality. Thin ice was introduced into the original ice model because of the possibility that the Oslofjord and Skagerak was an active ice stream and that the surface elevation of the ice was lower than for adjacent areas. These discrepancies occur for all plausible earth models and indicate that this hypothesis is improbable: it therefore seems more likely that during the LGM and immediate post-LGM interval thick ice extended over this region.

Another group of observations gives persistently negative discrepancies, where the predictions systematically over-predict the rebound. These correspond to some of the older observations from Ångerman River, northern Finland and some from Trondheimfjorden. The older Ångerman data are based on a varve chronology (Liden 1938) that remains poorly linked to the ^{14}C time scale for the older period and recent results by M. Berglund point to a possible discrepancy of about 800 years. The northern Finland data has been problematical, as already noted by M. Eronen. About half of the data points agree with the model predictions, the other half indicate predicted values that are too high: but which are the correct ones? Of these negative discrepancies, those for two Finnish sites at Lupojarvi and Kivilompolon, persist for the entire range of the earth-model space.

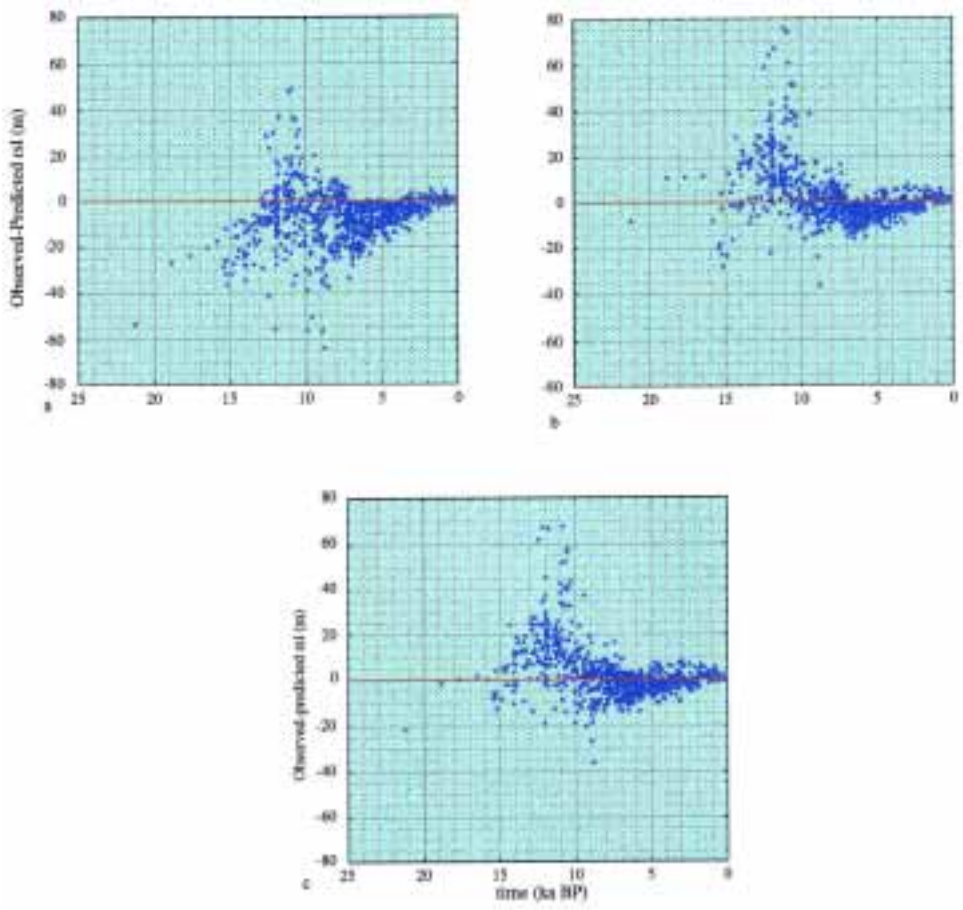

Figure 6. *Time series of the differences between observed and predicted sea levels ($\Delta\zeta_{observed}$-$\Delta\zeta_{predicted}$) for all Scandinavian data points with the predicted values based on an earth-model defined by the parameters (5). (a) Case 1 ice-model parameters. (b) Case 2 ice-model parameters with the single β^S scaling parameter. (c) Case 3 ice-model parameters which includes the change in ocean volume over the past 7000 years.*

Case 2. ESL-1 only, β^S = variable.

In the Case 2 solutions a single scaling parameter is introduced as unknown for the Scandinavian ice sheet and the solution is repeated (see Figure 7). In this case the Ψ^2_k and β^S results are shown separately in the η_{um}-- η_{lm} subspace for H_l=65 km. The least variance occurs at $H_l \sim$ 70 km, η_{um} =2.8x10^{20} Pa s, η_{lm} = 8x10^{21} Pa s with $\Psi^2_k \sim$ 5.3, and β^S = 0.86. Thus the earth-model parameters are not significantly modified through the introduction of the β^S parameter.

The least variance is substantially reduced and the discrepancies between observed and predicted sea levels for earth-model (5) show considerably closer clustering than in case 1 (c.f Figures 6a and 6b). However, the large positive anomalies previously noted are enhanced, indicating that a uniform scaling of the ice model is unsatisfactory. In contrast, a number of the large negative anomalies are reduced but those for the two Finnish locations noted before persist. The pattern of the residuals remains similar to those for the model with β^S=1.

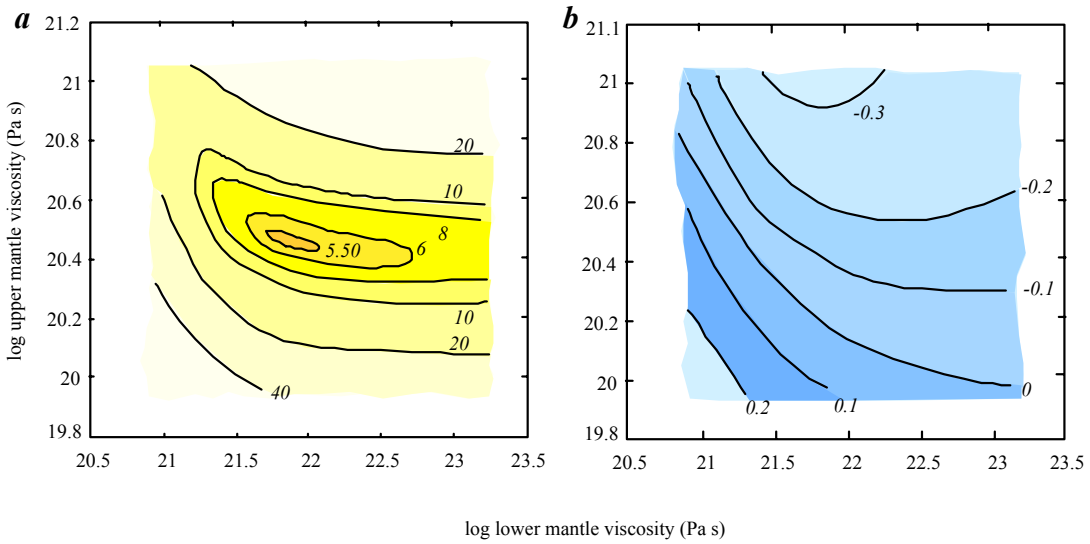

Figure 7. *Same as Figure 5a but for the model parameters of Case 2 which includes a single scaling parameter β^S. The overall least variance lies outside the illustrated sub space at H_l ~ 70 km, η_{um} =2.8x10^{20} Pa s, η_{lm} = 8x10^{21} Pa s with Ψ^2_k ~ 5.3 and β^S = 0.83. (b) The (1-β^S) estimates are shown for the same subspace as the variance estimates in (a).*

Case 3. ESL-1 and ESL-2.

In the above solutions the eustatic sea level for the past 7000 years has been held constant. Evidence indicates that this may not be a valid assumption and that ocean volumes increased after this time by perhaps enough to raise sea levels globally by 3-4m (Lambeck 2002). Estimates of this change have been made and the function describing this eustatic sea level for the past 7000 years is defined by ESL-2.

In Case 3 the model space has been explored for ESL-2 which includes this corrective term. Parameter searches were conducted and for both fixed (β^S=1) and varied values at β^S and the table below summarizes the corresponding results for the least-variance

solutions. The solutions yield the same earth-parameters for the two ESL models but the introduction of the new ESL function reduces the variances, although not by a significant amount. Figure 6c illustrates the residuals (observed-predicted) for the solution with ESL-2, variable β^S, and earth model (5).

Model	$\beta^S = 1$	β^S = variable
ESL-1	7.65	5.30 ($\beta^S = 0.86$)
ESL-2	7.31	4.94 ($\beta^S = 0.86$)

Discussion

The residuals for the minimum variance models in the above three cases show similar results. In all cases the residuals exhibit systematic variation with time in which the differences are predominantly negative in the time interval 0-8 ka, and positive in the interval 10-15 ka. This indicates an inadequacy of the single-parameter scaling model and that time variable β^S models may be more appropriate. Within any time interval there is also some scatter in these residuals and this is indicative of a spatial variability of the scaling parameter as well.

To further explore the variability of β^S a new strategy for parameter estimation is required in order to establish whether an effective separation of earth- and ice- model parameters is achieved. The above cases all lead to similar parameters for the earth-model but there is some trade-off between lower mantle viscosity and the β^S value: solutions with β^S=1 lead to lower values, ($\eta_{\rm lm}$ = (3-5)x10^{21} Pa s), than do solutions with variable β^S (for which $\eta_{\rm lm}$ = (5-10)x10^{21} Pa s). This is a consequence of the scaling being more effective for the longer wavelengths of the load that stress the intermediate and lower mantle. One possible strategy to deal with this problem is to set independent limits on the value of the lower-mantle viscosity. A suitable set of constraints may be derived from observations of the planet's global deformations recorded in the motions of artificial satellites (acceleration in the longitude of the node) and in the planetary rotation (changes in rate of rotation and in position of the rotation axis as the inertia tensor is modified through time.) These changes are particularly sensitive to the mantle viscosity and constrain the average value for this parameter to ~10^{22} Pa s (Johnston & Lambeck, 1999; Kaufmann & Lambeck, 2002). Another strategy is to use only the more recent part of the observed sea-level data on the basis that the earlier observations are more sensitive to the details of the ice sheet configuration than later observations. This approach requires that the terms 'more recent' and 'early' be more rigorously defined. To explore this methodology in more detail, several tests have been made in which time-subsets of the data sets are used. All of these proposed cases are based on the ESL-2 function only. In the two cases presented here (Cases 4 and 5) the parameter search is restricted to $\eta_{\rm lm} = 10^{22}$ Pa s, in accordance with the rotational results.

Case 4. T< 10 ka, ESL-2.

This case considers only observations between 0 and 10000 years BP. The variance function has been computed for the parameter range defined by (4.) The results are given in Figure 8 for β^S=1. The *E* solution is essentially the same as that for the previous solutions although the least variance is smaller than before (Ψ^2_k=4.3), reflecting the increasing uncertainties in the older, pre-10 ka observational data, and the inadequate modelling of the shorter wavelength signal contained in the early sea-level signal. The corresponding β^S value for solutions with the ice-scaling function is 0.8-0.9.

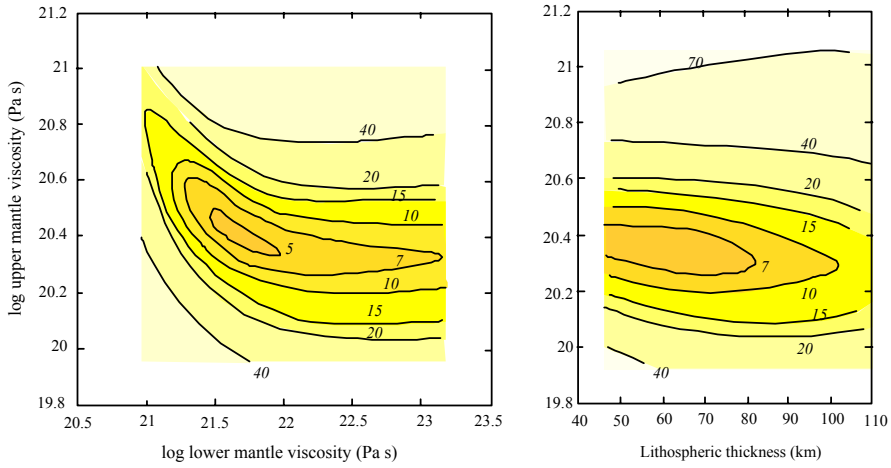

Figure 8. *The same as Figure 5 but for case 3 with the truncated T<10000 years data set. The solution for* $\eta_{lm}=10^{22}$ *Pa s is* H_l*~ 70 km,* η_{um} *~*$3x10^{20}$.

Case 5. T< 8 ka, ESL-2.

This case considers only observations after 8000 BP and the solution for the earth-model parameters is similar to that found previously and the corresponding β^S values are of the order 0.75-0.80. This reduction in the value of β^S (c.f. Case 3) could be suggestive of a time dependence of the scaling parameter

Discussion

Comparing the solutions for cases 3, 4, and 5, and containing β^S as unknown we have:

Case	H_l	η_{um}	η_{lm}	$\Psi^2_{k\,\|min}$	β^S
3 (all T)	75	$3x10^{20}$	$(5\text{-}10)x10^{21}$	5.0	0.84
4 (T<10 ka)	70	$3x10^{20}$	$(5\text{-}10)x10^{21}$	4.1	0.84
5 (T<8 ka)	80	$3.5x10^{20}$	$(5\text{-}10)x10^{21}$	2.8	0.78

The Earth-model parameters are effectively independent of the data set used and are comparable with the initial solution (5). Thus the earth-model parameters appear to be decoupled from the ice sheet parameters within this class of models. We can therefore define the earth model by these parameters and then use the comparison of predictions and observations to estimate an improved ice model using time and spatially variable scaling parameters. The change in ice-model parameter β^S is, however, significant, with the new solutions indicating that the original ice volumes of the Scandinavian ice sheet are over-estimated. This may be a consequence of the over-scaling of the early part of the 1998 ice-model, with the ice thickness before 19 ka BP scaled upwards by 50% in the current solution. This scaling was chosen to establish (i) by how much the ice volume could be modified without leading to unreasonable rebound results, and (ii) to arrive at a global ice budget that is in agreement with observations of sea-level change at sites far from the former ice margins. The scaling parameter in these new analyses, however, indicates that the scaling may have been excessive and we next explore the spatial variability of this parameter using earth-model (5) as reference.

5.4 Results: time-dependent scaling of the ice load

Case 6. Reduced ice thickness during the LGM

The relationship between the ice load and the rebound is not linear: the scaling of the LGM part of the ice model only, for example, impacts on the sea-level predictions throughout the post-LGM period. In Case 6 the LGM ice has been scaled downwards by 20% from that in the initial model but by 15.5 ka the ice volume is and remains the same as in the earlier Case 1 reference model. Solutions with and without a β^S factor yield essentially the same results which are also similar to the Case 2 solution. Figure 9a illustrates the outcome for earth-model (5) with β^S=1 and ESL-1. These residuals are very similar to those found for Case 2 (c.f. Figure 6b) indicating that the estimates of β^S are strongly influenced by the older part of the sea-level data-set. The solution including β^S as unknown yields β^S = 0.94 and suggests that a further reduction in LGM ice volume can be contemplated but this would not remove the oscillatory pattern remaining in the residuals seen in Figures 6b and 9a.

Case 7. Modification of the ice load at 15 ka BP.

The Case 6 modification of the ice model has the unintended consequence that the ice volumes after 16.5 ka briefly increase (see Figure 10). In Case 7 this artificial feature is removed by reducing the ice volumes in the interval 16.5 to 13 ka such that the ice volume decreases linearly over this interval. This results in a further reduction in the variance function but without impacting in any significant way on the distribution of the residuals (Figure 9b).

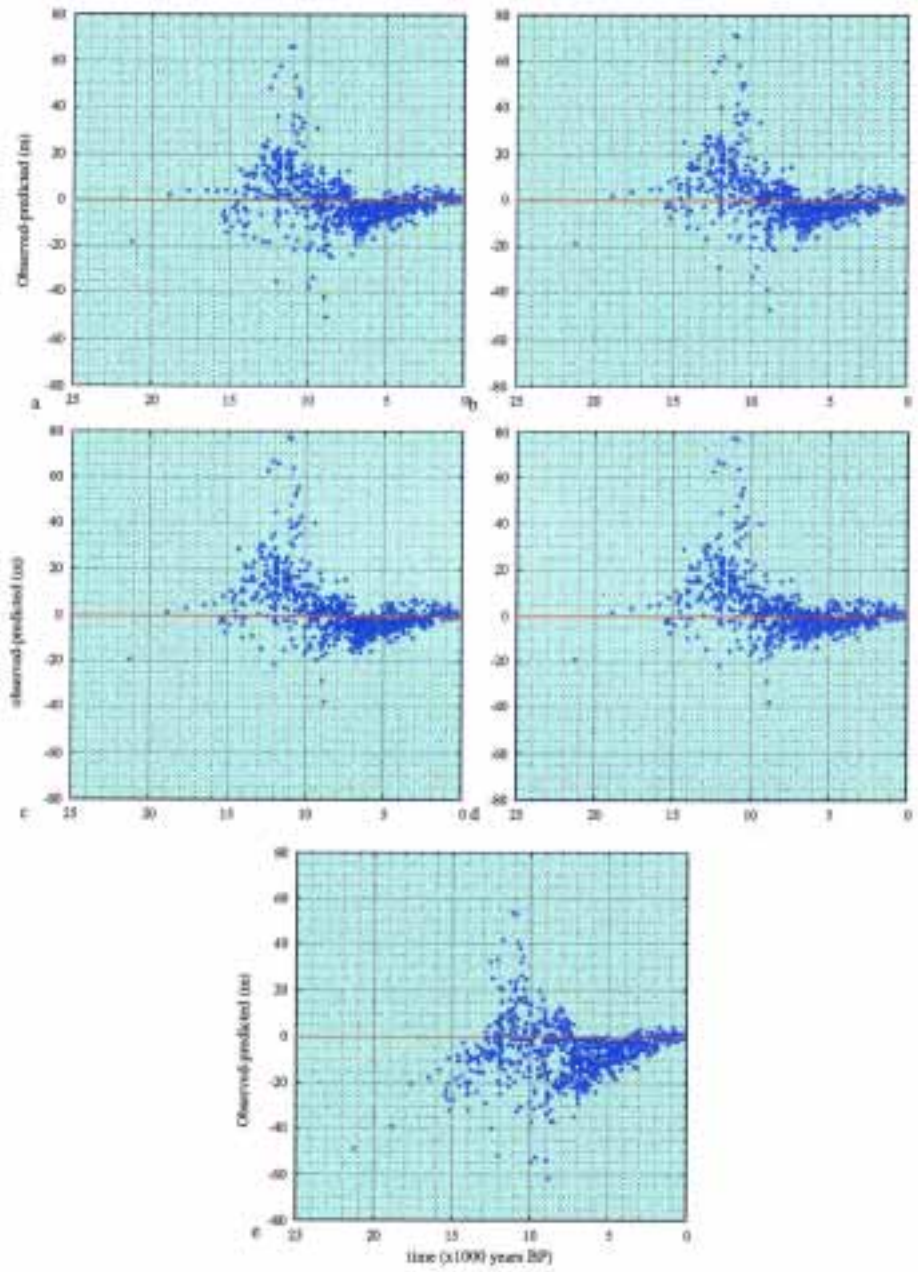

Figure 9. *Same as Figure 6 but but for (a) Case 6, (b) Case 7, and (c) Case 9. The corresponding equivalent sea-level functions are illustrated in Figure 10. All three cases assume* $\beta^S = 1$ *and ESL-1. (d) Same as (c) but with ESL-2. (e) Case 10, with the modified North American ice sheet.*

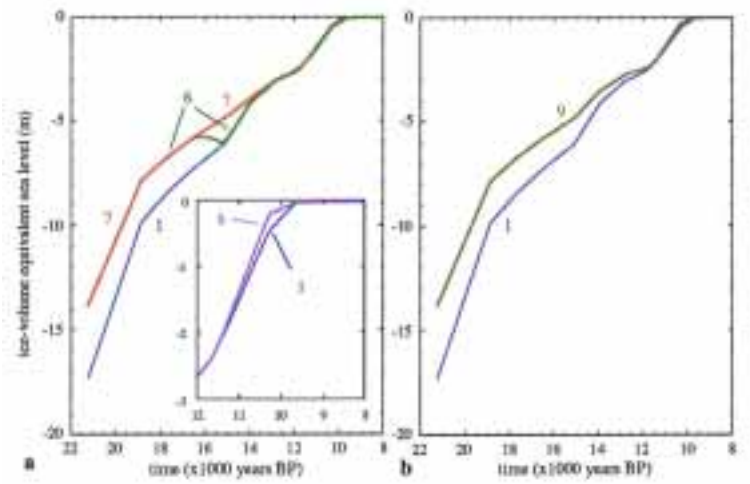

Figure 10. *The ice-volume equivalent sea-level function for the past 20000 years for (a) the ice models corresponding to Cases 1, 6, 7, 8 (inset) and (b) Cases 1 and 9.*

Case 8. Reduced ice thickness during the Holocene

In the next iteration we consider whether adjustment of the ice sheet during its later period has a significant impact on predicted sea levels for the post-glacial interval. We consider a case where the melting history is the same as in Case 6 up to 11.5 ka BP but melting then occurs more rapidly such that at about 10.5 to 10.3 the ice volumes are only half of that in the initial model. This change results in only marginal improvement in overall agreement between observations and predictions: For comparison with Case 6, the reduction in variance Ψ^2_k for model (5) with $\beta^S = 1$ and ESL-1 is from 6.59 to 6.51 and overall the rebound predictions are not strongly dependent on the Holocene part of the ice model. However, a closer examination of the spatial variation of the residuals does reveal some important differences for the two cases. In particular, for locations on the western and northern sides of the northern part of the Gulf of Bothnia predicted sea-levels show a greater sensitivity to this modification of the ice sheet than do the other localities. Here the reduced Holocene ice model in fact leads to improvement in residuals ($\Delta\zeta_{\text{observed}}$-$\Delta\zeta_{\text{predicted}}$) as is illustrated in Figure 11. This is consistent with recent evidence that the ice cover over northern Sweden during the early Holocene may have been significantly thinner than has been previously assumed (Kullman)

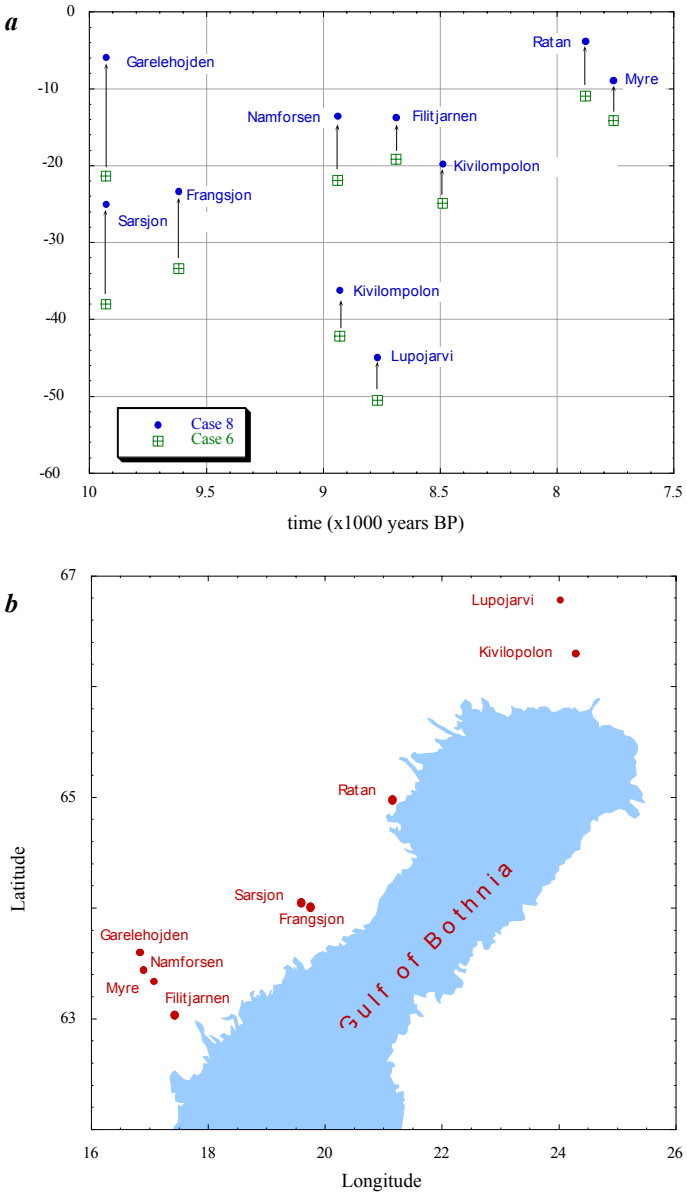

Figure 11. *(a) The residuals ($\Delta\zeta_{observed}$-$\Delta\zeta_{predicted}$) for sites in the northern Gulf of Bothnia region (see lower plot for locations) and for two ice-model configurations, Case 6 (green) and Case 8 (blue). In all instances the magnitudes of the residuals are reduced for the latter ice sheet configuration (shift indicated by the arrows). (b) site locations.*

Case 9. A combination of features of Cases 6-8

The last three tests indicate that a time dependent β^S function can result in some improvement in the predictive capability of the rebound model and that a modification of the starting model (Case 1) with:

(i) a reduction in ice volume during the LGM

(ii) reduction of ice volume during the Lateglacial period, and

(iii) reduction of ice volume during the Holocene period,

may lead to an improved solution. All three modifications point to a need to reduce the ice volumes but the reduction factor is not constant through time. The Lambeck et al. (1998) ice model was based on the assumption that any ice profile retained its shape throughout the glaciation and deglaciation stages whereas this was later modified to be the case only after 19 ka BP, with a change in profile occurring at this time to simulate a rapid collapse of the ice sheet (Lambeck et al. 2000). The assumption of constancy of the ice profile for the Lateglacial stage would not be valid if there has been substantial downwasting of the ice without necessarily a major retreat of the ice margins and this is what in fact the above results suggest, with major thinning of ice occurring in Holocene time.

This leads to the next modification of the ice sheet in which the above features (i) to (iii) are combined. In it, the LGM model corresponds to Case 6 for the interval before 19 ka BP and the Holocene model corresponds to the modification introduced in Case 8. For the intervening interval the ice thickness has been reduced consistent with the reduction in Case 7, but introducing a delay in melting during the Younger Dryas interval (Figure 10). Figure 9c illustrates the residuals ($\Delta\zeta_{\text{observed}}$-$\Delta\zeta_{\text{predicted}}$) for the reference Earth model with β^S=1 and ESL-1 and Figure 9d illustrates the case with β^S as unknown and ESL-2. Solutions (using the same ESL) with and without β^S lead to the same outcome: a reduced variance estimate, a marginally improved pattern of residuals in that the scatter within any time interval is reduced, the pronounced grouping of positive residuals within the interval 10-13 ka BP persists.

Case 10. A modified North American ice sheet.

Before introducing the spatial variability of the scaling parameter, two further tests have been carried out. First, the pattern of residuals for the Late Holocene tend to be negative, and while there is some spatial dependence of the residuals this may also be a consequence of the choice of North American ice sheet. Thus the tests have been repeated with different models for the North American ice sheet in which the contributions to global sea level are held constant so as to satisfy the global ESL function, but in which the distribution of the ice within the ice sheet is changed. The two classes of models used are based on (i) the multi-domed Laurentian ice model of Licciardi et al. (1998) (Case 1, above) and (ii) a single-domed ice model centred on the Hudson Bay and based on the model by Peltier and Andrews (1976) (this defines the Case 10 model). (The other parameters are the same as for Case 1.) The two lead to similar results (c.f. Figures 6a and 9e), with similar variance factor and a similar distribution of residuals, so that the results for the Scandinavian ice sheet are not strongly dependent on the details of the selected North American ice sheet.

Discussion

The above tests have all been conducted for the same earth model parameters (5) and it needs to be established whether the changes in the Scandinavian ice model introduced result in any modification of the earth model parameters. Thus a new search has been conducted through the earth-model space (4), using the Case 9 ice model as input. The results are illustrated in Figure 12 in an analogous manner to Figure 5. The least variance of Ψ^2_k=4.90 occurs at H_l~ 70 km, η_{um} ~3x10^{20} and η_{lm}=10^{22} Pa s. Solutions that include β^S yield essentially the same results, with H_l~75 km, η_{um}~3x10^{20} and η_{lm}=7~10^{21} Pa s, β^S=1.03, and Ψ^2_k=4.80, the small difference from the β^S=1 solution reflecting some residual trade-off between this scaling parameter and the lower mantle viscosity. These solutions are essentially the same as the Case 1-Case 2 solutions, and the ice sheet modifications have not resulted in a change in the earth-model solution. The least variance, however, remains large and is not significantly decreased with further modifications of the time dependence of β^S. Thus we next explore the spatial variability of using again the earth-model (5) and the Case-9 ice model as starting points.

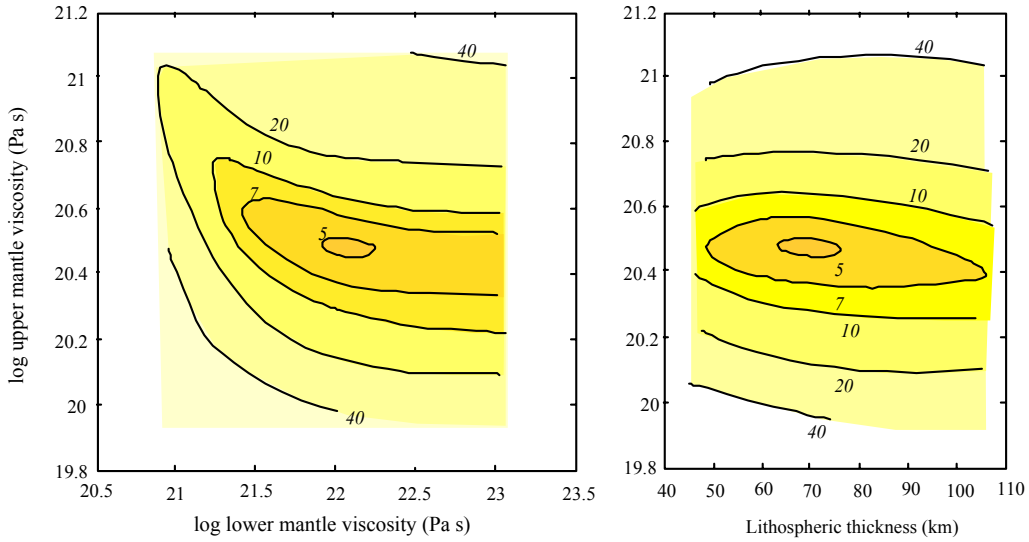

Figure 12. *Same as Figure 5 with the ice-model parameters corresponding to case 9, with β^S=1 and ESL-2. The overall least variance of occurs at H_l~ 70 km, η_{um} ~3x10^{20} and η_{lm}=10^{22} Pa s.*

5.5 Results: spatially variable scaling of the ice load

The above results have established that an effective separation of parameters has been achieved between the earth- and ice-model parameters and that further modifications of the ice sheet, consistent with the sea-level response, are unlikely to lead to major revision of the earth model. The time dependence of the global scaling parameter has led to some substantial modification of the ice load, particularly by reducing the ice load throughout the Lateglacial interval, or, equivalently, by bringing the melting history forward before about 12000 years BP (c.f. Figure 10). However, the residuals remain substantial for some localities and these cannot be reduced unless spatial variation in the scaling parameter is also introduced. The local scale parameter for any locality β_{loc}within the former ice margins can be estimated approximately from equation 2 as

$$\beta_{loc} = 1 + \{\Delta\zeta^{obs} - \Delta\zeta^{pred}\}/\delta\zeta_{iso}^{scan} \qquad (6)$$

where $\delta\zeta_{iso}^{scan}$ is the isostatic part of the sea-level response to the Scandinavian glacial loading only. The corresponding precision estimate of β_{loc} is approximately $\sigma_\beta=\sigma_{obs}/\delta\zeta_{iso}^{scan}$. Equation 6 implies that the dominant contribution to the sea-level change is from crustal rebound. Also, (6) assumes that the response is effectively local, that the contributions from adjacent ice areas are small compared with that from the local ice load. Neither assumption is strictly valid and therefore in the following calculation (i) only data with T>6000 years are used since these correspond approximately to data points for which the major contribution to the sea-level change is from the local rebound, and (ii) an iterative procedure will be used for estimating the β_{loc}. The ice model corresponding to Case 9 is used as the starting point.

If we consider only observations for which $|(1-\beta_{loc})/\sigma_\beta| > 2$ as being indicative of significant departure from the assumption $\beta_{loc}=1$, then we note immediately that the majority of sites for which the ice thickness in the Case 9 ice model is underestimated (i.e. $\beta_{loc} > 1$) correspond to coastal Norway, south of about Nord Trondelag, to Oslofjorden and to southwest Sweden (See Figure 13a). Other sites with $\beta_{loc}> 1$ occur within Varangerfjorden and the Kola Peninsula as well as four isolated data points in Finland. In contrast, sites with $\beta_{loc}< 1$ cluster in southern and western Finland (Figure 13b) indicating that ice thickness over southern Finland and, by extension, over the south eastern sector of the ice sheet, is overestimated in the ice-sheet model represented by Case 9. (The contradictory information from some of the Finnish data has already been alluded to and points to a need to reinterpret some of the field data. Most of the Finnish data for which $|(1-\beta_{loc})/\sigma_\beta| < 2$ point to $\beta_{loc} < 1$ and support the evidence that the ice thickness here is overestimated. Thus the four anomalous points identified in Figure 13a are rejected.) The other locality where the ice thickness appears to be overestimated is over the Troms and northern Nordland region of Norway.

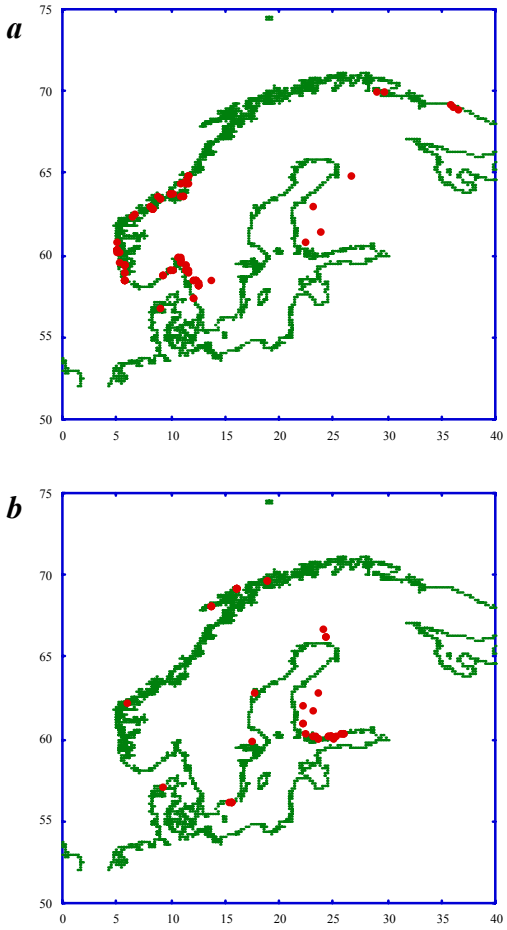

Figure 13. *Spatial variability of the β_{loc} function for observation points for which (a) $\beta_{loc} > 1$, subject to $|(1-\beta)/\sigma_\beta| > 2$: (b) $\beta_{loc} < 1$, subject to $|(1-\beta)/\sigma_\beta| > 2$.*

Summary of β_{loc} values by region and time interval

Region	**15>T>13**	**13>T>12**	**12>T>11**	**11>T>9**
N.W. Norway	0.94	0.82	0.79	0.75
Central Norway	1.10	1.17	1.14	1.27
S.W. Norway	1.11	1.24	1.28	1.28
Oslofjorden		1.32	1.36	1.30
S.W. Sweden	1.14	1.18	1.17	1.08

The distribution of the β_{loc} estimates from (6) for localities with a good distribution of data in time, indicates that, within uncertainties of the estimates (~10% of the β_{loc} values themselves), the scaling factor remains approximately constant with time (see above table). Thus in the next iteration of the ice-sheet modelling a time-averaged β_{loc}

parameter is calculated for each locality and these values are extrapolated and contoured across the entire region. The resulting spatially variable β_{loc} function is then convolved with the starting ice sheet to obtain the next iteration ice model. Increasing the ice thickness at any one locality increases the crustal rebound at that locality but for points beyond the region of increased ice the rebound is reduced. This non-linearity is resolved by iterating the solution several times until the variance of the overall fit of the model predictions to observations reaches a point beyond which further reduction is minimal. We have carried out 3 iterations based on earth-model (5). Figure 14 illustrates the resulting spatial variability of the scaling to be applied to the Case 9 ice sheet and the so-scaled ice model defines the Case 11 ice model. The net effect has been to (i) increase the ice thickness over the southwestern region of Norway, including the Oslofjorden by up to 40% and a smaller increase over Finnmark and (ii) decrease the ice thickness over southeastern Finland by up to 30% and by about 20% over Vesterålen and Lofoten. The modifications over the Gulf of Bothnia and western Finland are generally less than 10%.

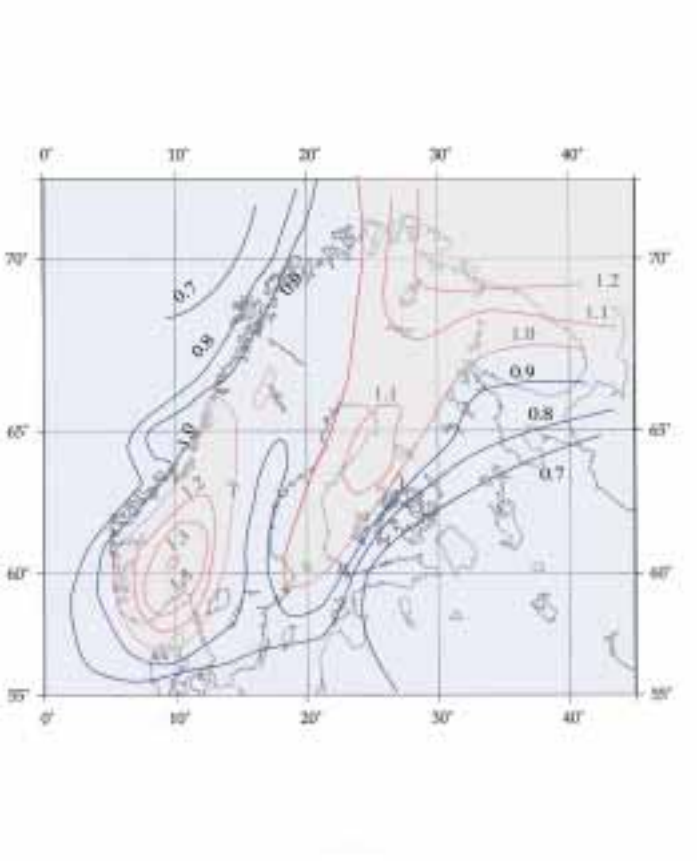

Figure 14. *Spatial variability of the β_{loc} function estimated from the inversion of the sea level data and to be applied to the Case 9 ice model to yield the Case 11 ice sheet. The solution is based on the earth-model parameters (5) and ESL-2.*

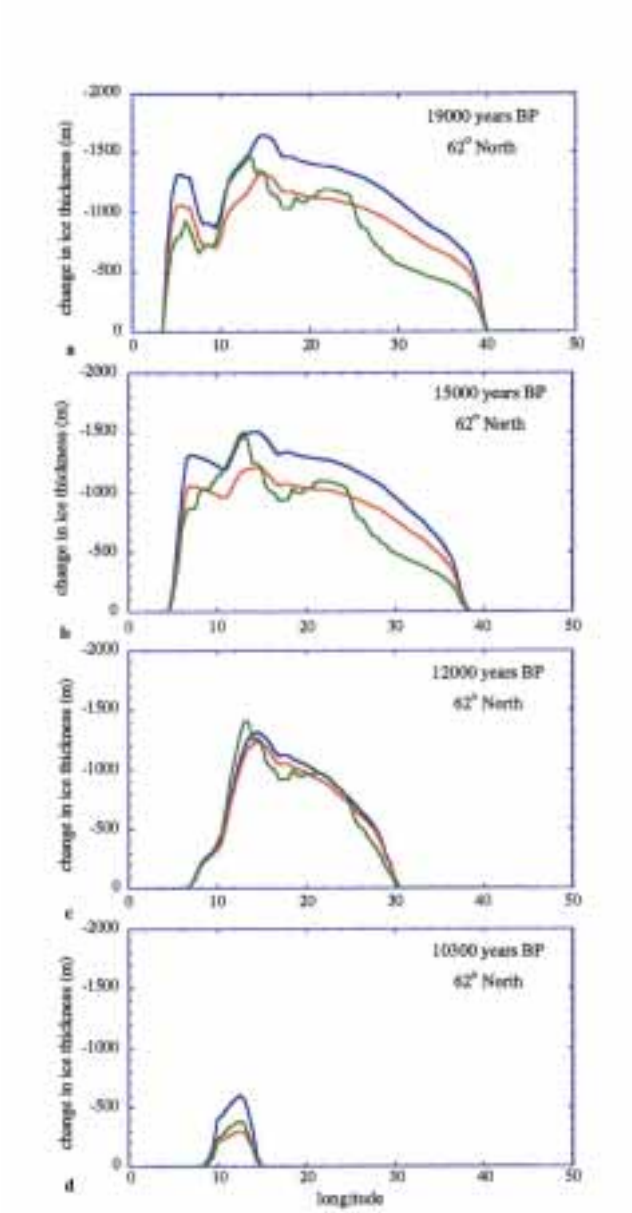

Figure 15. *Ice thickness profiles at 62^o N for three models: Case 1 (blue), Case-9 (red) and Case 11 (green) at four epochs.*

Figure 15 compares the ice-thickness profiles along the latitude circle 62^{o}N for three models: the starting ice model (Case 1, blue), the Case-9 ice (red) and the Case-11 ice model (green). Figure 16 illustrates the residuals for the complete data set and this can be compared with Figure 9d which corresponds to the Case 9 solution. The residuals are now much reduced although there remain a number of anomalous points. In northern Finland there are the previously identified anomalies where the observed

values lie well below the predicted values whereas for other sites in the same region the agreement is much better (Figure 17a).

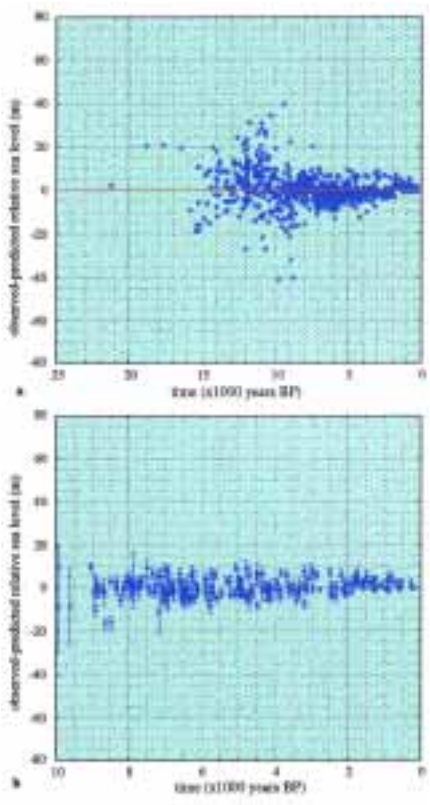

Figure 16. *Same as Figure 9 but for the case 11 ice model and earth-model (5). (a) all data from Fennoscandia: (b) data from Finland and the Bothnian coast of Sweden.*

In Oslofjorden, Ostfold, Vestfold, and Kragerø the agreement between observations and predictions is now generally satisfactory (Figures 17b,c) but there are also a few discrepancies. In particular, the model does not predict the very rapid fall in sea level noted in the Kragerø area between 11 and 9.5 ka BP. Similar misfits occur at some other locations, but not all, along the Norway coast at about the same time (Figures 17d,e). This may be a consequence of the radiocarbon dating of samples poor in carbon content at a time when the radiocarbon scale exhibited a plateau effect and needs to be further examined. Overall, the anomalous data points, defined here as $|(\Delta\zeta_{observed}-\Delta\zeta_{predicted})| > 20$ m, represent only 3% of the total data set. Rejection of these data points reduces the least variance for earth-model (5) to 2.73. For Finland and the Bothnia region, including the coastal zone of Sweden, the agreement between observations and predictions is mostly satisfactory when compared with observational accuracies (Figure 16b) although a few significant differences do occur. These can be mostly attributed to observational issues, with basin isolations, for example, having been identified as isolations from the Ancylus Lake but the age pointing to the isolation having occurred

within the Litorina interval (see, for example, the data set in Eronen et al., 1995). Again, the number of anomalous points is small and, whatever their cause, they do not affect any of the outcomes.

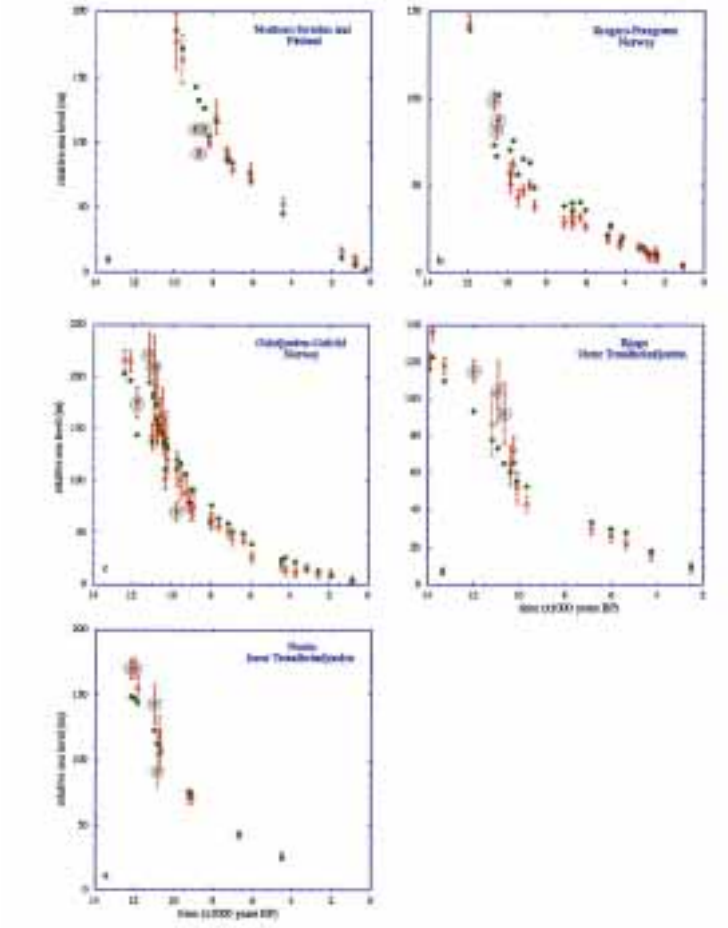

Figure 17. *Observed (open red circles with error bars) and predicted (filled green circles) of sea level in five different locations where the largest discrepancies seen in Figure 16a occur. Some of these anomalous points are highlighted by the blue circles.*

Before proceeding further with this solution we repeat the earlier search through the earth-model space for this revised ice sheet to establish whether the earth- and ice-model parameters remain effectively separated. The search is conducted through the same parameter space as before and the results for two selected parameter sub-spaces are shown in Figure 18: in this case the H_l -- η_{lm} space for two values of η_{um} since the strongest model dependence appears to be on lithospheric thickness and lower mantle viscosity, with some trade-off occurring between these two parameters (see the dashed line in Figure 18a). We adopt the following parameters to describe the observed shoreline elevation evidence:

H_l = 90 km,

η_{um} =3x10^{20} Pa s, (7)

η_{lm} = 7x10^{21} Pa s.

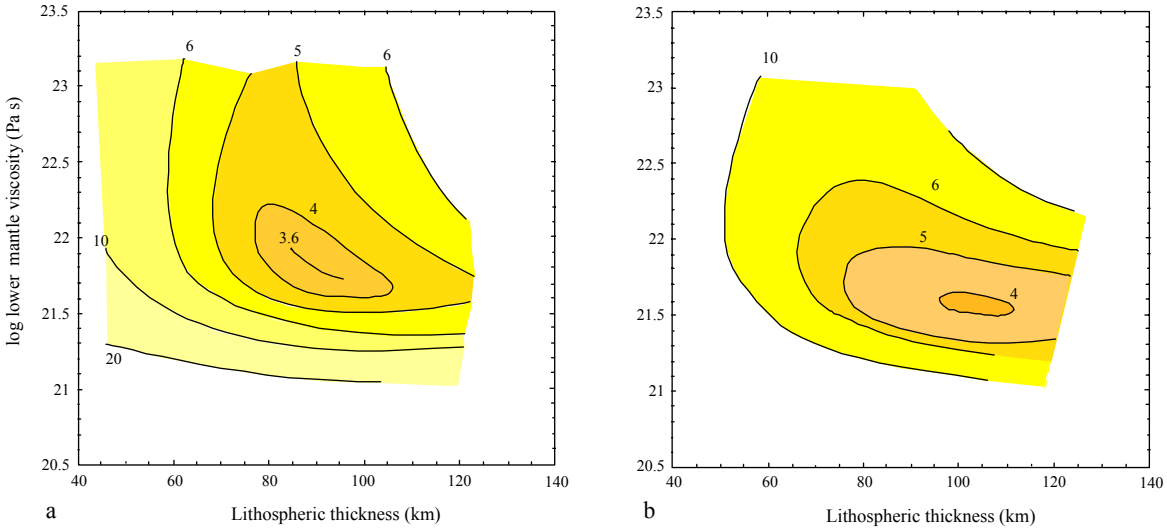

Figure 18. *The variance* Ψ^2_k *in* H_l *--* η_{lm} *space for two values of* η_{um}*. The ice-model parameters correspond to case 11, with* β^S *=1 and ESL-2. The overall least variance of occurs at* H_l*~ 90 km,* η_{um} *~3x10*^{20} *and* η_{lm}*=7x10*^{21} *Pa s.*

5.6 Results: the revised ice sheet

Figure 19 illustrates the ice thickness at selected epochs corresponding to the Case 11 ice model. The ice margins during the LGM and the subsequent retreat were fixed at the locations specified by Andersen (1981) and Pedersen (1995) although it has become clear that some modifications are required. In particular, the ice margin at the LGM did not everywhere reach its limits at the same time and in the northwest the ice may have been retreating at the same time that it was advancing in the south. Thus at the time of the nominal LGM, 20 ka BP, the ice margin in the southeast probably occurred within the margin shown in Figure 19a. Finland, however, lies well within the LGM ice margins and the rebound there is not strongly sensitive to the details of the ice movements at these margins. One feature of the inversion results is that the thickest LGM ice occurs over the northern part of the Gulf of Bothnia, ~ 2700 m, with a secondary maximum of ~2400 m over southern Sweden. This dual-domed character is more apparent when the ice elevation is mapped, as is illustrated in Figure 15 for the profile along the 62˚ North latitude circle and it appears to be feature required by the current data set. However, the secondary dome over northern Finland may be an artifact because (i) sea-level data from this region is limited, and (ii) there is inconsistency between some of the data points for this region as previously noted. The evidence from northern Finland clearly needs re-examination

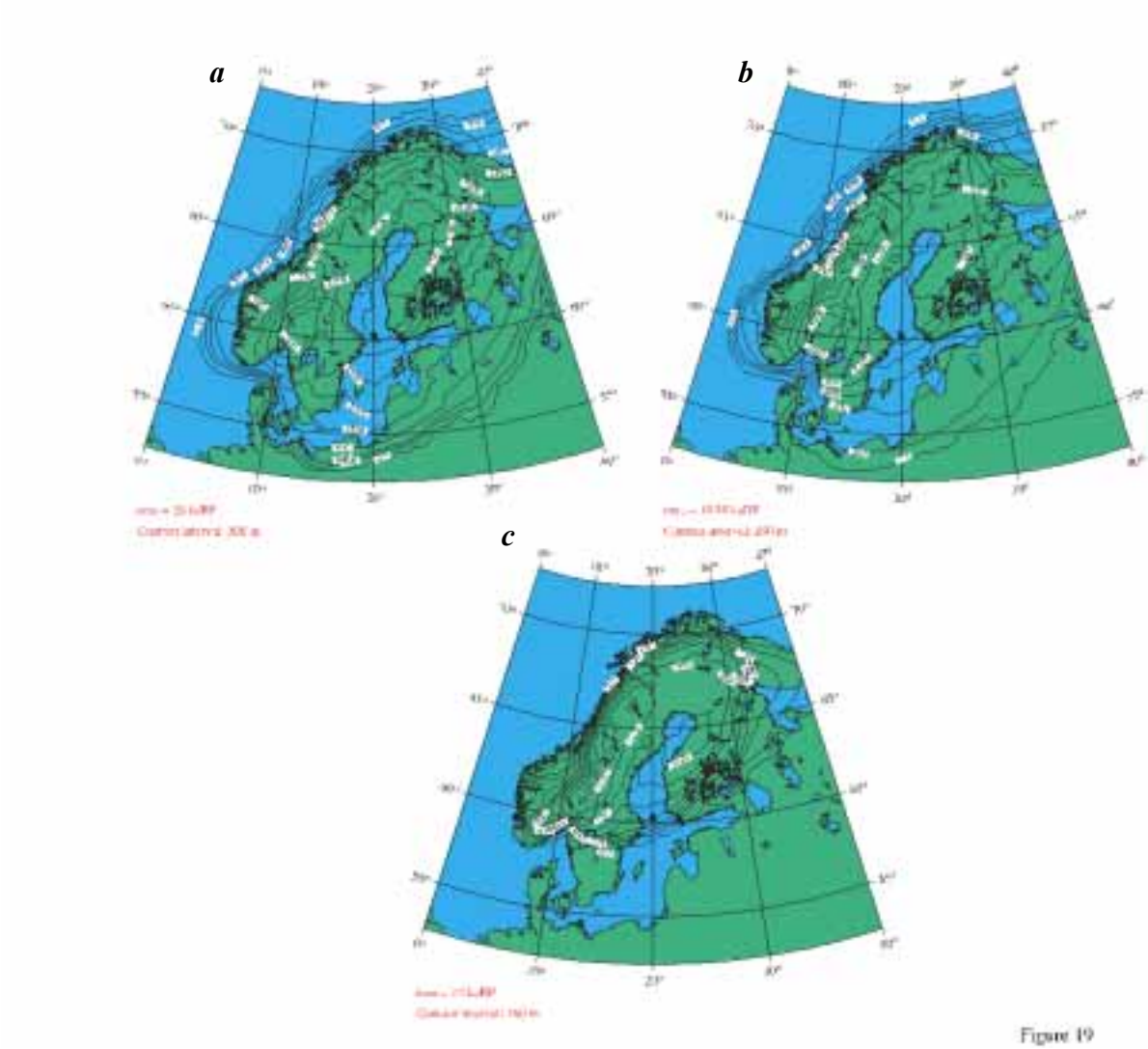

Figure 19. *Ice thickness maps for three epochs: (a) the time of the Last Glacial Maximum at 20 ka BP, (b) at ~19 ka after the occurrence of a substantial thinning of the ice, (c) at the time of the Younger Dryas between about 12.8 and 12 ka BP.*

The result at 20 ka corresponds to the maximum glaciation and that at 18.8 ka corresponds to an epoch imediately after the postulated ice sheet collapse. The subsequent reduction in ice thickness occurs more slowly as the ice retreats and the ice-height profiles along any section retain similar shapes retain By 14 ka BP the ice thickness.

The early collapse of the ice sheet is seen as a considerable thinning of the northern part of the ice sheet (Figure 19b) and it is likely that the ice margin in the southeast reached its maximum limit at the time of this event. The reduction of ice volume occurring in the model at the end of the LGM may be excessive but a series of tests in which the LGM ice, in the interval from 19 to 32, is significantly scaled downwards by a constant factor β_{LGM}, all lead to an increase in the least variance. Figure 20 summarizes the results of these tests for solutions based on the earth-model (5). The least variance

occurs for β_{LGM}= 0.98, essentially the same as the Case-11 solution. Thus the rapid decrease in ice volume at about 19 ka appears to be a robust feature of the inversions although, since the major reduction occurs over northern and central Finland, it is a subject to the reservation that the sea-level data from this region has been correctly interpreted. This reinforces the need to revisit and expand upon the field data from northern Bothnia.

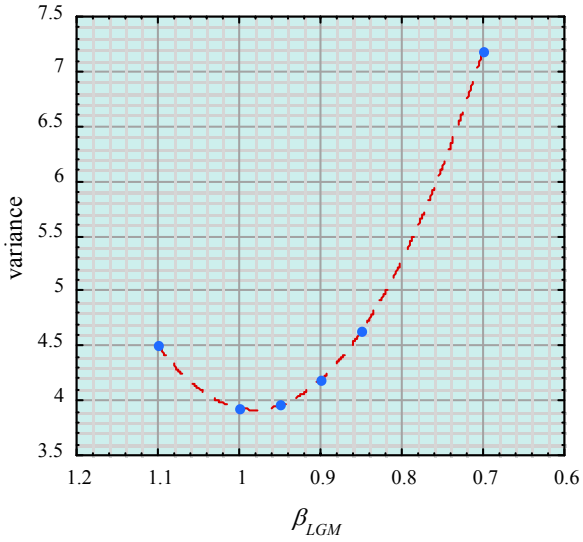

Figure 20. *Variance* Ψ^2_{k} *as function of* β_{LGM} *for ice model Case 11 with only the ice thickness during the LGM scaled by the factor* β_{LGM}

For these models with the β_{LGM} scaling, some trade-off may occur with the earth-model parameters, particularly with the lower mantle viscosity. Increasing the ice thickness of the long-wavelength components of the ice sheets results in a reduction in lower mantle viscosity estimate as shown by some of the earlier tests (Section 5.3) and it may be that for each scaling there exists an earth model that will yield a lower variance than given above. The computational time required to conduct a full search through the $E - \beta_{\mathrm{LGM}}$ parameter space is for the moment sufficiently long to rule out a full search. A multiple-processor parallel computational scheme is being developed within the Research School of Earth Sciences but it is not yet operational for this task.

5.7 Baltic Ice-Lake data: a check of model parameters

The Baltic Ice-Lake shoreline is well defined for much of the Baltic and its height exhibits a marked gradient, from below present sea level in the south to ~160 m at the locations of the Younger Dryas ice margins in both Finland and Sweden (Svensson, 1991). Its rapid drainage, when the ice retreated from central-southern Sweden thereby removing the ice dam, ensured good preservation of shorelines corresponding to the time just before the drainage. At some locations it has been possible to use isolation basin results to quantify the amount of lake lowering and the best results from southeast Sweden and Gotland indicate that this lowering was about 25-30 m.The gradients of these palaeo shorelines provide good constraints on the parameters defining the rebound

model as does the amplitude of the fall. If the observed elevation of the lake shoreline is $\Delta\zeta_o^{BIL}$ and the predicted value of mean sea level is, $\Delta\zeta_p^{BIL}$, then the two statistical functions that characterize the agreement between model predictions and observations are (i) the mean difference

$$\gamma = <(\Delta\zeta_o^{BIL} - \Delta\zeta_p^{BIL})/\sigma_o^2> \quad (8a)$$

and (ii) the variance

$$\Psi^2 = \Sigma \{(\Delta\zeta_o^{BIL} - \Delta\zeta_p^{BIL})^2/\sigma_o^2\}/(I-1) \quad (8b)$$

where σ_o^2 is the variance of the observed elevation and the summation is over the i=1...I observation. The model that is in best agreement with the observational evidence will be the one that yields a γ value within the observed range of 25-30 m and a minimum value for Ψ^2. The parameter estimation process is the same as before; forward prediction through the earth parameter space and estimating the above two parameters for each earth model within that space to identify those parameters that satisfy the above two conditions. The observational data base of Svensson (1991) is used with σ_o = 3m. Assuming that the time of the Baltic Ice Lake lowering occurred at 12 ka BP the results for H_l = 80 km are illustrated in Figure 21 and the following table for selected discrete H_l values summarizes some of the results.

The overall least variance of ~2.9 occurs for H_l = 85 km, η_{um} ~2.5×10^{20} and $\eta_{lm}>10^{22}$ Pa s with a lake lowering of 32 m, a solution for earth-model parameters that is consistent with the inversions from the shoreline elevation-age information previously discussed.

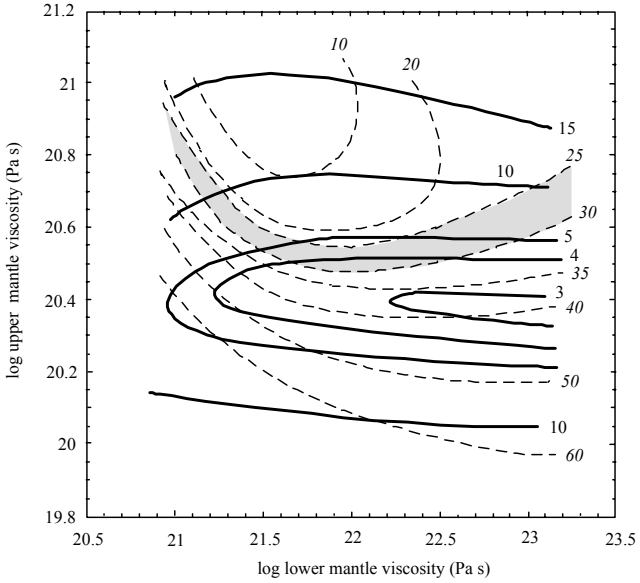

Figure 21. *Baltic Ice Lake results. Variance Ψ_k^2 and the mean offset γ (see eqn. 8) as function of mantle viscosity for H_l ~ 80 km. The solid lines define the variance and the dashed lines the offset. The shaded area defined the zone 25< γ <30 m corresponding to the observed values. The optimum solution will be the least variance value within this zone.*

Least variance solutions.

H_l (km)	η_{um} ($x10^{20}$ Pa s)	η_{um} ($x10^{22}$ Pa s)	Ψ^2	γ (m)
50	2	>1	7.0	51
65	2.5	>1	3.7	39
80	2.5	>1	2.9	36
100	3	>1	3.5	30
Minimum variance solutions for $25 < \gamma < 30$ m				
50	3.5	>1	11.7	30
65	3.5	>1	6.6	39
80	3	2	3.3	30
100	3	2	3.8	30

In these inversions the assumption is made that the timing of the drainage is known from observations such as those of Svensson (1991). The nominal time of this event is 10.3 ^{14}C ka BP or ~12 cal. ka, the time adopted in the above solution. There is some uncertainty about the radiocarbon time scale at this time period and the inversions could include the timing of the drainage as an unknown. Thus the results have been repeated using different assumptions about the chronology of the drainage. Figure 22 illustrates the results for three different times, T=11.5, 12 and 12.5 ka BP for this drainage event.

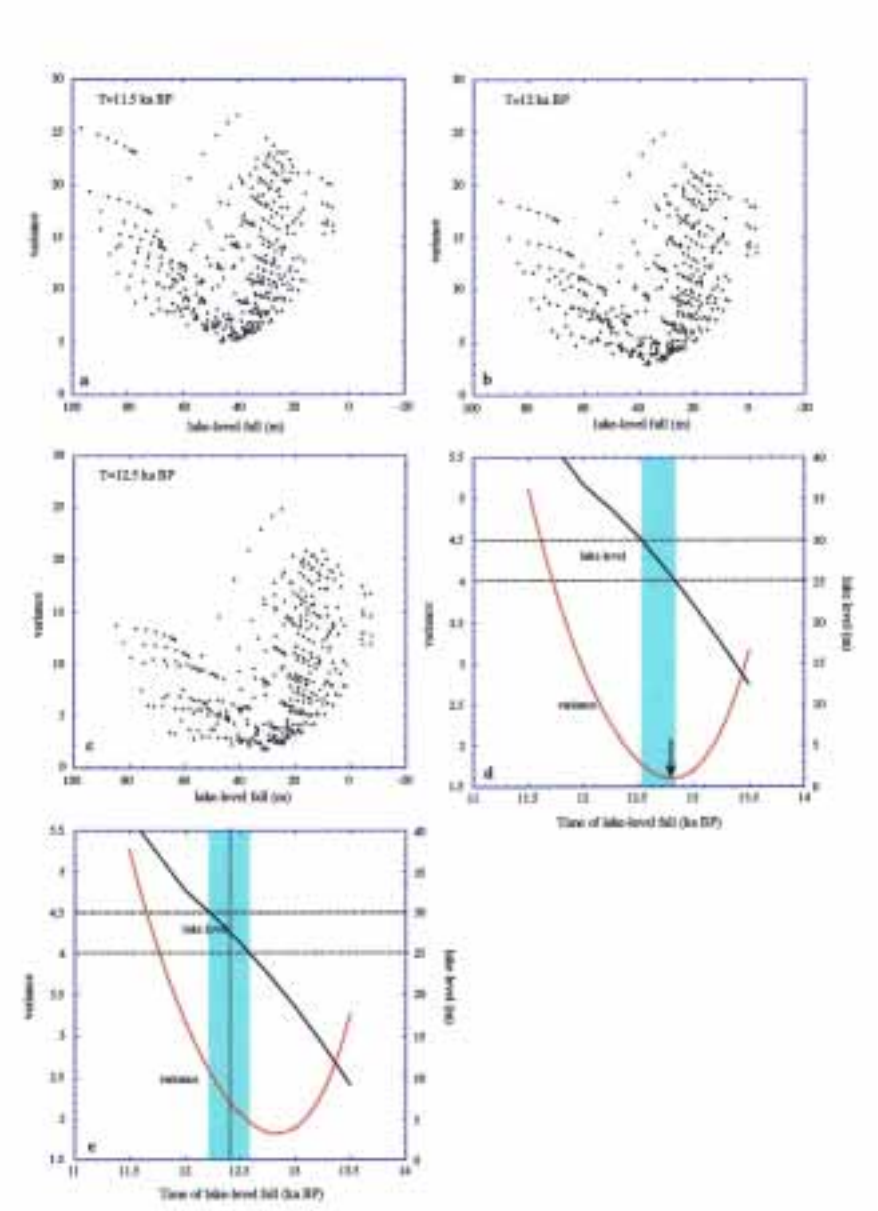

Figure 22. *(a-c) Variance* Ψ_k^2 *versus mean offset* γ *(lake-level fall) for earth models* E_k *for three different assumed drainage epochs. (d-e) Variance (LHS axis) and Lake level fall (RHS axis) as a function of the assumed epoch for the drainage event. (d) for the Baltic Ice Lake model (9). The blue zone corresponds to the values for T for which the amplitude of the drainage lie in the range 25-30m. (e) same as (d) but for the solution (10).*

For each epoch the Ψ^2 and γ have been estimated for a range of earth models in the parameter space (4) and the results are summarized in the table below. The earth model parameters remain effectively unaffected by the choice of the drainage epoch at

$$H_l = 80 \text{ km},$$
$$\eta_{um} \sim 2.5 \times 10^{20} \qquad (9)$$
$$\eta_{lm} = 3 \times 10^{22} \text{ Pa s}$$

but both the variance and the offset estimates are strongly dependent on this choice (Figure 22d). If we adopt the overall least variance solution as the optimum one then T= 12.8 ka and γ = 26 m. If we adopt $25 > \gamma > 30$ m, as suggested by the evidence from Kalmar and Gotland, then T= 12.7 ka: the estimates are internally consistent and we adopt T = 12.7 ± 0.1 ka for the time of the last and major drainage of the Baltic Ice Lake and 27 ± 2 for the lake level fall.

T (ka)	H_l (km)	η_{um} ($\times 10^{20}$ Pa s)	η_{lm} ($\times 10^{22}$ Pa s)	Ψ^2	γ (m)
11.5	80-90	2.5-3	2-5	5.0	45-47
12	80-90	2.5-3	1-5	2.9	36-38
12.5	75-85	2.5-3	0.7-5	1.8	30-32

6 RESULTS FROM GEOLOGICAL DATA INVERSIONS

The inversion of the geological evidence for relative sea-level change has resulted in a consistent model for describing the Scandinavian rebound for the post-LGM period. The results from the inversion of the shoreline age-height data and of the Baltic Ice Lake shoreline gradients yield comparable results. This is important because the two data sets are complementary. The Baltic Ice Lake data includes information from locations and for time intervals that are not well represented by the age-height data set, and the time interval for the former corresponds to a time interval for which the early-iteration inversions of the age-height information led to substantial discrepancies with the observed values. Thus the Baltic Ice Lake results confirm the modifications that led to the ice model represented by Case 9. Because of the complementarity of the two data sets, and because the two separate earth-model parameter solutions are comparable, we adopt as the optimum solution for the earth-model parameters the weighted mean of the two separate solutions. This yields

$$\begin{aligned} H_{\rm l} &= 80\text{-}90 \text{ km}, \\ \eta_{\rm um} &= 2.5\text{-}3\text{x}10^{20} \text{ Pa s}, \\ \eta_{\rm lm} &= 7\text{-}30\text{x}10^{21} \text{ Pa s}. \end{aligned} \qquad (10)$$

Figures 23-24 illustrate the essential comparisons for predictions based on this earth model and on the Case 9 ice model. The predicted values are based on $H_{\rm l}$ = 85 km, $\eta_{\rm um}$ =2.75x10^{20} Pa s and $\eta_{\rm lm}$ =10^{22} Pa s and the accuracy of the predictions are based on the root-mean-square of the differences with respect to their mean, of predicted sea levels for the above range (10) of earth-model parameters. Figure 23a shows the observed versus predicted values for all age-height field data, including the anomalous data points previously identified.

The correlation coefficient is 0.986. The solution with variable β^S yields the same result. With these results we should return to the original data base to examine whether the outlying points are of observational consequence or whether there is still scope for some model-parameter improvement. A scan of the time and spatial distribution of the anomalous data points has not revealed any systematic patterns but a careful re-scrutiny of the field data has not yet been attempted. Figure 23b illustrates the differences between the observed and predicted sea levels for the same data set with the variance estimates being the sum of the observed and predicted variances. These results are very similar to those based on the earth-model (7) because the dependence of the predictions on these parameters is small in the vicinity of these solutions.

Figure 23c illustrates the observed versus predicted sea levels at the time of the Baltic Ice Lake (with T_{BIL}-12.75), where the predicted values refer to coeval sea level while the observed levels correspond to the lake level, and the offset corresponds to the height of the Baltic Ice Lake above its coeval sea level. The correlation coefficient between the two is 0.996 and the offset is 22 m. This is less than the observed range of 25-30 m

discussed above because the mean of the two geological solutions with T_{BIL} = 12.75 is not the optimum solution for the Baltic Ice Lake data only. The principal difference is in the lower mantle viscosity on which the ice-lake data shows a quite strong dependency. This suggests that a further iteration of the entire solution, including the ice model, may be necessary before the two data sets are internally consistent with the earth- and ice-model parameters. An alternative approach is to solve for T_{BIL} for the earth model (10) which yields T_{BIL}= 12.40 ka (Fig. 22e) and the comparison illustrated in Figure 23d. Other than the value for T_{BIL} this solution is indistinguishable from the earlier result and we adopt this solution.

Figure 24 illustrates comparisons for Finland, including the Baltic Ice. Lake Data for Finland and the southern shore of the Gulf of Finland. The sea level data is from Eronen et al. (1995) and the lake-level data is from Svensson (1991). For the ice lake results the observed values have been corrected for the offset previously determined of 27.6 m. Agreement is mostly satisfactory, with the few anomalous points previously identified. The two lake level points marked S are from two localities near Hämeenlinna but other data points from the same region fall on the regression line. The differences, observed-predicted sea levels, are illustrated in Fig. 24b.

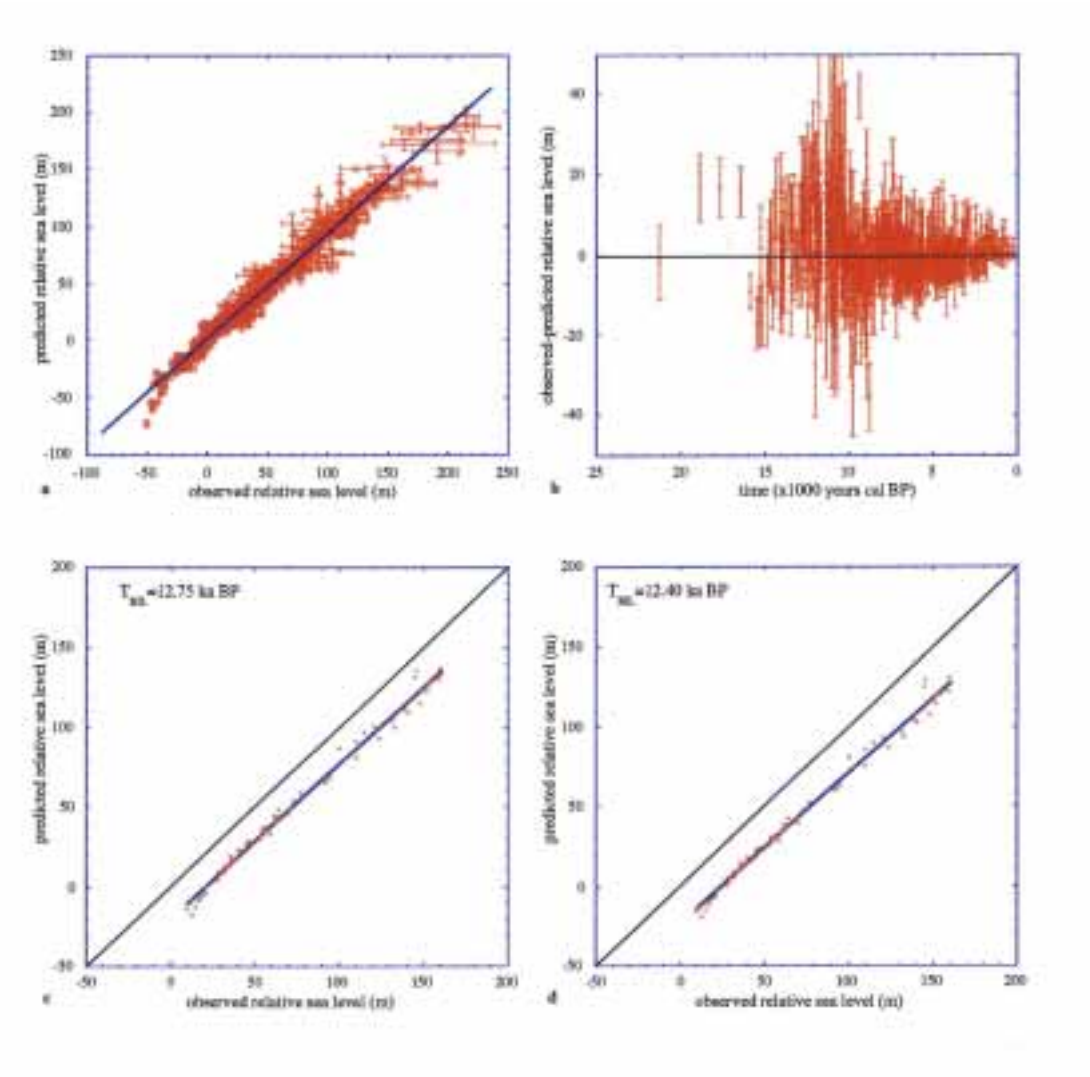

Figure 23. *Observed versus predicted shoreline elevations for (a) the Scandinavian geological age-elevation data set, and (c) for the Baltic Ice Lake data. (b) illustrates the observed-predicted sea levels for the case (a). For the Ice Lake results in (c) the predicted values are elevations above coeval sea level and the offset from the observed values is a measure of the height of the sill of the Baltic Ice Lake. For (c) the epoch of drainage is T_{BIL}=12.75 and in (d) it is for T_{BIL}=12.4 ka. The predictions are based on earth model (10) and the Case 9 ice model.*

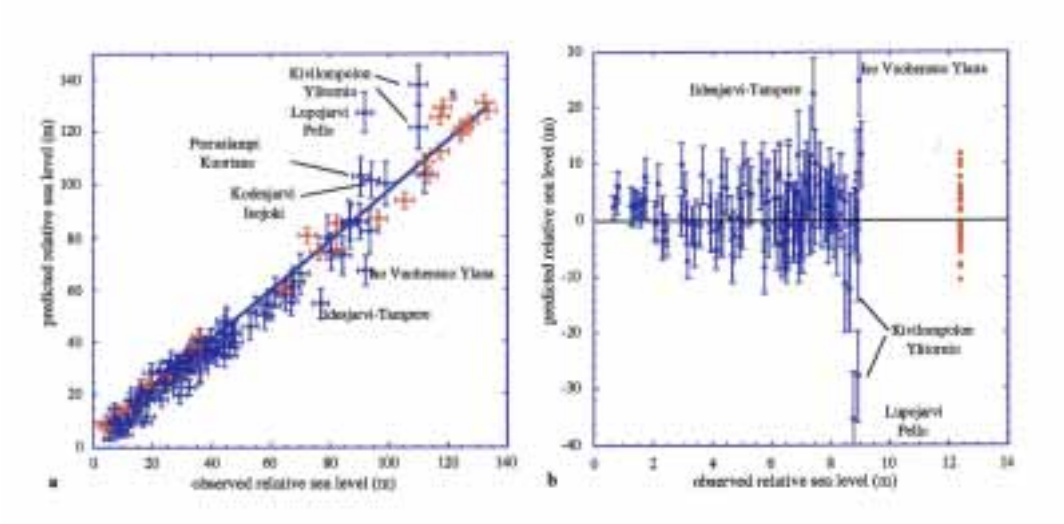

Figure 24. *Observed versus predicted shoreline elevations for the combined shoreline elevation and Baltic ice lake data set for Finland. (The ice lake data, in red, includes information from the southern shore of the Gulf of Finland.) (b) The observed less predicted sea levels for the same combined data set.*

While there may be scope for further refinement of the model in that the agreement between observations and predictions is not always satisfactory, a number of essential features of the model appear to be robust. These include the estimates of ice volume for the LGM and Lateglacial period, and the spatial distribution of the Lateglacial ice into at least two domes, one over southern Norway and southwestern Sweden, and another over the northern Bothnia region. The solution for the earth-model parameters is also robust with the principal subdivision of the mantle viscosity into three layers providing an effective description of the response. Some of the remaining differences between observed and predicted values can be attributed to observational issues because the anomalous data points are mostly inconsistent with other data from the same localities and for the same time intervals. Other differences occur at some margins of the former ice sheet and these can be attributed to inadequacies in the retreat history of the ice sheet. But the consequences of such limitations on predictions in the central Bothnian-Finland region are unlikely to be important because of the insensitivity of these predictions to the detail of the ice sheet at its margins. The solution inferred from the Baltic Ice Lake observations is consistent with the other geological solutions and with the Baltic Ice Lake drainage having occurred at about 12400 (calibrated) years ago resulting in a lowering of the Baltic by about 25-30 m. Thus the adopted model provides a sound basis for predicting the shoreline migrations within the Gulf of Bothnia and Finland for the Late- and Post-glacial periods when the Baltic was open to the Atlantic Ocean (section 6.1). The model should also be adequate for predicting the stress evolution due to the changing ice loads (section 8).

Once the sea-level change $\Delta\zeta(\varphi,t)$ is known and the present topography (and bathymetry), $h(\varphi,t_0)$, is available, then the elevation or depth of the palaeo-terrain at time t is given by

$$h(\varphi,t) = h(\varphi,t_0) - \Delta\zeta(\varphi,t) \qquad (11)$$

and the palaeo-shorelines for epoch t are defined by the contour $h(\varphi,t)=0$. For the initial reconstructions of the area as a whole (Figure 25) we have used the topography DTM 2.5 which is a 2.5' x 2.5' digital terrain model of Europe.

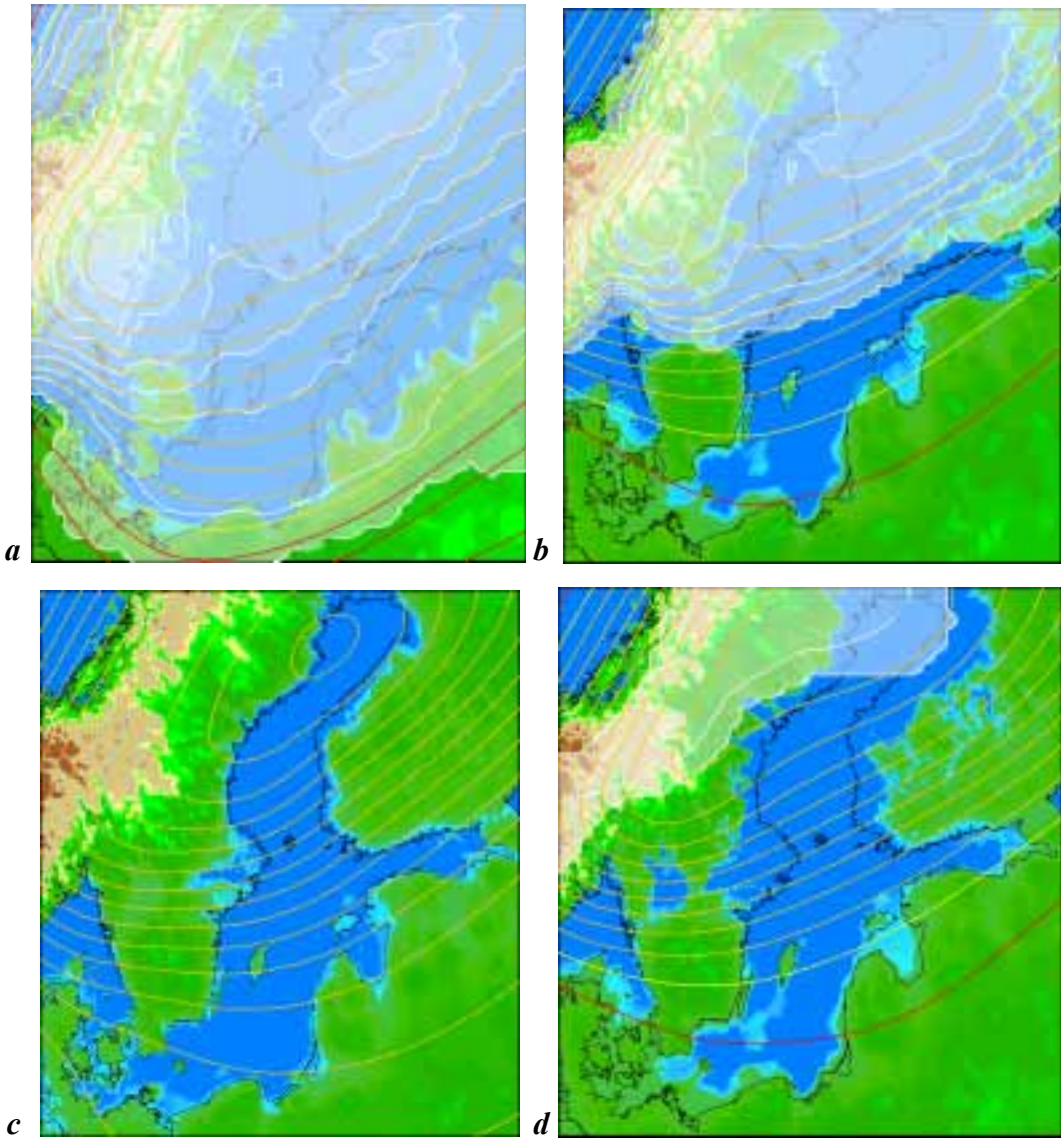

Figure 25. *Shoreline and lake-level reconstructions for four epochs. (a) the last Glacial Maximum. (b) the late stage of the Baltic Ice Lake at a nominal time of 12 ka BP. The lake level is 30 m above sea level at this time. (c) The time of the Ancylus transgression at ~ 9ka BP. The Ancylus lale level is 13 m above coeval sea level. (d) The time of the Litorina transgression at ~ 6 ka BP. The contour intervals for the sea-level isobases at the four epochs are 40, 30, 20 and 5 m respectively. The red contours correspond to negative values (any palaeo shorelines would be below present sea level) and the orange contours correspond to positive values. The yellow contour corresponds to 0. The ice thickness contour interval is 250 m. Green areas correspond to elevations above coeval sea level. Changes in green shading occur at 25, 50, 75m and higher intervals. Changes in blue shading correspond to depths of 5, 10, 15, 20, and 25 m.*

This topographic data base has limitations in some areas (see Figure 28 below, where areas of land appear in the upper Gulf of Bothnia or in the Gulf of Finland that should be below sea level at the present time) but the reconstructions illustrate the broad evolution of the area. The ice cover at 18 and 12 ka BP is indicated by the area in translucent blue and green, blue corresponding to areas below the ice where the base of the ice sheet is below the sea level for the epoch. The ice thickness is specified by the white contours. The relative sea level change since the epoch illustrated is given by the red (negative), yellow (zero) and orange (positive) contours. At 18 ka BP the region is ice covered and the rebound is dominated by a symmetrical pattern focussed on the northern part of the Gulf of Bothnia. Note that the secondary ice dome over southwestern Scandinavia results in a broad ridge of rebound that persists into earliest Holocene time but not into very recent time by which time the centre of rebound has migrated southwards. At 12 ka BP the southern Baltic is ice free but is separated from the Atlantic by both the ice barrier in southern-central Sweden and by the sills of the Danish straits. This corresponds to the nominal time of the end of the Baltic Ice Lake and the lake level will be about 25-30 higher than illustrated here with the outflow through Denmark. By 10 ka BP, shortly after the peak in the Ancylus transgression, the ice has retreated mostly to the mountains of Norway and Sweden with residual thin ice over northern Bothnia. At about this point in time the Baltic is separated from the Atlantic by the topography of Sweden and the Danish straits being above sea level for that epoch. Thus the actual lake level is about 10-15 m higher than indicated here. By 6000 years ago, corresponding to an early part of the Litorina phase, the Danish straits are open to the Atlantic and the Baltic begins to take on its present form.

The higher resolution GTOPO30 data base does not extend to the higher latitudes of Finland and does not include the marine areas. We have therefore digitized the 1:1700 000 bathymetric map of the Baltic Sea Area (Geol. Surv. Finland, 1981), gridded it onto a 30” grid and merged it with GTOPO30 to obtain higher resolution maps for areas south of 65˚N. But even with this data set the actual resolution is only about 1-2’ and a higher resolution grid is desirable for more detailed predictions, particularly for predicting the future changes in sea level caused by the ongoing rebound.

Figure 26 illustrates the results for the southern and western parts of Finland only. The rebound contours are with respect to sea level at the epoch shown but the Baltic shorelines now correspond to the lake level for times when the Baltic was isolated. For the pre-Litorina period the Baltic Ice Lake level, illustrated here for 12.5 ka, is taken to be 27.5 m above sea level as established above (the epochs are rounded to the nearest 500 years and the results can be taken to represent average conditions in an interval ± 250 years about the epoch shown). For the brief Yoldia phase (T=11.5 ka) the Baltic is assumed to have been at sea level but for the following Ancylus transgression phase the Baltic was again isolated from the open sea (Björck, 1995) and the lake level lies above coeval sea level. Because we do not have a comprehensive data set to repeat the Baltic Ice Lake solution for the Ancylus period we use the model proposed by Lambeck (1999) which is consistent with much of the field data. In this model an elevation of 13 m for the maximum Ancylus transgression, at a nominal epoch of 10.4 ka (9.4 ^{14}C ka), is adopted, although these values are less certain than the elevation and age of the Last

Baltic Ice Lake shoreline. An analysis of the Ancylus data, analogous to the Baltic Ice Lake analysis in section 5.7 should be done in a follow up study.

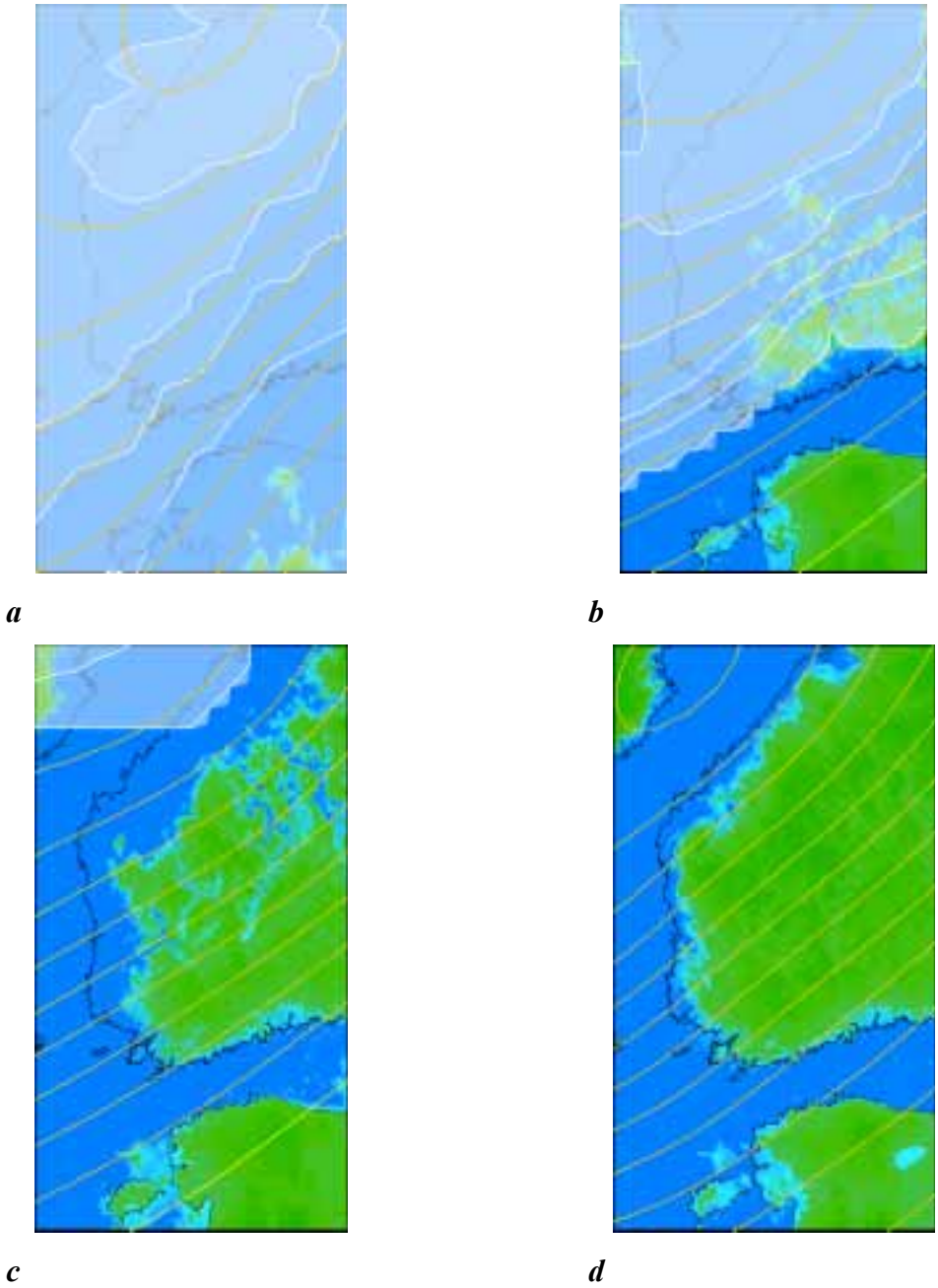

Figure 26. *Same as Figure 25 but for Finland and adjacent seas. The contour intervals are the same as for Figure 25 for the matching epoch.*

7 PRESENT-DAY TIDE GAUGE RECORDS: A COMPARISON OF OBSERVATIONS AND PREDICTIONS

The tide gauges in the Baltic region record the combined isostatic crustal rebound and the recent eustatic sea-level change for about the last 100 years. The former effects range up to about 10 mm/year in amplitude, and the latter are of the order 1-2 mm/year. The first results in an apparent fall in sea level within the Baltic region and the latter is a rise in sea level. The records from the Baltic region have been analysed in very considerable detail by Ekman (1988, 1996) and have previously been used to constrain rebound models by Lambeck et al. (1998b). The merit of the records is that, compared to other geodetic time series, they are of long duration and that, because of the marked coherence of the signal, gaps in the individual records can be filled using correlation analysis relative to nearby sites. We use the same records here to test the previous results obtained for the rebound parameters in the previous sections.

For the first tests we compare predicted present-day sea-level observations for some of the iterative ice models discussed above. The equation relating the observed and predicted values to the model parameters is

$$\Delta\zeta_o(\phi) + \varepsilon^o(\phi) = \Delta\zeta_p(\phi,k,I) + \Delta\zeta^e \qquad (12)$$

where the subscripts o and p denote observed and predicted values for the rate of change respectively, $\varepsilon^o(\phi)$is the observational error at position ϕ, and $\Delta\zeta^e$ is the rate of eustatic sea level change, being constant over the area. The earth-model parameters H, η_{um}, η_{lm} and the ice-model parameters *I* are contained within $\Delta\zeta_p$ (ϕ,k,*I*). For an earth model k the measure of model fit is

$$\psi_k^2 = \frac{1}{M}\sum_{m=1}^{M}\left[\frac{\dot{\Delta\zeta}_o^m - \dot{\Delta\zeta}_p^m(E_k)}{\sigma^m}\right]^2 \qquad (13)$$

where σ_m is the standard deviation of the observed rate of the m^{th} observation. A value of σ_m=0.3 mm/year is assumed for all sites (see discussion in Lambeck et al. 1998b). If the rebound model is correct, the estimates for σ_m are realistic, and there are no other contributions to the sea level change other than a secular eustatic rate, then the expected value of the dimensionless quantity ψ^2 is unity.

The Table below summarizes results for a series of tests with the same earth model (5) but for different iterations of the ice model. (In the geological solutions time is expressed backwards and the sign notation is that negative $\Delta\zeta^e$ means that sea levels 100 years were lower than today.) These outcomes indicate (i) that the predictions of present sea-level change are sensitive to the ice volumes at times of maximum glaciation (compare tests 1 and 2 which differ in the amount of ice at the time of the LGM), as well as sensitive to the rates of melting of the ice sheet (compare tests 2 and 3): (ii) that the predictions are not strongly dependent on the details of the spatial distribution of the ice within the ice sheet (compare tests 4 and 5): (iii) that the

variances for all tests are large, indicating that earth model parameters that describe adequately the response observed on the geological time scale may not be optimal for describing the response observed over the past 100 years: (iv) that the estimates of the mean rate of sea-level change for the past century lie between 1 and 2 mm/year, consistent with global estimates (Church et al., 2000).

Test	Ice model	$\Delta\zeta^e$ (mm/year)	ψ^2
1.	Case 1-3	-1.91	10.9
2.	Case 6	-1.36	13.9
3.	Case 7	-1.29	15.2
4.	Case 9	-1.23	17.9
5.	Case 11	-1.06	17.6

In the second series of tests, the ice model (Case 1) is held constant and the earth-model parameters are varied over a restricted range in the first instance. The outcomes are as follows, where the earth models are described by the three parameters H_l, η_{um}, η_{lm}.

Test	Earth model	$\Delta\zeta^e$ (mm/year)	ψ^2
6.	50, $3x10^{20}$, 10^{22}	-0.88	18.7
7.	100, $3x10^{20}$, 10^{22}	-1.23	19.0
8.	80, $3x10^{20}$, $5x10^{21}$	-0.55	23.6
9.	80, $3x10^{20}$, $2x10^{22}$	-1.34	14.6
10.	80, $2x10^{20}$, 10^{22}	-0.23	53.0
11.	80, $4x10^{20}$, 10^{22}	-1.65	4.03

These results exhibit a strong earth-model dependence, in particular for the upper mantle viscosity (compare tests 10 and 11) but also for the other two parameters. Of note is that only the last test yields variance estimates that begin to approach a satisfactory solution. Also, note that the estimates of the present-day eustatic sea-level rise are strongly dependent on this choice of parameters and earth models with relatively low values for H_l and η_{um} (tests 6 and 10) yield values for $\Delta\zeta^e$ that are much less than the globally observed values. In the next test we conduct a complete search through the parameter space as defined by (4). Figure 27 illustrates the outcomes in η_{um} - η_{lm} space for two values of H_l.

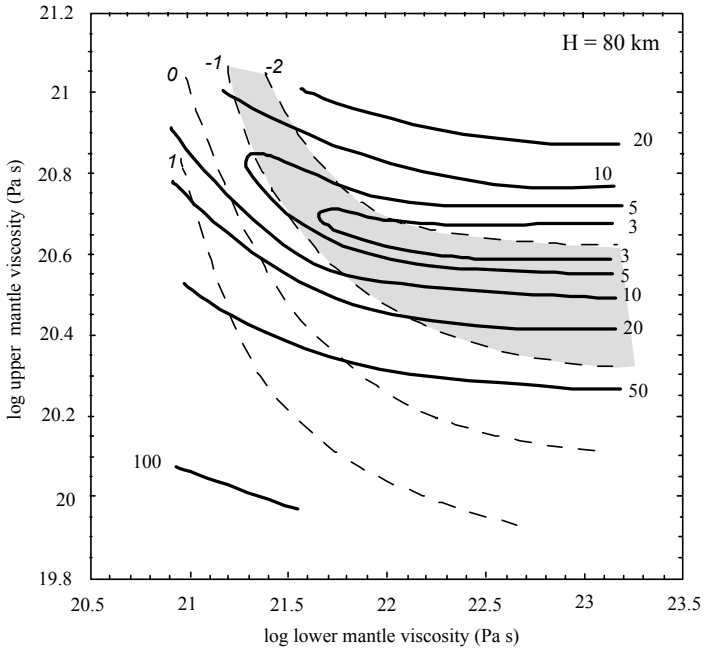

Figure 27. *Tide gauge results. Variance* Ψ^2_k *(thick lines) and the present-day eustatic sea level rise (dashed lines, italic numbers) based on the tide gauge data, as a function of* $\underline{\eta}_{um}$ *and* $\underline{\eta}_{lm}$ *for* H_{el} *= 80 km. The shaded zone defines the parameter space for which* $-1 < \Delta\zeta^e < -2$ *mm/year.*

The overall least variance in the parameter space (4) occurs at low values for η_{lm} but the corresponding eustatic sea-level rise estimates indicate past eustatic levels higher than those of today (i.e. a falling eustatic sea level) and these solutions are inconsistent with the global values. If the loose constraint

$$-0.5 > \Delta\zeta^e > -2.5$$

is imposed on the solution then the tide gauge data yields the following estimates for the earth-model parameters:

$$H_l = 90 \pm 10 \text{ km}$$
$$\eta_{um} = (4.25 \pm 0.25)\ 10^{20} \text{ Pa s} \qquad (14)$$
$$\eta_{lm} \geq 10^{22} \text{ Pa s}$$

Of these parameters η_{um} is best constrained as can be inferred from Figure 27 where for any fixed value of H_l or η_{um} the variance ψ^2 changes rapidly with η_{um} about either side of its local minimum value. Within this range

$$\psi^2 = 2.0$$
$$\Delta\zeta^e = -(1.8 - 2.1) \text{ mm/year}$$

Figure 28a illustrates the predicted rate of present sea level change due to the isostatic rebound only.

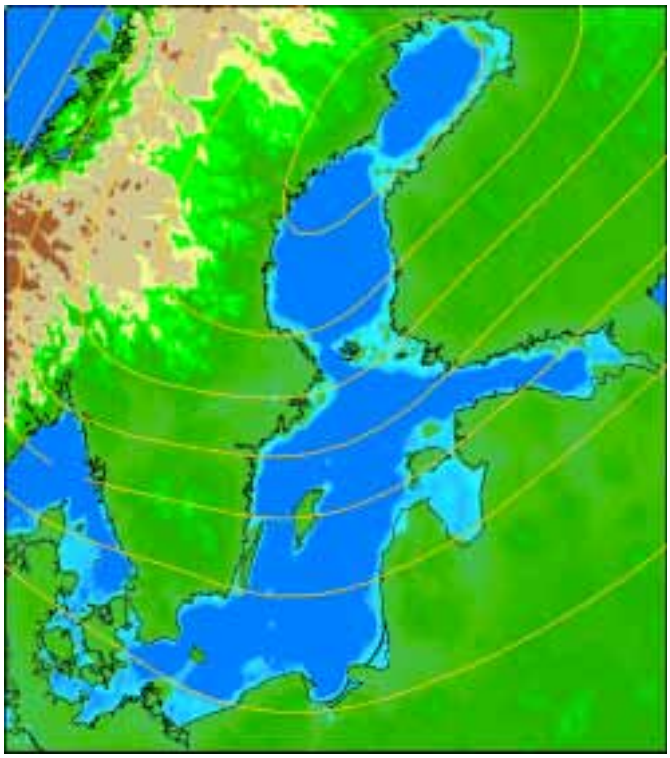

Figure 28. *Predicted rate of relative sea level change due to glacial isostasy only for the model (14). The contour interval is 1.25 mm/year. The maximum contour over northern Bothnia corresponds to a present rate of sea level fall of 8.75 mm/year and the maximum value is about 9.0 mm/year. The contour interval through Sjaelland, Denmark, is –1.25 mm/year.*

For the model used here, where present-day ocean volume rate of change is zero, this is effectively equal to the radial crustal rebound. Figure 28b gives the relative sea level change using the above estimate for the eustatic change.

7.1 Summary

The solution (14) for response parameters from tide gauge data is relatively insensitive to the details of the Fennoscandian ice sheet but is dependent on the magnitude of the ice load at the time of the LGM and the Lateglacial stage. This dependence is however less strong than for the geological-data inversions. The strategy we adopt is to fix the ice sheet, use the tide-gauge data to constrain the earth-model parameters and then use the concomitant estimate for the eustatic level to check our solution. One feature of the outcome is that the value obtained for upper mantle viscosity is consistently higher than that derived from the geological data (solution 7). This trend has been noted previously and our revised and improved results confirm it. It is possible that this may be indicative of non-linear behaviour of the mantle response: If a non-linear rheological response is modelled as an effectively linear body then the viscosity that yields best fit with the observations becomes stress dependent. During the early part of the unloading

phase, stress levels in the mantle are relatively high when compared with the residual stresses during the post-glacial phase. Hence the geodetic inversions- reflecting the relaxation that has occurred over the past century- can be expected to yield higher values for the effective viscosity of the mantle. This trend appears to be confirmed by this data set as well as by the instrumental records for lake tilting and preliminary GPS crustal displacement analyses. Lambeck et al. (1998b) examined the lake-tilt records for four large lakes, Vänern and Väattern in Sweden, and Päijänne and Saimaa in Finland. We have not revised these analyses here because with just four lakes the solutions are barely significant. However, the data is nonetheless important since it extends the instrument record to inland sites. The data set of Sirén (1951) should be updated and a revised analysis attempted. The preliminary analysis of the GPS data discussed above (section 4.2) also support the geodetic solutions but these results require further development and analysis.

The Baltic Ice Lake solution (9) tends to support the hypothesis of a non-linear response; the upper mantle viscosity of 2.5×10^{20} Pa s characteristic of the response at 12.4 ka BP being less than the value of $\sim 3 \times 10^{20}$ Pa s from the shoreline data (7) whose characteristic time will be less than T_{BIL}. The difference is small but because both solutions are very sensitive to upper mantle viscosity, it may be significant and warrants closer examination. A useful strategy may be to revisit the above solutions (Case 4, Case 5) in which only time-dependent subsets of data were used, but using the revised earth model. This is beyond the scope of the present study and probably should not be attempted until the observational data set has been improved.

Because of the different results for the Earth response obtained from the geological and geodetic data analyses stress calculations for recent times will be carried out with both models.

8 CRUSTAL STRESS CONSIDERATIONS

8.1 Introduction

The stress state in the upper layers of the Earth, in the crust and sub-crustal lithosphere, is the result of various tectonic processes that operate on different time scales. Some of these processes operate on time scales of millions of years, others on time scales of thousands of years. Topography and its isostatic compensation, as well as the plate tectonic movements of the lithospheric plates, produce a background tectonic stress field that, by its nature of formation, is likely to be close to the failure limit of the weaker parts of the crust. Both these stress-sources are a result of long-term geological processes and are unlikely to change on the human time-scale except for locations near plate margins where stress adjustments can be episodic and catastrophic in response to local conditions. If the plate-tectonic driving forces change only slowly over time than many of the anomalous stress generated by the internal structure of the crust and by the topography will have relaxed through deviatoric stress relaxation and the levelling tendency of surface erosion processes. Thus the stress states of old continental plate interiors may be considered to reflect primarily the plate-tectonic driving forces. The crust has a finite strength and differential stresses do remain but, because the geological structure or process that gave rise to the original stress field may no longer be obvious, the residual stresses are difficult, if not impossible, to predict from *a-priori* model considerations. Thus failure occurs in many old plate interiors for no apparent reason and at no predictable location. This is well illustrated by some of the large surface-rupturing earthquakes of the Australian continent, far from plate boundaries, without any topographically generated stress fields, and with no history of glaciation since Permian times (Lambeck et al., 1984). The analogy of Fennoscandia with the Australian continent is not irrelevant because of their similar Precambrian histories. Thus it should not be a foregone conclusion that if postglacial faulting has occurred in the former that it is the result of the last deglaciation.

Topographically generated stresses are anticipated to be small for Finland. Topography produced by mountain building processes in the geological past introduce maximum topographic stresses in the crust that are of the order $\rho\, g\, h$ where ρ is the density of topography of height h and g is the value of acceleration due to gravity. The topography is usually compensated isostatically through variations of density in the lithosphere and this internal lateral inhomogeneity further modifies the stress field. The mountain building forces usually involve thermal processes as well as mechanical ones and as the lithosphere cools after the orogenic event has run its course the stresses in the layer continue to evolve; relaxing in the lower regions and concentrating in the cooler upper parts. Thus the lithosphere can be expected to continue to deform, flowing viscously in the warmer and more ductile regions and fracturing in the colder brittle zone. When the topography of a region is geologically old a broad balance between these stresses and the residual strength of the lithosphere can be expected to have been attained, leaving a residual or background stress-state in the crust of typical magnitude $0.5\, \rho\, g\, h$ (Jeffreys, 1962; Lambeck 1981), that may be near the failure limits of the layer. Where these

background stresses are largest is where the gradients of the topography are greatest over distances comparable to the thickness of the lithosphere. This may occur at continental margins where the differences in elevation between mountains and adjacent sea floor can be substantial, but is unlikely to be significant in Finland.

The major plate-tectonic stress field will be a regional horizontal stress caused by boundary and basal forces acting on the tectonic plate. These stress differences can reach tens of MPa. In Scandinavia these are believed to be mainly compressional with a NW-SE orientation (Clauss et al. 1989; Stephansson et al. 1989) but the exact description of this stress field remains a matter of debate due to uncertainties in the relative importance of the forces acting on the plate: ridge push, trench pull, viscous drag at the base of the plate etc.

A process that may be more significant on the human time scale and in Finland is the incremental stress introduced by cycles of glacial loading and unloading. With ice sheets attaining some two kilometers in thickness, the magnitudes of the additional stresses are of the order of 20 MPa, comparable to some of the other stress fields but fluctuating on much shorter time scales, of $10^3 – 10^4$ years. The important question is whether within the plate interiors such changes in stress regime, when superimposed on the background stress field, can lead to the crust exceeding its local failure limit.

The problem is one of formulating (i) the evolution of the stress field in this crust under these time-dependent forces and the stress field associated with the in-built background stress and (ii) the brittle deformational response of the layer to this stress field. Will failure occur, and if so where? A successful solution of this problem requires a knowledge and quantification of the physical processes and of the rheology of the layer with all its small scale structure that has been incorporated into it through geological time. Such a model of the lithosphere is not yet available and at present one can only seek approximate solutions to the problem, solutions that characterise the principal elements of the processes, that point to outcomes that are robust, and that can be superimposed upon detailed local stress fields when these have been observationally determined.

While it is the present stress field that is likely to be of greatest interest to those concerned with the stability of the crust, the palaeo-stress field is also important for testing any outcomes because of evidence that post-glaciation failure of the crust has occurred and the possibility that this may have been triggered by the glacial unloading. The formulation of the stress must therefore include a description of the evolution of the stress field during at least a full glacial cycle.

8.2 Glacial Stresses

The stress calculation for loading of the earth by a time-dependent surface load follows several steps: (i) the definition of the surface load, in this case of the cyclic exchange between the ice sheets and the oceans, (ii) the evaluation of the displacement field of the surface and of the planet's interior, (iii) the evaluation of the strain field within the planet, particularly within the lithosphere, (iv) the establishment of an appropriate rheology, (iv) the evaluation of the deviatoric stress field, and (v) an evaluation of possible failure mechanisms.

The surface load assumed for this study is the above described Scandinavian ice load (Case 9), supplemented with the ice loads of other ice sheets, and the changing water load in the ocean basins and adjacent seas. The ice load is defined for the last glacial cycle starting with the Last Interglacial or OIS-5e using the pre-LGM ice sheet fluctuations established by Lambeck and Chappell (2001).

The surface strain field is not simply a function of radial and the effects of tangential displacements must also be considered, as has been briefly discussed above in the context of using GPS observations of horizontal crustal displacements to constrain the rebound-model parameters. Furthermore, the strain fields below the surface are required if the depth dependence of stress is to be examined. This has required some modification of the numerical code at the expense of increased computation time.

The strain and stress components are predicted using the general rebound formulation for a spherical, radially stratified earth model, with a linear Maxwell visco-elastic response so that the Love Number formulation can be used. This has the advantage of maintaining a gravitationally consistent description of the ice-water load, and of allowing analysis of detailed load geometries through harmonic decomposition of the load and superpositioning of the responses to each harmonic component. It has the disadvantage of the need to assume lateral homogeneity, as was also the case for the above sea-level analyses. The theory assumes an elastic lithosphere over a viscoelastic mantle (Johnston et al. 1998). The strain field is calculated from the displacements and rates of displacement in the mantle through time and from this the complete deviatoric stress tensors are calculated using the standard formalism relating stress to strain rate with appropriate boundary conditions. The latter include zero traction at the top of the plate and the normal stress at the surface determined by the load. The normal stress at iso-density surfaces within the earth is specified by the buoyancy force due to the displacement of more dense material during deformation. For the calculation of the stress, but not the strain field, we assume incompressibility in the lithosphere as this facilitates considerably the solution through the property relating the radial displacement gradient to the displacement as a function of position (e.g. Johnston et al. 1998). The lithosphere itself has depth-dependent elastic parameters as before. The full stress tensor is defined by six elements τ_{rr}, $\tau_{r\theta}$, $\tau_{r\lambda}$, $\tau_{\theta\theta}$, $\tau_{\lambda\lambda}$, $\tau_{\theta\lambda}$ where r is the radial direction, (positive outwards), θ is the direction in the meridian, (positive south – the direction of increasing colatitude), and φ is along a latitude circle, (positive eastward).

A useful quantity for assessing the impact of these incremental stress fields is the Fault Stability Margin (*FSM*) (Figure 29).

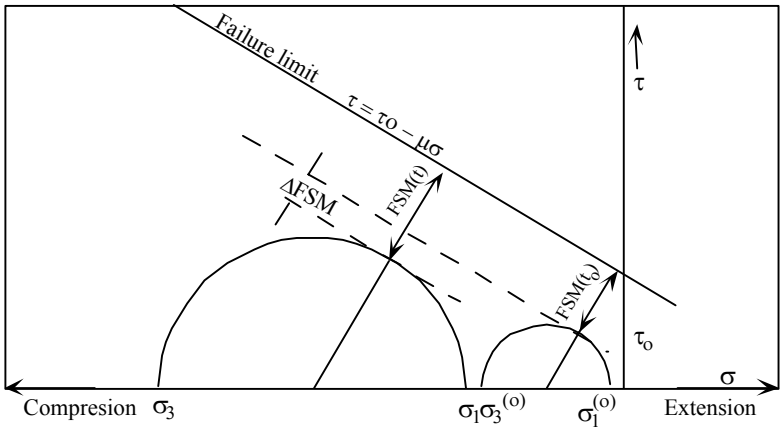

Figure 29. *Definition of the Fault Stability Margin FSM. Compressive stresses are negative.* $\sigma_1^{(0)}$ *and* $\sigma_3^{(0)}$ *are the maximum and minimum principal stresses of the reference state and* σ_1 *and* σ_3 *are the maximum minimum principal stresses of the perturbed state.* ΔFSM *is the change in the Fault Stability Margin. In this case it is positive and the incremental stress stabilises the fault.*

This is a measure of the additional stress required to cause failure in a material. If σ_1, σ_2, and σ_3 represent the maximum, intermediate and minimum (extensional) principal stress components, then the Fault Stability Margin is defined as

$$FSM = \beta\,[2\,\tau_0 - \mu(\sigma_1 + \sigma_3)] - (\sigma_1 - \sigma_3)/2 \qquad (15a)$$

where

$$\beta = \sin(\tan^{-1}\mu)/(2\mu) = (1+\mu^2)^{-1/2}/2 \qquad (15b)$$

The cohesion τ_0 and the friction coefficient μ define the failure limit of the material according to Byerlee's law

$$\tau = \tau_0 - \mu\,\sigma \qquad (15c)$$

where τ is the shear stress on the fault plane and σ is the stress normal to the fault plane (e.g. Johnson 1970; Jaeger & Cook 1979). Typically $\mu \approx 0.6$. In terms of a conventional Mohr representation of stress, the FSM is the minimum distance of the Mohr circle from the failure limit. The position of this limit is usually not known but its slope is defined by μ. In the above definition of the *FSM* the principal stresses represent the total stress field and in the present case include the stresses induced by the time-dependent surface load of ice and water, a horizontal in-plane plate-tectonic stress, and a depth-dependent hydrostatic stress. These last two are functions of position only on the time scales under consideration here.

The change in Fault Stability Margin from the initial stress state $\tau_{i,j}^{(0)}$ is given by

$$\Delta FSM = FSM - FSM^{(0)} \qquad (16)$$

where $FSM^{(0)}$ is the value for the pre-load condition (the hydrostatic and plate-tectonic stress fields). The change in Fault Stability Margin is therefore represented by the amount by which the Mohr circle is displaced towards or away from the failure criteria limit when an incremental stress is added to the background stress. Negative values of

ΔFSM result when the Mohr circle is shifted towards the failure limit and the incremental stress field enhances the likelihood of faulting for optimally oriented 'virtual' faults (see Wu et al., 1998). That is, existing faults close to this orientation where the background stress is close to critical may be reactivated under the influence of the glacial unloading. Positive values for the ΔFSM enhance fault stability.

We consider initially only the stress field along a longitudinal section at 24˚E. Figure 30 illustrates the load-stress components τ_{rr}, $\tau_{\theta\theta}$, $\tau_{\lambda\lambda}$ at the surface for different epochs. Both $\tau_{r\theta}$, and $\tau_{r\lambda}$ are zero because of the imposed boundary conditions and $\tau_{\theta\lambda}$ is mostly small because of the near-symmetry of the ice load about the northern Gulf of Bothnia. Thus, in this example, τ_{rr}, $\tau_{\theta\theta}$, $\tau_{\lambda\lambda}$ are approximately principal stresses. The reference state is one of hydrostatic equilibrium at the penultimate interglacial. That is $\sigma_1^{(0)} = \sigma_2^{(0)} = \sigma_3^{(0)} = \rho g D$ where D is depth below the surface. Tests in which the onset occurs earlier yield very similar results, indicating that the memory of earlier cycles of glaciation is lost after about two full cycles.

Maximum stresses at the time of the LGM attain about 30 MPa in $\tau_{r,r}$ consistent with an ice load of ~ 2500 m over northern Finland at that time. Values for $\tau_{\theta\theta}$, $\tau_{\lambda\lambda}$ are about twice that and all three stresses are compressional and remain so beneath the ice load. A significant reduction in the stress levels occurs during the deglaciation while central Fennoscandinavia remains ice covered (see results for T=18 ka and T=12 ka), but when northern Finland becomes ice free (T~10 ka) the maximum stresses there are still about 50% of their LGM values. The main difference from the earlier period is that one of the principal stresses, τ_{rr}, has approached zero as the last ice vanishes (non-zero values are achieved because of the water loads in the northern Gulf of Bothnia and in the Gulf of Finland (see T=0). At the present time the stresses have not relaxed entirely and are about 5 MPa at the surface in the northern part of the Gulf of Bothnia. Outside the area of loading the signs of the stresses change and the state is one of extension. This is consistent with standard stress patterns for loading of plates.

The corresponding ΔFSM at the surface is illustrated in Fig 31a for six epochs. Beneath the centre of the ice load at the time of the LGM (T=22 ka), the principal stresses are compressional and the effect of the ice is to enhance stability; the Mohr circle is moved away from the failure limit. At the margins of the ice sheet the ΔFSM is strongly negative for the early epochs (c.f. the results for T= 22 ka and 18 ka) and crustal stability here is reduced. The principal deviatoric stress here is horizontal extension (c.f. Fig. 30)and any pre-existing normal faults with an approximately east-west orientation could be reactivated by the glacial unloading. For the early deglaciation history the ice margins lie south of the southern Baltic shore and in southwestern Finland the crust is stabilised by the ice load. By the time this region becomes ice free, shortly after 12 Ka, the ΔFSM values are small, ~ 1-3 MPa and the present-day values are ~ 1 MPa only. Further north, at ~ 68˚ N near Porttipahdan tekojärvi, the ΔFSM values reach their maximum negative values of ~ 5 MPa at ~ 10 ka BP. Here in Lateglacial time the principal stresses are all compressional and any appropriately oriented faults could be reactivated as thrust faults during the immediate post-glacial period.

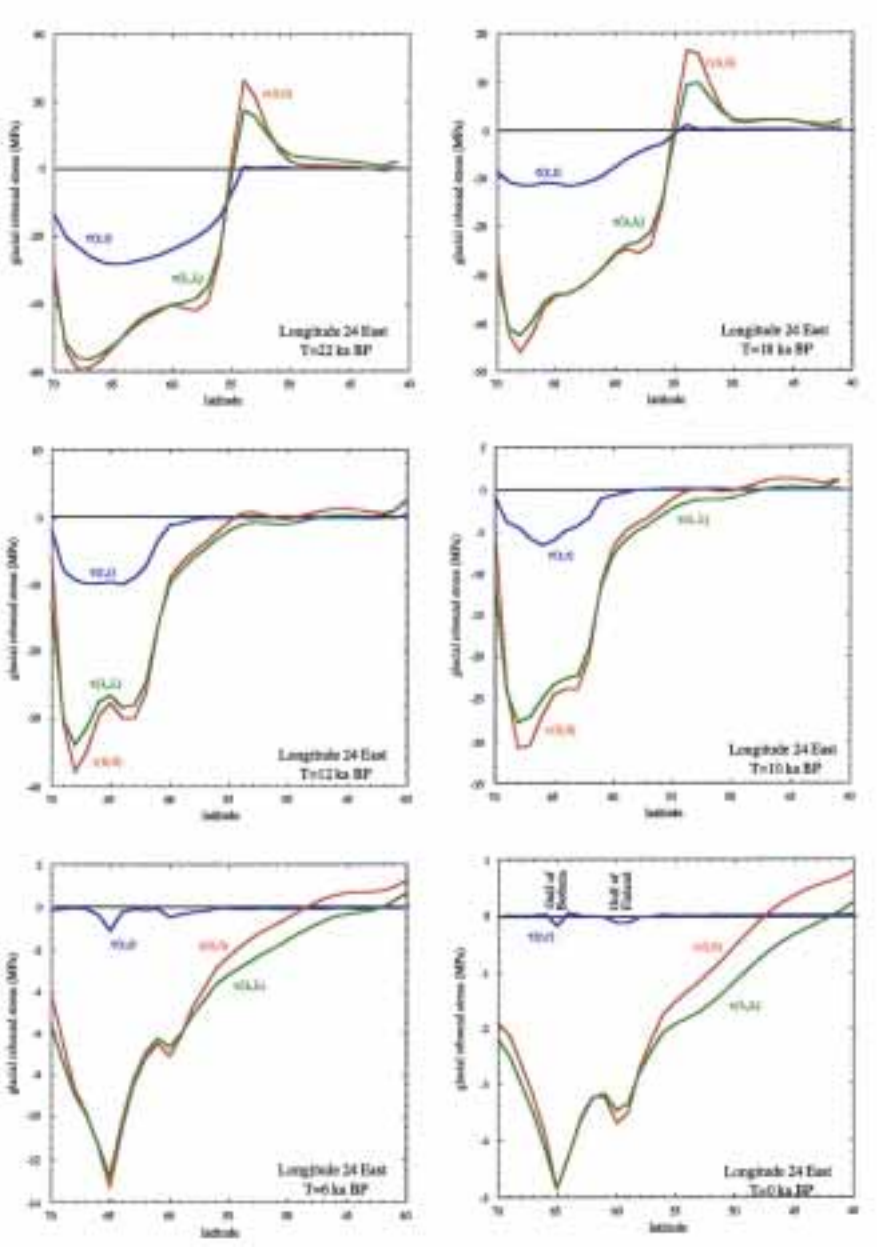

Figure 30. *Stress components τ_{rr}, $\tau_{\theta\theta}$, $\tau_{\lambda\lambda}$ at the surface along a section at 24˚ longitude for different epochs. Note the different scales for the stress axes. Negative stresses are compressional.*

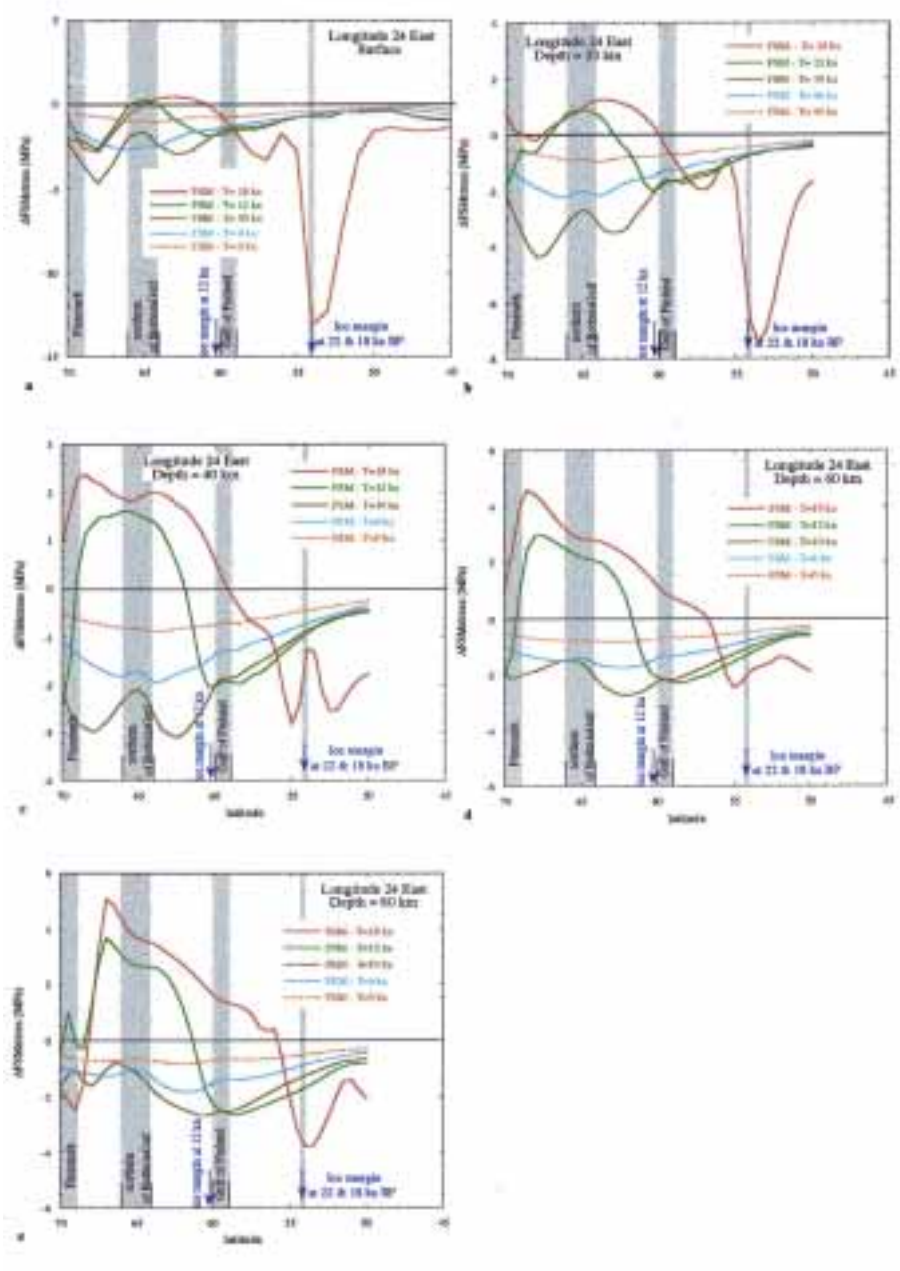

Figure 31. *ΔFSM at the surface and at depth along a section at 24˚longitude. The numbers in the legend refer to depth in km and time in ka.*

Fig. 31 also illustrates the predicted Δ*FSM* at a number of depths within the lithosphere. Because the loads at the times considered here are supported in part by the sub-lithospheric mantle, the depth dependence of stress is not the same as for a plate or shell over a fluid. Thus there in no correspondence to the 'middle plane' of the latter within the lithosphere of the viscoelastic mantle model, and so the deviatoric stress at the base of the lithosphere is not a mirror image of that at the surface. For as long as substantial ice remains the lithosphere beneath the loaded area has positive Δ*FSM* values at all

depths but once the vertical stress is reduced the Δ*FSM* become negative. Compare, for example, the results for T= 12 ka and T= 10 ka at ~ 65˚ N. The maximum negative values reach ~3 MPa within Finland at ~10 ka BP but the amplitudes decrease rapidly to <1 MPa by the present time.

The plate tectonics stress field can be inferred from the present-day near stress orientation measurements on the assumption that these stresses now dominate the largely relaxed glacial-load stresses. Such measurements (Stephansson 1989, 1993; Claus et al. 1989) show considerable variability probably due to topographic stresses and to internal crustal structures including faults. Stress indicators from depths of 300 m or greater show greater consistency and point to a mainly NW-SE direction of maximum compression. Thus we assume that the principal tectonic stress is one of compression with the maximum stress orientation being NW-SE. We do not specify the stress magnitude since they are largely unknown but also because their values are not critical in defining the Δ*FSM* and it is only the stress difference that is important (Wu & Hasegawa, 1996). Estimates of ~ 5 MPa for the stress drop on some of the palaeo faults of Sweden Arvidsson 1996) suggest that an appropriate value for the maximum stress difference for the plate-tectonic stress is ~ 5 MPa and we adopt this value for the preliminary analysis.

Figure 32 illustrates the results along the same longitude section as before for the case of the inplane force. In fact, the solutions do not differ greatly from the zero in-plane stress results because the background stress field is constant in space and time and its modification of the *differences* in principal stresses is mostly minor. For the part of the section between the Bothnia and Finland Gulfs the current Δ*FSM* values are negative but small at all depths. That is, the residual glacial loading stresses tend to move the crust closer to its failure limits and existing surface faults could be preferentially activated. Throughout the late glacial period (T< 18 ka BP) negative Δ*FSM* are predicted across this region with the maximum values occurring at the time when the region became ice free (T$\underline{\sim}$ 10 ka BP). Figure 33 illustrates the stress components and Δ*FSM* at 63˚N, 24˚E (near Lappajärvi) for three depths as a function of time. At all depths the present Δ*FSM* is less than 1MPa in magnitude compared with maximum magnitudes of 4 MPa at ~10 ka BP. Thus any failure within the crust triggered by glacial loading and unloading will have occurred preferentially at the time the region became ice free, all other factors contributing to crustal instability remaining unchanged.

The above results (Figs 30-33) have been based on the starting ice model (Case 1) but since the subsequent perturbations to this model are small, mostly less than 10% of the ice thickness, the above conclusion remains unchanged. Also, the results have been based on the geological estimates for the earth-model parameters but as indicated by the analysis of the geodetic data, the effective parameters may be time dependent. Thus the results in Figure 33 have been repeated for the same ice model but using the geodetic parameters (14). The pattern of the stress distribution and evolution changes little (Fig. 34) but the magnitudes are increased, reflecting the higher value for the upper mantle viscosity and the increased relaxation time constant. However, the ratio of the present negative Δ*FSM* values compared with the maximum magnitudes at ~ 10 ka BP remain

very similar and if stress has been released by brittle failure it will have most likely occurred at the time of ice retreat. The depth dependence of Δ*FSM* is illustrated in the fourth panel of Figure 34 indicating that, at least in central Finland Δ*FSM* decreases with depth throughout the crust.

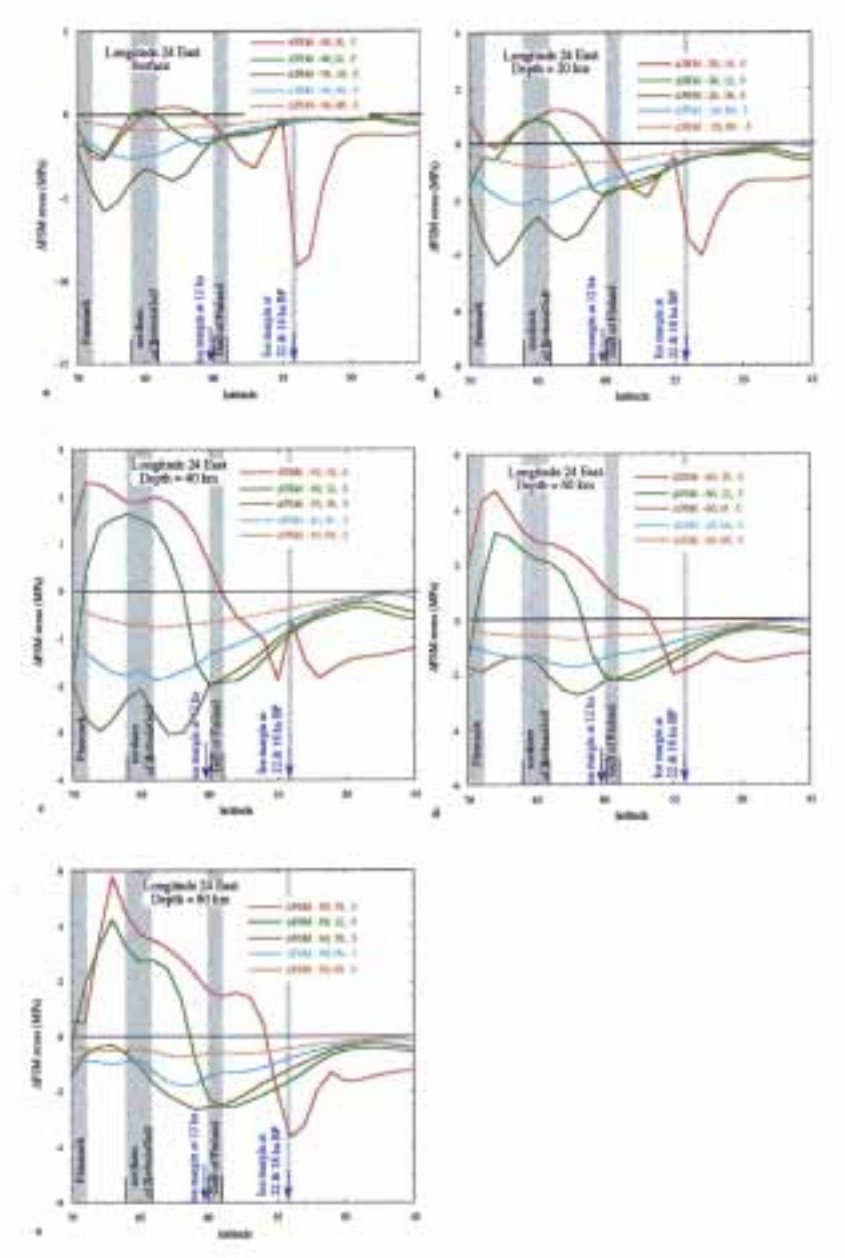

Figure 32. *ΔFSM with in-plane stress of -5 MPa (compression) at the surface and at depth along a section at 24˚ longitude. The numbers in the legend refer to depth in km, time in ka and in-plane stress in MPa.*

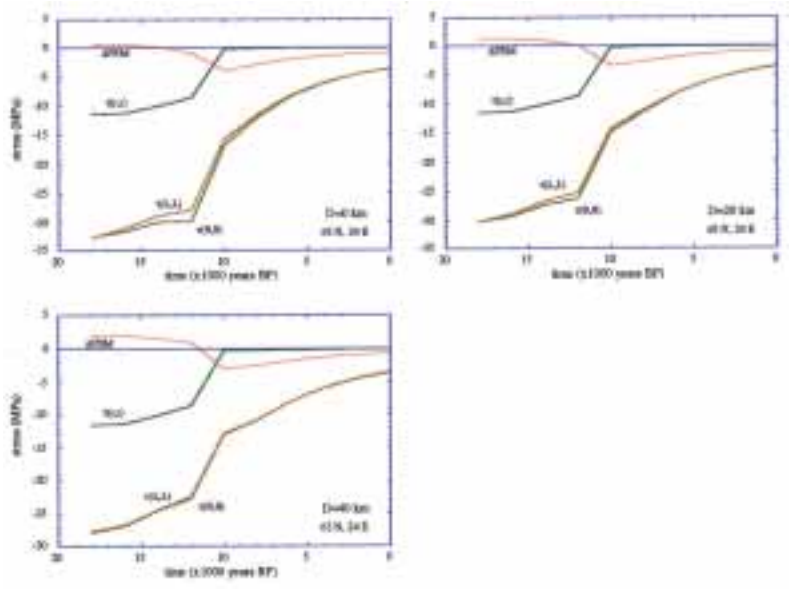

Figure 33. *Stress components τ_{rr}, $\tau_{\theta\theta}$, $\tau_{\lambda\lambda}$ and ΔFSM at 63˚N, 24˚E , as a function of depth D and time, based on the earth-model solution (10)*

The spatial variability of the surface stresses is illustrated in Figures 35 and 36 for a number of epochs. The ellipses in Figure 35 illustrate the orientation of the principal axes and the relative value of the maximum and minimum horizontal principal stresses is indicated by the ellipticity. With one exception, at T= 12 ka, these principal stresses are all compressional. The magnitudes of the maximum stress is given by the colour coding.

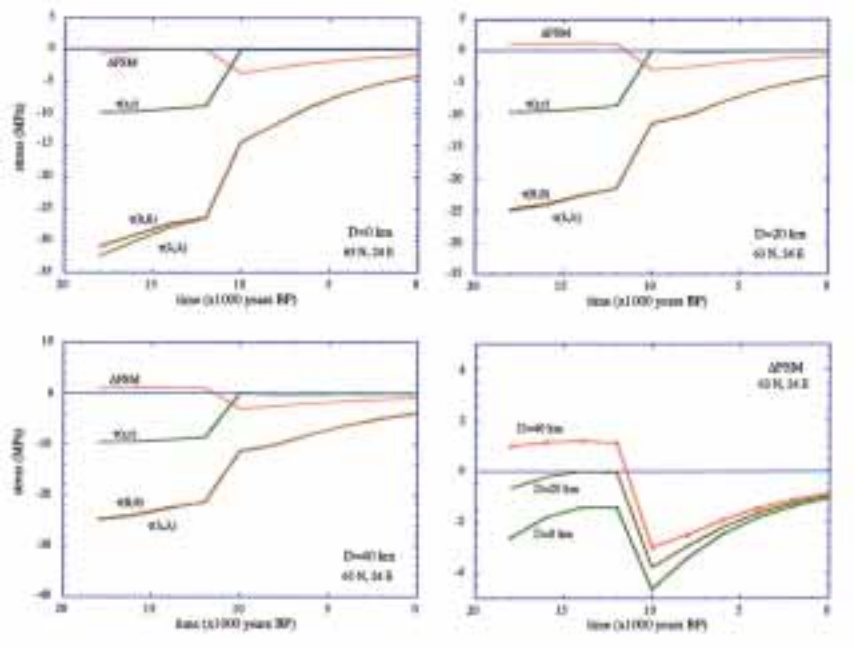

Figure 34. *Same as Fig. 33 but based on the earth-model solution 14. The fourth panel gives the depth dependence of ΔFSM.*

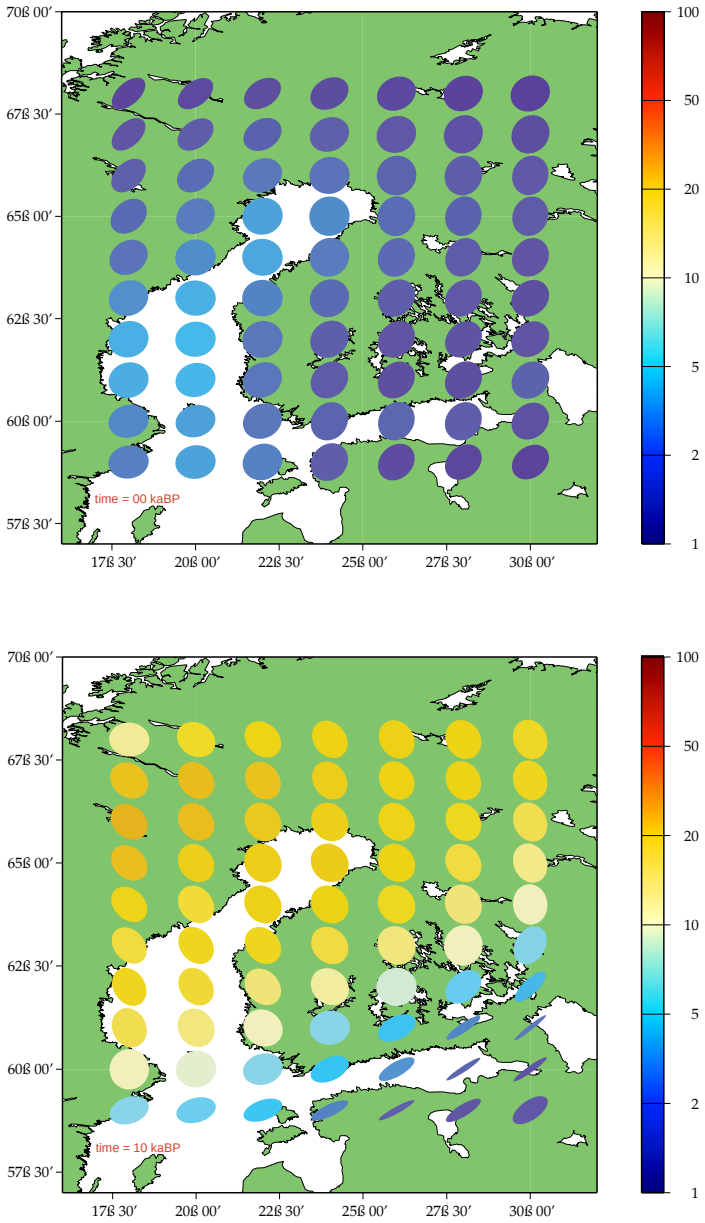

Figure 35. *Spatial variability of ΔFSM. The horizontal principal stress components at the surface due to the glacial rebound only for four epochs. The orientation of the ellipses indicate the directions of the principal stresses and the ellipticity specifies the relative magnitudes of the two stresses. The amplitude is specified by the colour coding with the numerical values in MPa. Only for T= 12 ka BP are there regions where these stresses are not compresssional.*

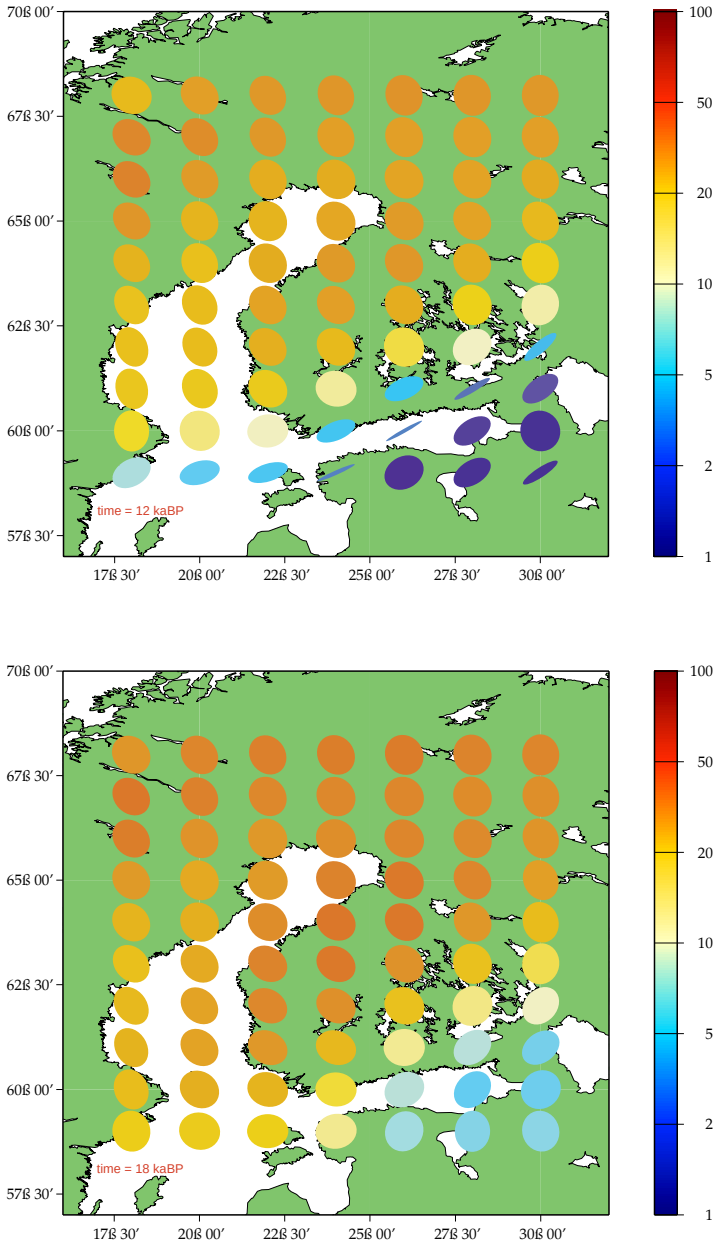

Figure 35. *(continued)*

The contours in Figure 36 give the ΔFSM for the specified epochs and the colour coded circles refer to the style of faulting that is preferentially activated by the glacial-load stress field This is thrust faulting throughout except for the southeast corner where this changes to normal faulting at about 12 ka BP.

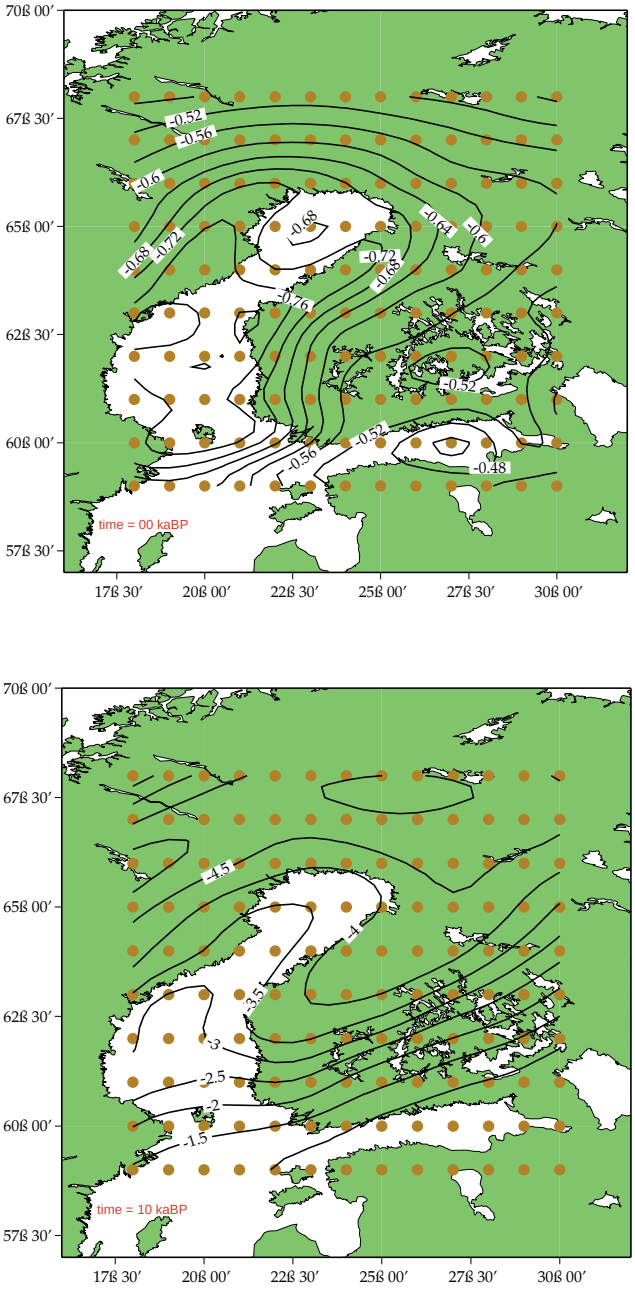

Figure 36. *The ΔFSM at the surface for four epochs. The magnitudes are given by the contours and the style of faulting is given by the colour coding (orange-brown thrust; blue normal). Only for T= 12 ka BP are there regions where the style of faulting is different from thrusting.*

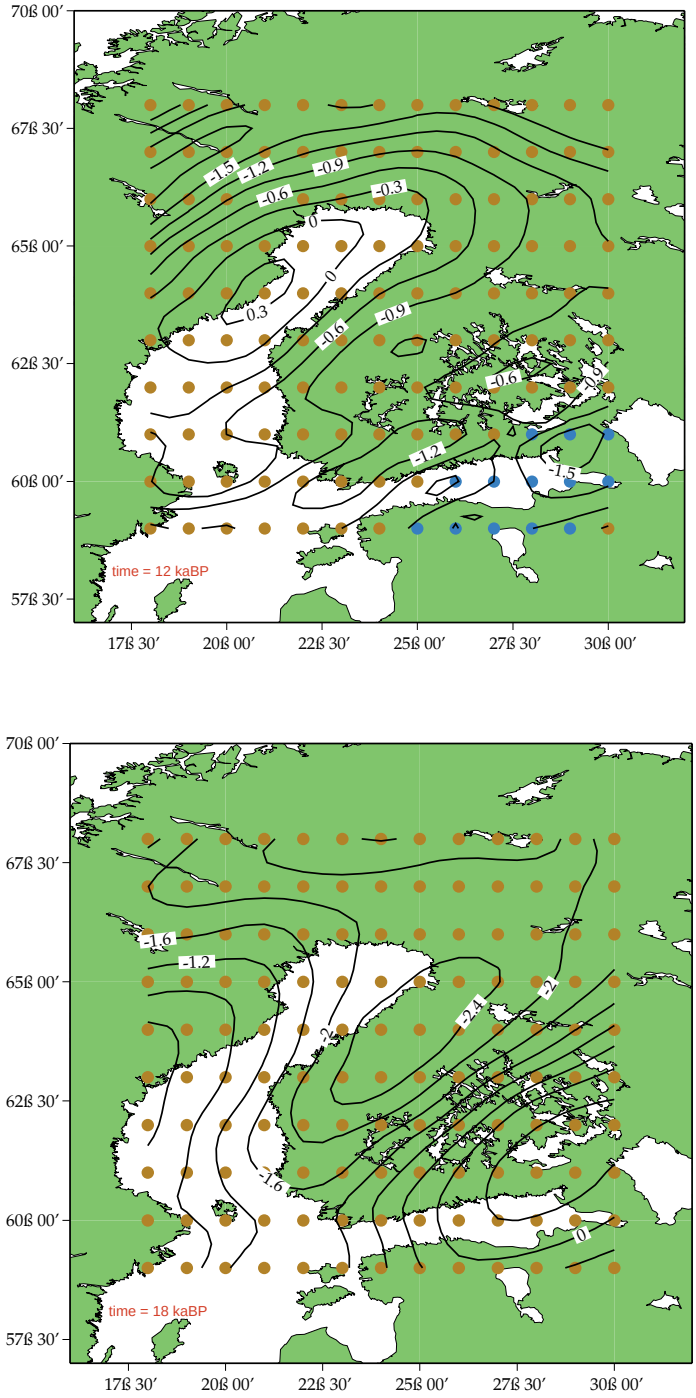

Figure 36. *(continued)*

For areas covered by thick ice all three principal stresses are compressional and the ice load stabilizes the crust against failure. Beyond the ice margin, however, the effect of loading is to develop extensional horizontal principal stresses (Figures 30, 31) and this occurs at ~12 ka in southeastern Finland and within the Gulf of Finland. At this time the area first became ice free but relatively thick ice still existed to the northwest. Thus here the horizontal principal stresses are extensional while the radial stress is zero so

that if the strength of the crust is exceeded failure will occur by normal faulting. At 10 ka much of Finland was ice free but the horizontal principal stresses are negative throughout. Thus any failure during this period is predicted to occur as thrust faulting. This is also the time when the destabilization of the crust is greatest at its surface with ΔFSM values of up to –4 to –5 MPa in central and northern Finland. From this time onwards the same pattern of stress is maintained but the magnitudes decrease. Thus at the present epoch all horizontal principal stresses are compressional across the region and $\tau_{rr} = 0$ (except the Gulf where τ_{rr} departs from zero by a small amount because of the changing water load with respect to the original stress state.) Thus everywhere the largest compressive force is horizontal and the least (or zero) compressive force is vertical and if failure were to occur it would be by thrusting. The two horizontal stresses are mostly comparable in magnitude and there is no strongly preferred orientation of faults susceptible to reactivation. However, the corresponding ΔFSM values are of smaller magnitude across the entire region than they were at earlier post-glacial epochs. Hence if failure occurred, it is likely to have taken place in the Lateglacial stage: by normal faulting in southeastern Finland circa 12-11 ka BP and by thrust faulting in central and northeastern Finland.

9 CONCLUSIONS

The results obtained in the current study of the rebound for Scandinavia represents considerable improvement over the previously published solutions in terms of agreement between observations and predictions. This is the case for the geological data as well as for the geodetic data and the new model parameters provide a robust description of the ice history and earth response function which can be used for predictive purposes and can be further tested against new data sets not previously considered. In this report we use this model to make a number of internally consistent geographic reconstructions and predictions. These include:

(a) The ice cover over Scandinavia since the Last Glacial Maximum, particularly for the Lateglacial period.

(b) The sea-level change and shoreline evolution for the Baltic area since the time the region became ice free for the last time.

(c) The predicted rates of present-day crustal rebound and sea-level change within the Baltic Basin.

(d) The evolution of the stress field in the crust since the time of the last glaciation and the prediction of the present-day residual stress field.

These results provide a regional picture of evolution since the last glaciation over Finland and the adjacent areas. Glacial rebound is mostly a long-wavelength and rather continuous change over time although localised crustal failure may have occurred in some localities when the ice retreated. Overall, there is no compelling evidence from the field data of relative sea-level change for substantial discontinuities in the earth response. Thus with high resolution topographic data, including bathymetry, it is possible to develop higher resolution geographic reconstructions. At present we do not have this information available to us.

While we consider that the present results are robust, there remains scope for further improvement, both in the modelling and in the observational evidence for rebound. These are summarized below.

9.1 Observational issues

Several data sets immediately come to mind for further testing of the model:

(a) The highest coastline data. Some problems have been identified with the geological data from northern Finland and the marine-limit data may provide an immediate check on the model for this region. Observation of the elevation of the marine limit provides a constraint on the amount of rebound and the position of the ice margin, although the age of the shoreline is not usually determined directly but inferred from the chronology of the ice retreat. Thus before we can incorporate this information chronology of the retreat of the ice across this region should be verified against field data that post-dates the compilation used by Pedersen (1995).

(b) GPS data for crustal displacement. The results presented here are preliminary and require further development. We are looking for a signal of the order of mm/year against instrumental and environmental noise that is at least as great and longer time series are required. Data modelling issues have also been identified, most notably the matter of how one maintains a reference frame when the European continent is deforming internally due to glacial rebound. The importance of this data set is at least threefold: the horizontal displacements provide a different constraint on rheological parameters than do the radial displacements, they provide measures of rebound within the land mass where tide gauge records are unavailable, and they provide a measure of rebound independent of recent ocean-volume changes.

(c) The geodetic levelling data set. In the uplifting areas of Finland and Sweden rates of rebound are required to adjust levelling measurements made at different epochs. If rebound models are used for this, is it still legitimate to use these data to test the models? For rebound modelling the levelling data is of value because it extends the recent record inland away from the coast and hence increases the spatial resolution of the observational data set. Both the levelling and GPS data are not very sensitive to the details of the past ice sheet but they are functions of the ice volumes through time. Hence they complement the geological data in any reconstructions of the ice history. Also, the results here have raised the possibility that the earth-response is not linear and this merits follow-up studies.

(d) The lake tilting analyses previously carried out for four major lakes in Finland and Sweden have indicated that this information provides a useful constraint on modelling recent crustal deformation. We are aware that more records exist but do not know their quality. This should be further investigated.

Of the currently used geological data sets a few anomalies have been identified and there is a need to go back to some of the original data to establish whether these anomalies are data related or indicative of rapid changes that are not captured by the models. Many of these data points were already considered as suspect by the original investigators because of inconsistencies between radiocarbon and stratigraphic ages but it may be that a careful comparison of predictions with observations can elucidate the causes. This needs to be done in cooperation with the original investigators. Particularly important in this respect is the data from northern Finland and there is a need to expand the data base there. Another area where there has been inadequate data is the eastern and southern margin of the Gulf of Finland. We have recently become aware of the new data from the University of Helsinki, and of new field work carried out on the southern margin of the Gulf of Finland. This should provide a useful test of the model and we will incorporate this in an appendix to this report at an early opportunity.

The Baltic Ice Lake data has provided a powerful constraint in the modelling. The timing of the Ancylus transgression remains more uncertain and the analysis carried out here for the BIL should be extended to the later lake stages, primarily to constrain the timing of the major phases in the evolution of the Baltic. An interesting outcome of the BIL analysis is that the time of drainage appears to have been earlier than the nominal

age of 12 ka BP (10.3 14C ka BP) at about 12.4 ka. If this is not consistent with other evidence then it points to scope for further model improvements, possibly to a need to modify the ice model for the early part of the Lateglacial.

9.2 Modelling issues

The range of earth models explored has remained restricted to a three-layer mantle model. Earlier work confirmed that such models are wholly adequate for describing rebound phenomenon and for predicting changes in shorelines. But for geophysical purposes a greater resolution in depth needs to be explored. While the ice sheet parameters remain uncertain, and dependent on the rebound, it is not immediately obvious whether such higher resolution models simply lead to trade-offs with the ice parameters when formal inverse procedures are used. The computational requirements for the extension of the forward modelling approach to higher resolution models, while keeping the parameter search to as large a range of values as possible, is substantial. We are developing multiple-processor parallel computational methods and when available we will extend the analysis to a greater range of parameterisation of the mantle.

The other vexing issue that remains unresolved is the degree of lateral variation in mantle rheology. That some occurs has been established by comparing different regions of the globe (Lambeck et al., 2002a) but preliminary analyses of the Scandinavian data has not indicated that this is necessary within Scandinavia. Whether solutions can be made for both ice and lateral mantle parameters as unknowns remains uncertain.

A third issue about mantle rheology is the issue of whether the linear rheology adopted here is adequate. A first examination of this issue is to repeat the tests carried out in section 5 (Cases 4 and 5) for the latest iteration ice model.

9.3 Stress considerations

For the stress predictions, the interactions of the glacial stress fluctuations with the background tectonic stress requires greater knowledge of the background stresses than we currently possess. But the essential conclusion is that these stresses have relaxed to a considerable degree and that the present-day residual stresses are small. If all other factors contributing to the total stress and to the crust's response to stress have not changed, it is unlikely that crustal failure will occur from this source.

The stress calculations used here are simplified in that they assume a relatively simple and laterally homogeneous crust and we need to relax these assumptions. The modelling methods used here for the sea-level predictions are global because of the need to consider contributions from the distant ice sheets and because of the need to include the water loading on the crust. The stress calculation for Scandinavia is not wholly insensitive to the changing ice sheet over North America but an alternate strategy is to separate the stress fields into a regional one, calculated for the distant ice

sheets using the global theory, and a local one for the Scandinavian ice sheet using high-resolution flat-earth models with greater depth and lateral structure. This has yet to be attempted.

The results provided here do support the concept that crustal failure may have occurred at the end of the glaciation. We have not been able to examine closely the field evidence for this in Finland and this needs to be done in collaboration with Finnish scientists.

10 REFERENCES

Andersen, B.G., 1981. Late Weichselian ice sheets in Eurasia and Greenland. In *The Last Great Ice Sheets*, (G.H. Denton, and T.J. Hughes, Eds.) J.Wiley, New York, 1-65.

Bard, E., 1998. Geochemical and geophysical implications of the radiocarbon calibration. *Geochim. Cosmochim. Acta*, **62**, 2025-2038.

Cathles, L.M., 1975. *The Viscosity of the Earth's Mantle*. Princeton University Press, Princeton, NJ.

Claus, B., Marquardt, G. and Fuchs, K., 1989. Stress orientations in the North Sea and Fennoscandia. In *Earthquakes at North-Atlantic Passive Margins*, (S. Gregerson and P. Basham, Eds.) Kluwer Dordrecht, 277-287.

Ekman, M., 1996. A consistent map of the postglacial uplift of Fennoscandia. *Terra Nova*, **8**, 158-165.

Eronen, M., et al., 1995. Land uplift in the Olkilvoto-Pyhäjärvi area, southwestern Finland, during the last 8000 years. *Nuclear Waste Commission of Finnish Power Companies, Helsinki.*

Feigl, K., et al., Space geodetic measurements of crustal deformation in central and southern California, *J. Geophys. Res.,* **98**, 21677-21712.

Fjeldskaar, W., 1994. Viscosity and thickness of the asthenosphere detected from the Fennoscandian uplift. *Earth Planet. Sci. Lett.*, **126**, 399-410.

Fjeldskaar, W., 1997. Flexural rigidity of Fennoscandia inferred from the postglacial uplift. *Tectonics*, **16**, 596-608.

Herring, T.A., 1997. GLOBK global Kalman filter VLBI and GPS analysis program., *Mass. Inst. Tech.,* Cambridge, Mass., (Version 4.1.)

Jaeger, J.C. and Cook, N.G.W., 1979. *Fundamentals of Rock Mechanics*, (3rd edition), Chapman and Hall, London.

James, T.S. and Morgan, W.J., 1990. Horizontal motions due to post-glacial rebound. *Geophys. Res. Lett.*, **17**, 7, 957-960.

Jeffreys, H., 1970. *The Earth* (5th edn). Cambridge University Press.

Johnson, A.M., 1970. *Physical Processes in Geology*, Freeman, Cooper & co., San Francisco.

Johnston P., Wu, P. and Lambeck, K., 1998. Dependence of horizontal stress magnitude on load dimension in glacial rebound models. *Geophys. J. Int.*, **132**, 41-60.

Johnston, P. and Lambeck, K., 1999. Postglacial rebound and sea-level contributions to changes in the geoid and the Earth's rotation axis. *Geophys. J. Int*., **136**, 537-558.

Kauffman, G. and Lambeck, K., 2002. Glacial isostatic adjustment and the radial viscosity profile from inverse modelling. *J. Geophys. Res.,* ETG-5.1.-5.15.

King, R.N. and Bock, Y., 1999. Documentation for the GAMIT GPS analysis software, release 9.6., *Mass. Inst. Tech.*, Cambridge, Mass.

Kullman, L., 2001. A new approach to postglacial forest-history of northern Scandinavia. Review of megafossil and macrofossil evidence. *Recent. Res. Devel. Ecol.,* **1**, 1-19.

Lambeck, K., 1993. Glacial rebound and sea-level change: An example of a relationship between mantle and surface processes. *Tectonophysics*, **223**, 15-37.

Lambeck, K., 1998. On the choice of timescale in glacial rebound modelling: mantle viscosity estimates and the radiocarbon timescale. *Geophys. J. Int.*, **134**, 647-651.

Lambeck, K. 1999. Shoreline displacement in southern-central Sweden and the evolution of the Baltic Sea since the last maximum glaciation. *J. Geol. Soc. Lond*., **156**, 465-486.

Lambeck, K., and Chappell, J., 2001. Sea Level Change through the last Glacial Cycle. *Science,* **292***,* 679-686.

Lambeck, K. et al., 1996. Glacial rebound of the British Isles – III. Constraints on mantle viscosity. *Geophys. J. Int.*, **125**, 340-354.

Lambeck, K., Smither, C. & Ekman, M., 1998b. Tests of glacial rebound models for Fennoscandinavia based on instrumented sea- and lake-level records. *Geophys. J. Int.*, **135**, 375-387

Lambeck, K., Smither, C. & Johnston, P., 1998a. Sea-level change, glacial rebound and mantle viscosity for northern Europe. *Geophys. J. Int.,* **134**, 102-144.

Lambeck, K., et al., 2000. Global ice volumes at the Last Glacial Maximum. *Earth Planet. Sci. Lett.,* **181**, 513-527.

Lambeck, K., Yokoyama, Y., & Purcell, A., 2002a. Into and Out of the Last glacial Maximum Sea Level Change During Oxygen Isotope Stages 3-2. *Quaternary Science Reviews*, **21**, 343-360.

Lambeck, K., Yokoyama, Y. Purcell, A. 2002b. Reply to the Comment by W.R. Peltier. *Quaternary Science Reviews*, **21**, 415-418.

Lambeck, K., 2002. Sea-Level Change from Mid-Holocene to Recent Time: An Australian Example with Global Implications. In *Ice Sheets, Sea level and the Dynamic Earth,* (J.X. Mitrovica and B. Vermeersen, Eds.) Geodynamics Series 29, American Geophysical Union, Washington DC, 33-50.

Lambeck, K., et al., 2003. Water-load definition in the glacio-hydro-isostatic sea-level equation. *Quat. Sci. Rev.*, **22**, 309-318.

Licciardi, J.M., et al. 1998. Deglaciation of a soft-bedded Laurentide Ice Sheet. *Quaternary Science Reviews*, **17**, 427-448.

Liden, R. 1938. Den senkvartara strandförskjutningens forlopp och kronologi i Angermanland. *Geol. Fören. Furhandl.* Bd. **60**, H3.

Milne, G.A., et al., 2001. Space geodetic constraints on glacial isostatic adjustment in Fennoscandia. *Science*. **291**, 2381-2385.

Milne, G.A. and Mitrovica, J.X. 1998. Postglacial sea-level change on a rotating earth. *Geophys. J. Int.,* **133**, 1-19.

Mitrovica, J.X. and Milne, G.A. 2003. On postglacial sea level: 1. General theory. *Geophys. J. Int.*, in press

Påsse, T., 1998. Lake-tilting, a method for estimation of glacio-isostatic uplift. *Boreas,* **27**, 69-80.

Pedersen, S.S. 1995. Israndslinier i Norden. *Danm. Geol. Unders.,* Copenhagen.

Peltier, W.R. and Andrews, J.T., 1976. Glacio-isostatic adjustment – 1. The forward problem. *Geophys. J. Roy. Astr. Soc.* **46**, 605-646.

Peltier, W.R., 2002. Comments on the paper of Yokoyama et al. (2000) entitled "Timing of the Last Glacial Maximum from observed sea level minima." *Quat. Sci. Rev.,* **21**, 409-414.

Sirén, A., 1951. On computing the land uplift from the lake water level records in Finland. *Fennia*, **73**, 5, 1-181.

Stephansson, O., 1989. Stress Measurements and modeling of crustal rock mechanics in Fennoscandia. In *Earthquakes at North Atlantic Passive Margins: Neotectonics and Postglacial Rebound,* (S. Gregersen and P. Basham, Eds.), NATO ASI Series, Kluwer Academic Publishers, Dordrecht, 213-229.

Stone, J.O., et al., 2003. Holocene Deglaciation of Marie Byrd Land, West Antarctica. *Science*, **299**, 99-102.

Svensson, N-O., 1991. Late Weichselian and Early Holocene shore displacement in the Central Baltic Sea. *Quat. Int.*, **9**, 7-26.

Wu, P., Johnston, P. and Lambeck, K., 1999. Postglacial rebound and fault instability in Fennoscandia. *Geophys. J. Int.*, **139**, 657-670.

Yokoyama, Y., et al., 2000. Timing of the Last Glacial Maximum from observed sea level minima. *Nature*, **406**, 713-716.

POSIVA-reports 2003, situation 11/2003

POSIVA 2003-01
Vertical and Horizontal Seismic Profiling Investigations at Olkiluoto, 2001
Calin Cosma, Nicoleta Enescu, Erick Adam, Lucian Balu
Vibrometric Oy
March 2003
ISBN 951-652-115-0

POSIVA 2003-02
Baseline Conditions at Olkiluoto
Posiva Oy
September 2003
ISBN 951-652-116-9

POSIVA 2003-03
ONKALO Underground Characterisation and Research Programme (UCRP)
Posiva Oy
September 2003
ISBN 951-652-117-7

POSIVA 2003-04
Thermal Analyses of Spent Nuclear Fuel Repository
Kari Ikonen, VTT Processes
June 2003
ISBN 951-652-118-5

POSIVA 2003-05
Programme of Monitoring at Olkiluoto During Construction and Operation of the ONKALO
Posiva Oy
December 2003
ISBN 951-652-119-3

POSIVA 2003-06
Assessment of disturbances caused by construction and operation of ONKALO
Timo Vieno, Jarmo Lehikoinen, Jari Löfman, Henrik Nordman
VTT Processes
Ferenc Mészáros
The Relief Laboratory
October 2003
ISBN 951-652-120-7

POSIVA 2003-07 Hydrochemical Interpretation of Baseline Groundwater Conditions at the Olkiluoto Site.
Petteri Pitkänen, Ari Luukkonen, Sami Partamies
VTT Building and Transport
ISBN 951-652-121-5

POSIVA 2003-08 Air-oxidation Tests with Gd-doped UO_2
Preliminary Dissolution Experiments with Pre-oxidized Gd-doped UO_{2+x}
Kaija Ollila, VTT Processes
Kristian Lindqvist, Geological Survey of Finland
ISBN 951-652-122-3

POSIVA 2003-09 Narrow Gap Arc Welding Experiments of Thick Copper Sections
Rami Pohja, Heikki Vestman, Petra Jauhiainen, Hannu Hänninen
Helsinki University of Technology
Laboratory of Engineering Materials
ISBN 951-652-123-1

POSIVA 2003-10 Glacial Rebound and Crustal Stress in Finland
Kurt Lambeck, Anthony Purcell
Research School of Earth Sciences,
The Australian National University
November 2003
ISBN 951-652-124-X